
Lappeenrannan teknillinen korkeakoulu
Lappeenranta University of Technology

Markku Hauta-Kasari

COMPUTATIONAL TECHNIQUES FOR SPECTRAL IMAGE ANALYSIS

Acta Universitatis
Lappeenrantaensis 81

ISBN 978-952-214-785-1 (PDF)

Lappeenrannan teknillinen korkeakoulu
Lappeenranta University of Technology

Markku Hauta-Kasari

COMPUTATIONAL TECHNIQUES FOR SPECTRAL IMAGE ANALYSIS

Thesis for the degree of Doctor of Philosophy to be presented with due permission for public examination and criticism in the Auditorium in the Students' Union Building at Lappeenranta University of Technology, Lappeenranta, Finland on the 20th of May, 1999, at noon.

Acta Universitatis
Lappeenrantaensis
81

Supervisor

Professor Jussi Parkkinen
Department of Information Technology
Lappeenranta University of Technology
FINLAND

Reviewers

Professor Moncef Gabbouj
Signal Processing Laboratory
Department of Information Technology
Tampere University of Technology
FINLAND

Professor Risto Myllylä
Optoelectronics and Measurement Technology Laboratory
Department of Electrical Engineering
University of Oulu
FINLAND

Opponent

Professor Erkki Oja
Laboratory of Computer and Information Science
Helsinki University of Technology
FINLAND

ISBN 951-764-333-0
ISSN 1456-4491

Lappeenrannan teknillinen korkeakoulu
Monistamo 1999

Preface

The work presented in this thesis has been carried out at the Laboratory of Information Processing in the Department of Information Technology of the Lappeenranta University of Technology, Finland, between summer 1995 and spring 1999. An important period of this thesis is my stay as a visiting researcher at the Graduate School of Science and Engineering of the Saitama University, Japan, between autumn 1996 and autumn 1998.

I want to express my deep gratitude to my supervisor Professor Jussi Parkkinen for the guidance and for the fruitful discussions throughout this thesis. Professor Parkkinen encouraged me to do this work and he organized facilities for the research.

My deep gratitude belongs also to Professor Satoru Toyooka at the Saitama University, Japan. Professor Toyooka was my supervisor during my two years stay in Japan. I want to thank Professor Toyooka for being my host in Japan, which was a wonderful experience, both in research and life experience. I am also very thankful to my friend Miss Kanae Miyazawa for the pleasant cooperation during my stay in Japan.

I wish to thank Dr. Reiner Lenz at the Linköping University, Sweden, for being my host on summer 1996, when I visited his laboratory for a month. Dr. Reiner Lenz also guided me with many valuable comments and advices during my work. I am also indebted to Professor Timo Jääskeläinen at the University of Joensuu, Finland, and Professor Heikki Kälviäinen at the Lappeenranta University of Technology. I thank the staff of the Department of Information Technology at the Lappeenranta University of Technology for stimulating atmosphere.

Finally, I thank my parents Tuula and Pentti and my sister Kaisa for their encouragement.

The financial support of the Lappeenranta University of Technology, Japanese Ministry for Education (Monbusho), Jenny and Antti Wihuri Foundation, South Karelia Regional Fund of the Finnish Cultural Foundation, Emil Aaltonen Foundation, Foundation of Technology, and Finnish Cultural Foundation is gratefully acknowledged.

Lappeenranta, May 1999

Markku Hauta-Kasari

Abstract

Acta Universitatis Lappeenrantaensis 81

Markku Hauta-Kasari

Computational Techniques for Spectral Image Analysis

Lappeenranta 1999

ISBN 951-764-333-0
ISSN 1456-4491
UDK 004.93'1 : 004.932 : 681.3.019 : 535.65

Keywords: Color, color constancy, color filter, color spectra, illumination estimation, multispectral texture, optical pattern recognition, spectral image, spectral imaging

Multispectral images are becoming more common in the field of remote sensing, computer vision, and industrial applications. Due to the high accuracy of the multispectral information, it can be used as an important quality factor in the inspection of industrial products. Recently, the development on multispectral imaging systems and the computational analysis on the multispectral images have been the focus of a growing interest.

In this thesis, three areas of multispectral image analysis are considered. First, a method for analyzing multispectral textured images was developed. The method is based on a spectral cooccurrence matrix, which contains information of the joint distribution of spectral classes in a spectral domain. Next, a procedure for estimating the illumination spectrum of the color images was developed. Proposed method can be used, for example, in color constancy, color correction, and in the content based search from color image databases. Finally, color filters for the optical pattern recognition were designed, and a prototype of a spectral vision system was constructed. The spectral vision system can be used to acquire a low-dimensional component image set for the two-dimensional spectral image reconstruction. The data obtained by the spectral vision system is small and therefore convenient for storing and transmitting a spectral image.

Abbreviations

ALSM	Averaged Learning Subspace Method
AOTF	Acousto-Optic Tunable Filter
BMU	Best-Matching Unit
CCD	Charged Couple Device
CIE	Commission Internationale de l'Éclairage
CIE xyY	CIE xyY color coordinate system
CIELAB	CIE $L^*a^*b^*$ color coordinate system
CIELUV	CIE Luv color coordinate system
DCT	Discrete Cosine Transform
ICA	Independent Component Analysis
IR	Infrared
k-NN	k-nearest neighbor classifier
LCSLM	Liquid Crystal Spatial Light Modulator
LVF	Linear Variable Filter
MLP	Multilayer perceptron neural network
NCS	Natural Color System
PCA	Principal Component Analysis
PGP	Prism-Grating-Prism
RGB	Red-Green-Blue color coordinate system
SOM	Self-Organizing Map
SVD	Singular Value Decomposition
UV	Ultraviolet
WTA	Winner Take All

List of Publications

1. HAUTA-KASARI M., PARKKINEN J., JAASKELAINEN T., AND LENZ R., Generalized Cooccurrence Matrix for Multispectral Texture Analysis, in *Proceedings, 13th International Conference on Pattern Recognition, (ICPR'96), Vienna, Austria, August 25-29, 1996*, Vol. II, pages 785-789.

2. HAUTA-KASARI M., PARKKINEN J., JAASKELAINEN T., AND LENZ R., Multispectral Texture Segmentation Based on the Spectral Cooccurrence Matrix, *Pattern Analysis and Applications*. In Press.

3. LENZ R., MEER P., AND HAUTA-KASARI M., Spectral-Based Illumination Estimation and Color Correction, *Color Research and Application*, Vol. 24, No. 2, April, 1999, pages 98-111.

4. HAUTA-KASARI M., WANG W., TOYOOKA S., PARKKINEN J., AND LENZ R., Unsupervised Filtering of Munsell Spectra, in *Proceedings, 3rd Asian Conference on Computer Vision, (ACCV'98), Hong Kong, January 8-10, 1998*, Vol. I of *Lecture Notes in Computer Science 1351*, R. Chin and T.-C. Pong, Eds., Springer 1998, pages 248-255.

5. HAUTA-KASARI M., MIYAZAWA K., TOYOOKA S., AND PARKKINEN J., A Prototype of the Spectral Vision System, in *Proceedigns, 11th Scandinavian Conference on Image Analysis, (SCIA'99), Greenland, June 7-11, 1999*. In Press.

In this thesis these publications are referred as *publication 1*, *publication 2*, *publication 3*, *publication 4*, and *publication 5*.

CHAPTER I

Introduction

Color is becoming an important quality factor in industrial processes. The accuracy of the color representation depends on the measuring system and the color coordinate system used. Usually color is represented by three-dimensional color coordinate models, which are based on the model of human color vision system, in which there are three different types of photoreseptors [50]. Typical three-dimensional color coordinate models are CIE xyY, CIELAB, CIELUV, and RGB models [39, 50, 107].

The color analysis based on the three-dimensional color coordinate systems is computationally effective and the accuracy of the color representation is enough for many applications. Also the present color imaging systems are mostly based on the use of color cameras with three color filters. However, there are some restrictions in these color models. The three-dimensional color coordinate systems may have a problem of metamerism [11, 12, 33, 39, 97], in which one three-dimensional color coordinate vector corresponds to several different color spectra. One type of metamerism is that human cannot distinguish the color of two objects under a certain illumination, but when the illumination is changed, the difference between the color of two objects can be recognized. In addition, sometimes the interesting part of the measurement can be outside the visible part of the electromagnetic spectrum, *e.g.* in the ultraviolet (UV) or near infrared/infrared (IR) region.

Basing on the physical approach, the highest accuracy of the color representation can be obtained by representing the color as a color spectrum, which is measured in the visible wavelength range from 380nm to 780nm of the electromagnetic spectrum. Two-dimensional high-quality color images, in which every pixel contains a color spectrum, are called multispectral or spectral images. The spectral based representation of color avoids the problem of metamerism and the spectra can be also measured outside the visible light area, for example in the UV or IR regions.

The importance of color image processing is growing and the trend is to multispectral images. The technical development in spectral imaging devices has received a great deal of attention recently. Multispectral imaging systems have application areas such as remote sensing [3, 8, 80, 81], environmental monitoring [45, 82], material analysis [62], computer vision [51], and industrial quality control [40]. The spectral information has been used, for example, to improve the color reproduction of electronic endoscopes [27, 92], to simulate

adaptation in the human vision system [63], and to analyze skin color [41, 42]. Recently, the multispectral images of natural scenes have been used to investigate the coding in the human vision system [78, 85]. In the analysis of works of art, the use of multispectral imaging is a promising noninvasive approach [2].

The high-quality color images measured by the multispectral imaging systems have to be analyzed by new methods of the color image analysis. For example, if the spectral imaging system is tuned to measure the visible light from 400nm to 700nm at 1nm intervals, then a measured image contains 301 spectral channels, and the total size of the 8bits/pixel, 256 × 256 pixels spectral image is about 158 megabytes. The multispectral image contains a large amount of data and therefore the transmission and storing of it can be unconvenient. The compression and acquisition of the spectral images needs also new techniques in order to be convenient to use in the field of high-quality color image processing.

The objective for this thesis is to study computational techniques for spectral image analysis. The main interest is in the multispectral images, where the number of spectral channels is more than 30. The aims and a scope of this thesis contain an investigation of a method for multispectral texture analysis, a study of spectral based illumination estimation and a production of a prototype for the spectral imaging system, which we call as the spectral vision system.

The thesis is divided into seven chapters. Following the introduction in Chapter 1, the principles of color and texture representation are given in Chapters 2 and 3, respectively. A method for analyzing multispectral textured images is described in Chapter 4. In Chapter 5 the spectral based illumination estimation procedure is proposed. In Chapter 6 a prototype of the spectral vision system is presented and Chapter 7 provides the discussion and conclusions of this thesis.

Summary of the publications

In *publication 1* the generalization of the gray level cooccurrence matrix was proposed for the multispectral texture analysis. The novelty of the proposed method is that the cooccurrence is defined as a joint distribution of the spectral classes in a spectral domain. From the generalized cooccurrence matrix, five Haralick's features were calculated. The experiments of multispectral texture segmentation with synthetic data were performed. The author of this thesis participated in the development of the method, programmed the procedure, performed the experiments, and wrote the publication.

In *publication 2* the generalized cooccurrence matrix based method was tested with natural multispectral images. Furthermore, the cooccurrence matrix itself was used as a feature vector for the classification process. The experimental results of segmenting natural multispectral textures were performed. The author of this thesis participated in the development of the method, performed experiments, and wrote the publication.

In *publication 3* a statistical technique based on the spectral-based illumination estimation for solving the problem of color constancy was proposed. It was used for the color correction and for the content based search from the color image database. The idea of the method was developed by Dr. Reiner Lenz and Professor Peter Meer. The author of this thesis participated in the program development and in some experiments of the publication.

In *publication 4* a new computational approach for designing broad band color filters for the low-dimensional spectral imaging system was proposed. The author of this thesis participated in the development of the method, programmed the procedure, performed the experiments, and wrote the publication.

In *publication 5* a prototype of the low-dimensional spectral vision system was proposed. The optical setup was constructed and the color filters designed by the computer simulations in *publication 4* were implemented optically. The experiments of acquiring two-dimensional spectral images were permormed. The author of this thesis participated in the development of the method and in the construction of the optical setup. He programmed the procedure, performed the experiments, and wrote the publication.

CHAPTER II

Color Representation

Color of an object detected by a human being is a sensation which is produced by the human brain [50] and therefore it is hard to define the color. Using a physical approach, the color information is conveyed by light approaching the eye originating from the observed object. Thus the color of the object is a continuous function of wavelength of the electromagnetic radiation in the visible light range from 380nm to 780nm. In practical use the wavelength range from 400nm to 700nm has been used. The spectrum of this radiation can be measured and represented as a vector

$$\tau(\lambda) = [\tau(\lambda_1), \tau(\lambda_2), \ldots, \tau(\lambda_n)]^T, \tag{2.1}$$

where λ is the wavelength and T denotes the transpose. For example, the spectrum τ sampled at 5nm intervals from $\lambda_1 = 400$nm to $\lambda_{61} = 700$nm can be defined as a vector in a 61-dimensional Euclidean space. Figure 2.1 shows an example of the color spectrum of green and red objects.

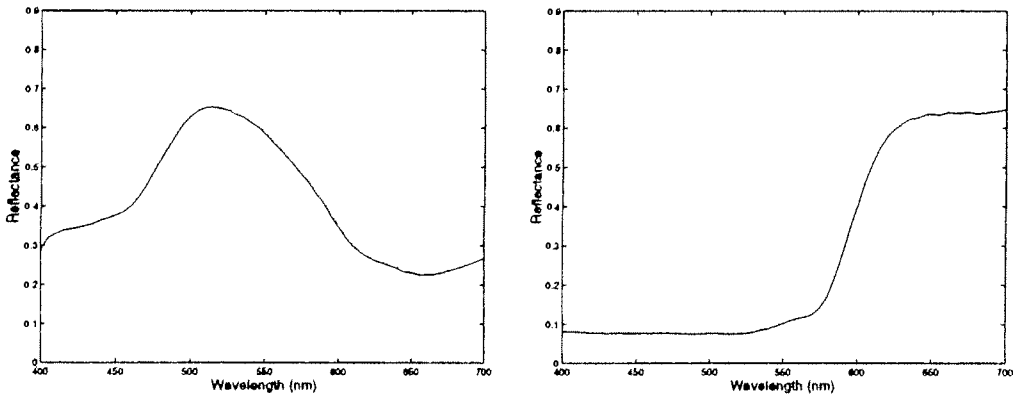

a) b)

Figure 2.1: Example of the color spectrum of a) green and b) red object.

The measured radiation is effected by the relative spectral power distribution $E(\lambda)$ of the illuminant. Thus the measured radiation is defined as the product

$$\tau(\lambda) = S(\lambda)E(\lambda), \tag{2.2}$$

where $S(\lambda)$ is the spectral reflectance, transmittance or radiance of the object [39, 50, 107]. There are a number of standard light sources recommended by the Commission Internationale de l'Éclairage (CIE). These are commonly called the illuminants A, B, C, and D_{65}. For the standard daylight D illuminants, CIE has also recommended the representations D_{50}, D_{55}, and D_{75} [39]. These standard light sources have different spectra which correspond to the illumination conditions of the measurement. The measured radiation is also effected by the spectral sensitivity of the measuring sensors, but they are not modeled here.

2.1 Three-dimensional colorspaces

The color is usually represented by three-dimensional color vision models. These models are based on the model of human color vision system, in which there are three different types of photoreseptors. Typical three-dimensional color vision models are CIE 1931 xyY, CIELAB, CIELUV, and RGB models. Most of these three-dimensional color coordinate systems are calculated from the tristimulus values (X, Y, Z) which are calculated over the spectrum $\tau(\lambda)$

$$\begin{aligned} X &= k\int \tau(\lambda)\bar{x}(\lambda)\, d\lambda \\ Y &= k\int \tau(\lambda)\bar{y}(\lambda)\, d\lambda \\ Z &= k\int \tau(\lambda)\bar{z}(\lambda)\, d\lambda, \end{aligned} \tag{2.3}$$

where the functions $\bar{x}(\lambda)$, $\bar{y}(\lambda)$, and $\bar{z}(\lambda)$ are the human color-matching curves defined by the CIE. The normalizing factor k is chosen as

$$k = \frac{100}{\int E(\lambda)\bar{y}(\lambda)\, d\lambda}. \tag{2.4}$$

The color-matching curves $\bar{x}(\lambda)$, $\bar{y}(\lambda)$, and $\bar{z}(\lambda)$ have been defined according to the results of the experiments with human observes. Figure 2.2 shows the color-matching curves $\bar{x}(\lambda)$, $\bar{y}(\lambda)$, and $\bar{z}(\lambda)$ at the wavelength range from 380nm to 780nm.

From the tristimulus values (X, Y, Z), other color coordinate systems can be derived. The CIE 1931 (x, y, z) coordinates are defined as follows

$$\begin{aligned} x &= \frac{X}{X+Y+Z} \\ y &= \frac{Y}{X+Y+Z} \\ z &= \frac{Z}{X+Y+Z}, \end{aligned} \tag{2.5}$$

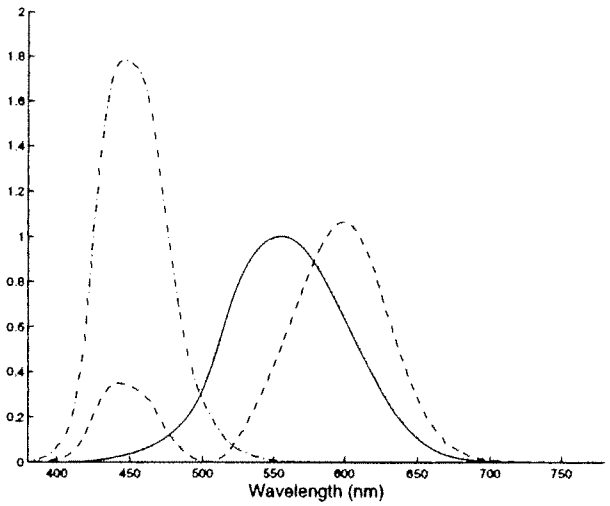

Figure 2.2: CIE 1931 color-matching functions $\bar{x}$ (dashed curve), $\bar{y}$ (solid curve) and $\bar{z}$ (dash-dotted curve).

where $x+y+z=1$. The CIE 1931 chromaticity diagram represents the two-dimensional color space of the x and y coordinates. In this model the disadvantage is that the visual color differences are not equal in all parts of the diagram. CIE has defined more uniform color coordinate systems to avoid the nonuniformity of the color differences. One system proposed is the CIELAB system, which is also called the CIE 1976 $L^*a^*b^*$ system. CIE 1976 $L^*a^*b^*$ color coordinates are defined as follows

$$\begin{aligned} L^* &= 116\,(Y/Y_o)^{1/3} - 16 \\ a^* &= 500\,[(X/X_o)^{1/3} - (Y/Y_o)^{1/3}] \\ b^* &= 200\,[(Y/Y_o)^{1/3} - (Z/Z_o)^{1/3}]\,, \end{aligned} \tag{2.6}$$

where X_o, Y_o, and Z_o are the X, Y, and Z coordinates of the reference white. The color coordinates in Eq. (2.6) are valid if the ratios X/X_o, Y/Y_o, and Z/Z_o are larger than 0.008856. If Y/Y_o is equal or less than 0.008856, then L^* is defined as $L^* = 903.3(Y/Y_o)$. If any of the ratios X/X_o, Y/Y_o, or Z/Z_o for a^* and b^* is equal or less than 0.008856, then it is replaced by $7.787F + 16/116$, where F is X/X_o, Y/Y_o, or Z/Z_o.

The color difference ΔE^* between two colors in $L^*a^*b^*$ color coordinate system is defined as

$$\Delta E^* = \sqrt{\Delta L^{*2} + \Delta a^{*2} + \Delta b^{*2}}. \tag{2.7}$$

A detailed description of the three-dimensional color coordinate systems can be found in Refs. [39, 50, 107].

2.2 Spectral based representation of color

Basing on the physical approach, the highest accuracy of the color representation can be obtained by representing the color as a measured color spectrum. The color spectrum can be measured, for example, by a spectrophotometer, by an acousto-optic tunable filter (AOTF) [24, 25], by a radiometer [45], or by a CCD camera with a set of narrow band interference filters [52]. Figure 2.3 shows an example of the color reflectance spectrum (solid line) measured by the spectrophotometer from an orange color plate. The spectrum is sampled at the wavelength range from 400nm to 700nm at 5nm intervals and it contains 61 components. Figure 2.3 shows also a metameric spectrum (dash-dotted line) for the orange color spectrum. The metameric spectrum for the real spectrum was generated computationally. The (X, Y, Z) tristimulus values for this metameric pair of color spectra are equal under the CIE standard illumination D_{65}. Therefore, the RGB color coordinates calculated from the (X, Y, Z) for these spectra are equal under the illumination D_{65}, but, for example, under the illumination A, the RGB color coordinates for these spectra are different. Table 2.1 shows the RGB color coordinates for these two spectra.

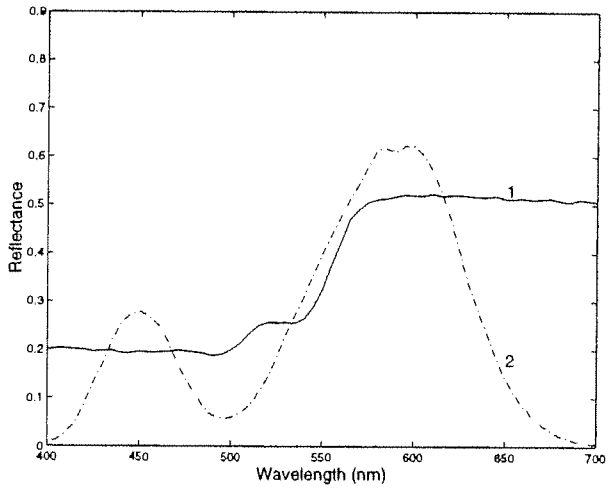

Figure 2.3: Example of metameric pair of color spectra.

Table 2.1: RGB color coordinates for the metameric pair of spectra. The Spectrum 1 and Spectrum 2 correspond to the spectra marked as 1 and 2 in Figure 2.3, respectively.

Illumination	CIE D_{65}		CIE A	
	Spectrum 1	Spectrum 2	Spectrum 1	Spectrum 2
R	51.82	51.82	83.39	76.18
G	34.86	34.86	33.33	34.93
B	21.32	21.32	6.83	6.46

From the computational analysis point of view, the effective analysis of a large amount of high-dimensional spectra can be too restricted. Usually, the shape of the color spectrum is smooth and the spectra strongly correlate with each other. It has been shown that the spectral data can be represented accurately by the linear combination of a few basis spectra, *i.e.* basis vectors [9, 15, 22, 44, 48, 60, 61, 76, 77, 106, 108]. Recently, the linear models for the infrared spectra and for the outdoor illumination spectra have been published [36, 93]. Usually these linear models are based on the use of the principal component analysis (PCA) for defining the basis vectors.

Parkkinen *et al.* [77] showed that a large spectral database can be described accurately by a few basis vectors calculated by the subspace method [68], which is based on the Karhunen-Loève expansion. In Ref. [77] the spectral database measured from the *Munsell Book of Color* [66] containing 1257 color spectra was described accurately from 3 to 8 basis vectors. This basis can be also used to represent natural colors with a sufficient accuracy [44]. In this thesis, some of the results are compared with the results obtained by the subspace method and therefore the subspace method is briefly reviewed next.

To compute the basis vectors for the color spectra, the correlation matrix R of the spectra set is used:

$$R = \sum_{i=1}^{N} \tau_i(\lambda)\tau_i(\lambda)^T, \tag{2.8}$$

where the index i means ith spectrum in the set of N measured spectra. The eigenvectors ϕ are the solutions of the equation

$$R\phi = \sigma\phi, \tag{2.9}$$

where σ are the eigenvalues of R. From the columns of the matrix ϕ, the first p eigenvectors, corresponding to the p largest eigenvalues, form a basis B for the subspace of dimension p. Figure 2.4 shows the basis vector set of 8 vectors for the Munsell spectral database containing 1269 color spectra sampled from 400nm to 700nm at 5nm intervals. These basis vectors contain 99.99% of the total variance of the database. A reconstruction τ' of the original spectrum τ can be obtained by the linear combination of the basis vectors

$$\tau' = BB^T\tau, \tag{2.10}$$

where the columns of matrix B are the basis vectors. See Refs. [56] and [77] for the detailed analysis of the basis vectors for the Munsell spectral database.

By the use of subspace method it is possible to compress a large amount of spectral data. The subspace method can be also used in spectral classification where the subspaces can be trained to represent the spectral classes. In Chapter 4 of this thesis, the Averaged Learning Subspace Method (ALSM) of Oja [68] is used to classify color spectra. In Ref. [63] the self-organizing PCA was used to simulate color-vision deficiency and white-light adaptation characteristics. The basis vectors of the subspace method have been implemented optically for measuring color spectra [34] and for classifying color spectra [46].

Two-dimensional spectral images, in which every pixel contains a color spectrum, can be measured, for example, by a CCD-camera with narrow band interference filters [2, 52, 78] or broad band filters [32, 65], by AOTF [24, 25], by Fourier-transform based methods [43], or by the line scanning based spectral cameras [40]. In this thesis the

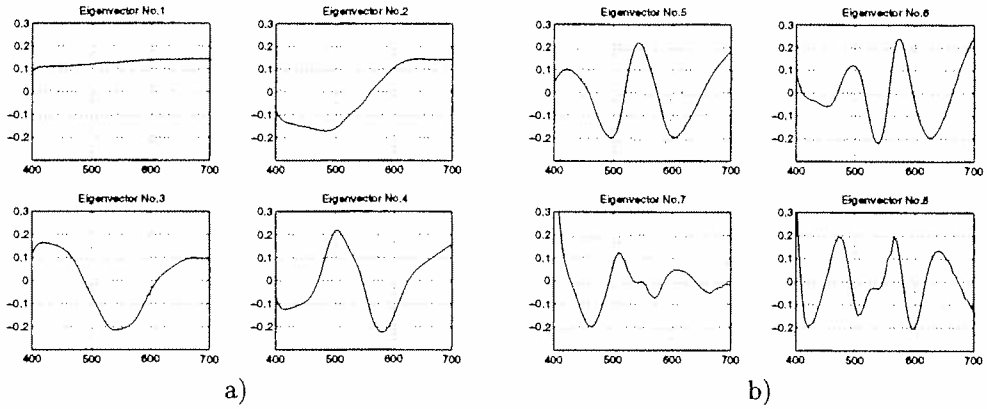

Figure 2.4: Eigenvectors of the subspace method a) No.1-4, b) No.5-8.

color is mainly represented using the spectral information of the spectral images as such, without calculating the three-dimensional color coordinates. Figure 2.5 shows an example of the spectral image.

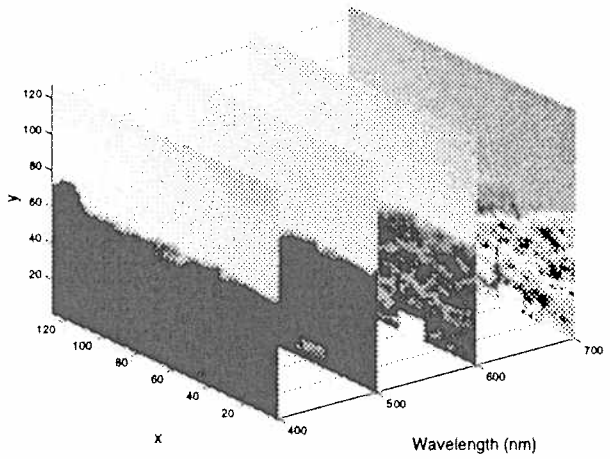

Figure 2.5: Example of the spectral image measured at the wavelength range from 400nm to 700nm at 10 nm intervals [78]. Wavelength bands 400nm, 500nm, 600nm and 700nm are shown.

2.3 Spectral databases used in this thesis

In this work we mainly experimented with commonly available spectral databases. During this work, there were only a few spectral databases and spectral images containing

more than 30 channels commonly available. In *publication 5* the author of this thesis measured all color spectra and spectral images. The following spectral databases were used:

1. In *publication 1* the spectral database measured by the radiometer from the canopy of growing trees (Scots pine, Norway spruce, and birch) [45] was used. The spectral database was measured at the Väisälä laboratory, University of Joensuu, Finland, by Dr. Raimo Silvennoinen. Database contains 1056 spectra measured at the wavelength range from 390nm to 850nm at 5nm intervals and it is available at the www-server of the Lappeenranta University of Technology, Finland, http://www.it.lut.fi/research/color/lutcs_database.html.
2. In *publication 2* the spectral image database of Parraga *et al.* [78] was used. The database consists of 29 spectral images measured from the natural scenes by a CCD-camera with 31 narrow band interference filters at the wavelength range from 400nm to 700nm at 10nm intervals. Each spectral image contains a total of 31 monochrome 256 × 256 pixels images as 8bits/pixel format. The database and a more detailed description are available at the www-server http://www.crs4.it/~gjb/ftpJOSAtab.html.
3. In *publication 3* the spectral database measured from the Natural Color System (NCS) [30] containing 1513 spectra was used. The spectra were measured at the wavelength range from 380nm to 780nm at 5nm intervals. Database was obtained from the Scandinavian Color Institute in Stockholm, Sweden, by courtesy of Professor Björn Kruse, Linköping University, Sweden.
4. In *publications 3, 4,* and *5* the spectral database measured by the spectrophotometer of 1269 color chips from the *Munsell Book of Color* [66] was used. Database was measured at the Väisälä laboratory, University of Joensuu, Finland, by Mr. Jouni Hiltunen. The spectra was measured at the wavelength range from 380nm to 800nm at 1nm intervals. The spectral database is available at the www-server of the Lappeenranta University of Technology, Finland, http://www.it.lut.fi/research/color/lutcs_database.html.

CHAPTER III

Texture Representation

3.1 Gray level texture

Texture is a property of a surface. In natural environment the objects like wood, grass, sand, rock, textile, and skin contain textured regions. In digital images, the texture is a context dependent feature, *i.e.* texture can not be defined for a pixel, but for a small region in the image. A well-known texture database of gray level images is the Brodatz album [5].

Methods for gray level texture analysis have been widely studied over the last three decades. Texture is hard to define and there are several methods and different approaches for texture analysis in digital image analysis. Usually these methods are based on the use of statistical approaches [47]. Typical features used in the statistical texture analysis are based on the gray level cooccurrence matrices, gray level difference matrices, run length matrices [21], Fourier power spectra, auto-correlation functions, and random-field models [28, 47]. Comparative studies of the gray level texture features can be found *e.g.* in Refs. [67] and [73].

One of the most successful texture analysis method is based on the second-order statistics of texture and is represented as a gray level cooccurrence matrix of Haralick *et al.* [29]. Cooccurrence is defined as a joint distribution of gray levels of two pixels separated by a given displacement $(\Delta x, \Delta y)$. The gray level cooccurrence matrix P is defined as

$$P(i,j) = \{\#\text{pair}(i,j) | \text{image}(x,y) = i \wedge \text{image}(x+\Delta x, y+\Delta y) = j\}, \qquad (3.1)$$

where i, j are gray levels. The cooccurrence matrix is calculated by the following algorithm. The time complexity for the Algorithm 3.1 is $O(n)$, where n is the number of locations $\approx$ the number of pixels in an image.

Algorithm 3.1: Gray level cooccurrence matrix.

begin
  forall gray levels $i, j \in$ image
    $P(i,j) = 0$;
  endfor
  forall locations $(x,y) \in$ image and $(x+\Delta x, y+\Delta y) \in$ image
    $i =$ image(x,y);
    $j =$ image$(x+\Delta x, y+\Delta y)$;
    $P(i,j) = P(i,j) + 1$;
  endfor
end

Haralick *et al.* [29] described fourteen features extracted from the cooccurrence matrix. Usually only a few of them are used and in this study the following five of them were used:

$$\begin{aligned}
\text{Energy} &= \sum_i \sum_j P^2(i,j) \\
\text{Entropy} &= -\sum_i \sum_j P(i,j) \log P(i,j) \\
\text{Contrast} &= \sum_i \sum_j (i-j)^2 P(i,j) \\
\text{Correlation} &= \sum_i \sum_j \frac{1}{\sigma_x \sigma_y}(i-\mu_x)(j-\mu_y)P(i,j) \\
\text{Homogeneity} &= \sum_i \sum_j \frac{P(i,j)}{1+|i-j|},
\end{aligned} \tag{3.2}$$

where μ_x, μ_y, σ_x, and σ_y are the means and standard deviations of summing the rows and columns of P, respectively.

The cooccurrence matrix can be computed with different displacements which can be represented as a pair $(\Delta x, \Delta y)$ in cartesian coordinates or (d, β) in polar coordinates. The directions with angles $\beta = 0°$, $45°$, $90°$, $135°$ of the horizontal axis are usually used and the features of these matrices can be combined for the classification process. The best displacement for the cooccurrence matrix calculation can be approximated by analyzing the periodicity of the texture. In Ref. [71] the χ^2 and κ statistics were compared and it was shown that κ statistics was a better choice for choosing the best displacement for the cooccurrence matrix calculation.

Oja and Valkealahti [72] have proposed a method for quantizing the multidimensional texture histograms by the Self-Organizing Map (SOM) of Kohonen [54]. In Ref. [72] the reduced multidimensional histograms of the cooccurrence matrices were directly used for the classification of gray level and color textures. Recently, Valkealahti and Oja [101] speeded up the method proposed in [72] and published high classification accuracies for the gray level Brodatz textures. Also in Ref. [70] the cooccurrence matrix itself was used as a feature without calculating any features from it. Allam *et al.* [1] used the orthonormal decomposition of the cooccurrence matrix as a texture feature. The

methods of statistical pattern recognition and neural networks have been widely used for classifying the texture features [67, 70, 73, 79, 88].

3.2 Color texture

Methods developed for texture analysis have been proposed to represent the spatial aspect of the texture, but the color aspect in textures has not received as much attention. When color textures are considered, both the texture and color must be analyzed. Two color textures may have the same color and different structure, or different color and same structure, or different color and different structure [89].

The color texture analysis based on the three-dimensional color representation has been under a growing interest recently. Tan and Kittler [94, 95, 96] have proposed supervised color texture analysis methods which use the Discrete Cosine Transform (DCT) features extracted from the color textures. In Ref. [94] eight DCT texture features were extracted from each of the three RGB color bands for classifying color textures. In Ref. [95] eight DCT texture features were computed only for the intensity image and they were augmented by six color features derived from the color histogram. Messer and Kittler [64] have compared the statistical and neural network based methods in color texture analysis. The results of using color codebooks [89], Markov models [75], and spatial correlation functions [37, 55] for modeling color textures have been published. The color texture segmentation methods have been proposed *e.g.* in Refs. [75] and [90]. Recently, Saber and Tekalp [87] proposed an integration of the color and texture features for content-based image retrieval from the color image databases.

In this thesis, the main interest is in the spectral images which contain more than 30 spectral channels at the wavelength range from 400nm to 700nm. In our approach, we are interested in the high accuracy of the spectral information over the wavelength axis. For this reason, we don't compress the number of channels in the measured spectral images or calculate the three-dimensional color representations for them. Some of the color texture analysis methods described in the previous paragraph can be adapted successfully to spectral images, but in that case the methods will be computationally too restricted. For example, the color histogram calculations for the high-dimensional spectral data will be computationally too demanding for the machine vision applications. In this thesis, the aim is to propose a method which uses the spectral information of the measurement as such, but the number of spectra in a spectral image is quantized. This idea was also motivated by the spectral imaging system, which we recently developed in *publication 5*. The multispectral texture analysis method described in the next chapter can be partly implemented optically using the spectral vision system which provides an advantage of the parallel image processing. Figure 3.1 shows an example of the color texture used in the experiments of *publication 2*.

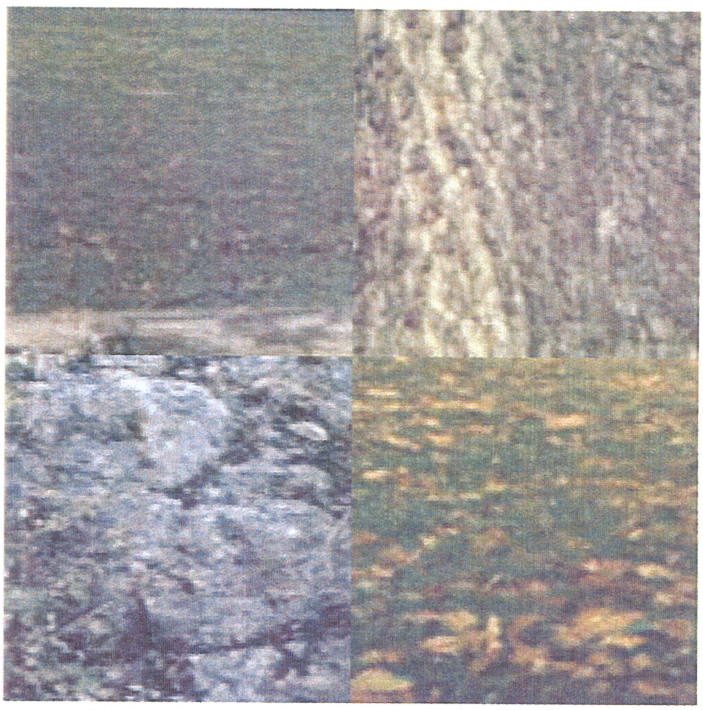

Figure 3.1: Example of the color texture.

CHAPTER IV

Multispectral Texture

Multispectral textures contain the spectral and spatial domains [83]. An important question related to human vision system is that should the spectral and spatial domains be analyzed simultaneously or separately. In this thesis we are not trying to explain the connection to the human visual system, but we are going to propose a computational model for multispectral texture representation.

Many texture analysis methods proposed for the gray level textures are based on the natural lightness based ordering of the gray levels. The color texture analysis based on the three-dimensional color representation is also usually done by analyzing the component images separately, for example in the case of RGB color textures, the color channels R, G, and B are processed separately by the gray level texture analysis methods. However, in the case of multispectral images, the number of spectral channels is large and therefore the analysis based on the separate analysis of each channel is computationally difficult. In the remote sensing, the common way is to classify the spectral domain [7, 16] and in the spatial domain, the texture features are calculated from a few selected bands or channels in an image [3, 8, 80]. In this thesis the aim is to propose a computationally effective method which uses the spectral and spatial information of all bands in a multispectral image.

In the case of multispectral images, the pixel values are color spectra (*i.e.* vectors), and there is no natural order for them. The generalization of the gray level texture analysis methods for the multispectral images is therefore not always straightforward. Mathematically, one moves from scalar values into a multidimensional vector space, where the order of the vectors is not uniquely defined [10, 58].

The number of high-dimensional spectra in a spectral image is large and it is computationally difficult to analyze the whole spectra as such. Therefore we reduce the spectral information in an image into a lower number of spectra. In the proposed method, a two-phase process is used: first, the spectral domain is quantized and labeled according to the quantized spectra. Then, the spatial domain is represented by the joint distribution of the spectral classes in the spectral domain. The joint distribution is represented as a cooccurrence matrix which is a generalization of the gray level cooccurrence matrix of Haralick. In this thesis it is also called as a spectral cooccurrence matrix. Chang and Wang [6] have used the color cooccurrence matrix based method to analyze three-

dimensional color textures. In their method they first quantized the color in an image, labeled the color domain according to the quantized spectra, and then used the cooccurrence matrix based method for the labeled image.

4.1 Quantization of the spectral domain

In our method we first quantize the spectral domain of the multispectral images. In the quantization, two methods, supervised and unsupervised, are used: the Averaged Learning Subspace Method (ALSM) of Oja [68] and the Self-Organizing Map (SOM) of Kohonen [54]. In the case of ALSM the spectral subspaces are first trained with known classification. Then the spectral domain is classified into spectral subspaces according to the projection criterion. In the case of SOM the spectral domain is first clustered into spectral clusters and then the spectral domain is classified into these clusters according to the shortest distance. Next the ALSM and SOM are briefly reviewed.

Averaged Learning Subspace Method (ALSM)

As discussed in Chapter 2, the principal component analysis (PCA) based methods have been shown to be powerful statistical techniques for reducing the dimensionality of the spectral data. One group of the PCA based classification methods are the learning subspace methods which are especially suitable for classifying the spectral type data [68].

The classification procedure can be performed as follows. First, the color spectra from the set of colors with known classification are measured. Then, the subspaces for each class are formed. The eigenvectors ϕ corresponding to the first p largest eigenvalues are chosen as a basis for the color subspaces representing each class ω. The equations for forming the subspaces are given in Chapter 2.

In the initialization phase of the ALSM the learning set is classified to color subspaces according to the projection criterion. Note that in this phase the initial correlation matrices R were formed by using Eq. (2.8) and in the following equation the matrices $C_1^{(i)}$ are equal to the correlation matrices R in the first iteration step $m = 1$. If there are misclassifications, then in the next iteration the subspaces are rotated by changing the matrices $C_m^{(i)}$ as follows:

$$C_m^{(i)} = C_{m-1}^{(i)} + \sum_{j \neq i} a K_m^{(i,j)} - \sum_{j \neq i} b K_m^{(j,i)}, \tag{4.1}$$

where $C_{m-1}^{(i)}$ is the matrix of a class $\omega^{(i)}$ at iteration $(m-1)$, and a and b are small numbers defining the weighting for misclassification. $K_m^{(i,j)}$ is a conditional correlation matrix formed by the pattern vectors that belong to class $\omega^{(i)}$, but have been classified at iteration m to class $\omega^{(j)}$. Learning process continues until the results are correct or stable.

After learning, the spectral domain of the multispectral image is classified to the spectral classes using a projection criterion

$$\begin{aligned} &x \text{ belongs to class } \omega^{(i)}, \\ &\text{if } \textstyle\sum_{s=1}^{p} (x^T \phi_s^{(i)})^2 > \sum_{s=1}^{p} (x^T \phi_s^{(j)})^2, \forall\, i \neq j, \end{aligned} \tag{4.2}$$

where the spectrum τ is classified to class where its projection is longest. The spectral image is finally labeled according to the spectral class numbers. The algorithm for the ALSM is given as follows.

Algorithm 4.1: Averaged Learning Subspace Method.

begin
  k = number of classes;
  set iteration parameter $m = 1$;
  compute correlation matrices $C_m^{(1)}, \ldots, C_m^{(k)}$;
  form initial subspaces with dimensions p;
  repeat
    $m = m + 1$;
    forall $\tau \in$ training set
      classify τ according to Eq. (4.2);
        if τ is misclassified **then**
          update matrices $K_m^{(i,j)}$ and $K_m^{(j,i)}$;
    endfor
    for $i = 1$ **to** k **do**
      update matrices $C_m^{(i)}$ according to Eq. (4.1);
      form new subspaces with dimensions p;
    endfor
  until classification is correct or stable
end

Self-Organizing Map (SOM)

The self-organizing maps are based on unsupervised competitive learning which can be used to cluster the input data [54]. In this thesis the one-dimensional SOM is used. By the use of SOM the spectral domain of the spectral images is clustered, and after learning, the weight vectors of the SOM are used as characteristics vectors for the spectral clusters.

First, the input data is normalized to unit norm and the map is initialized by the center vector of the input data. At each iteration of the unsupervised learning, the weight vector m_c, which has the closest Euclidean distance to the randomly selected input vector x, is chosen as the winner neuron

$$\|x - m_c\| = \min_i \{\|x - m_i\|\}, \tag{4.3}$$

where i is the index of the weight vectors. The winner m_c is also called as the Best-Matching Unit (BMU) [54]. The updating process of the weights including the winner m_c and its topological neighborhood N_c is defined as follows [54]

$$m_i(t+1) = \begin{cases} m_i(t) + \alpha(t)[x(t) - m_i(t)] & , \text{if } i \in N_c(t) \\ m_i(t) & , \text{otherwise,} \end{cases} \tag{4.4}$$

where t is the iteration parameter and $\alpha(t)$ is a learning rate, $0 \leq \alpha(t) \leq 1$. The learning rate decreases exponentially during the learning. Also the size of the neighborhood N_c

decreases during the learning. The following algorithm shows the steps for the self-organizing learning.

Algorithm 4.2: Self-Organizing Map.

begin
  e = number of iterations;
  normalize the input data to unit norm;
  initialize the SOM by the center vector of the input data;
  for $t = 1$ **to** e **do**
    take randomly vector x from the input data;
    find the BMU m_c for x by Eq. (4.3);
    update the weights m_i by Eq. (4.4);
    decrease the learning rate α and the size of neighborhood N_c;
  endfor
end

The result of the self-organizing process is a map where the weight vectors m are adapted towards the characteristics vectors of the spectral clusters in the spectral domain. After learning the spectral domain is classified and labeled by the use of the self-organized map by finding the Best-Matching Unit from the map for each spectrum in the spectral domain. Figure 4.1 shows the self-organized maps computed in *publication 2*. The one-dimensional map with 10 weight vectors in Figure 4.1 a) was formed for the 30720 training spectra extracted from the spectral images. In Figure 4.1 b) the map was formed for the 30720 RGB vectors extracted from the corresponding RGB images at the same pixel locations as the spectral data.

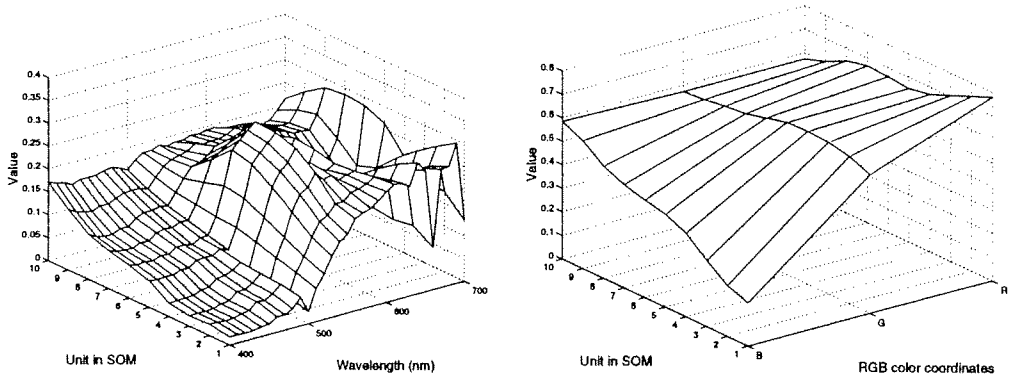

a) b)

Figure 4.1: Self-organized maps for the a) spectral data and b) RGB data extracted from the same locations at the spectral and RGB images.

4.2 Multispectral texture representation

After the spectral quantization the spectral domain was labeled according to the quantized spectra. Now each pixel in a quantized image represents a spectral class or a spectral cluster of the spectral domain. For the labeled image we use the gray level cooccurrence matrix based method which is generalized for spectral images. The idea is that we use the labeled image obtained from the spectral quantization process and define the cooccurrence as a joint distribution of spectral classes. The spectral cooccurrence matrix $P(i,j)$ is defined as follows:

$$P(i,j) = \{\#\text{pair}(p,q) | p(x,y) \in i \wedge q(x+\Delta x, y+\Delta y) \in j\}, \tag{4.5}$$

where i and j are spectral classes for the spectra p and q, associated with the pixels at the points (x,y) and $(x+\Delta x, y+\Delta y)$, respectively. The algorithm for calculating the spectral cooccurrence matrix is as follows.

Algorithm 4.3: Spectral cooccurrence matrix.

begin
  Q = quantized spectra by ALSM or SOM;
  forall locations $(x,y) \in$ image
    label the image according to the quantized spectra;
  endfor
  forall classes $i,j \in$ labeled image
    $P(i,j) = 0$;
  endfor
  forall locations $(x,y) \in$ image and $(x+\Delta x, y+\Delta y) \in$ image
    i = class for spectrum $p(x,y)$;
    j = class for spectrum $q(x+\Delta x, y+\Delta y)$;
    $P(i,j) = P(i,j) + 1$;
  endfor
end

Before the spectral cooccurrence matrix method in Algorithm 4.3 is applied, the spectra is quantized by the ALSM or SOM. This quantization can be time consuming, depending on the learning iterations needed in the learning process. However, after learning, the spectral classes learned by the sufficient learning data can be used to represent also the spectra which were not included in the learning data. Therefore, the spectral classes are trained for the specific application only once. The labeling of the image depends on the number of pixels and the number of spectral classes in an image. In the experiments of this thesis, the maximum of 10 spectral classes were used and therefore the number of comparisons in finding the best-matching class for spectra is small. Thus the time complexity for the labeling process is $O(n)$ where n is the number of pixels in the image. The time complexity for the latter part of the Algorithm 4.3 is the same as for the gray level cooccurrence matrix in Algorithm 3.1, $O(n)$. The total time complexity for the spectral cooccurrence matrix, excluding the spectral quantization, is $O(2n)$ and it belongs to the complexity class $O(n)$.

One problem in this method is to define the spectral classes properly. If we are comparing a fixed set of textures with each other, then the order of the spectral classes, computed for

the fixed texture set is enough. However, if the cooccurrence matrices shall be uniquely constructed, then the global, unique order for the spectral classes should be found. The meaning of Haralick features in Eq. (3.2) for the spectral cooccurrence matrix can be different to those calculated for the gray level cooccurrence matrix. Depending on the defined order of the spectral classes, it is possible that the spectra pair close to each other can be classified to classes far from each other. In this case the spectral cooccurrence matrix is quite different compared to the gray level cooccurrence matrix. The most critical features are the location dependent features: contrast, correlation, and homogeneity. However, the spectral quantization done by SOM can be a promising approach for the natural order of the spectral data.

After the construction of the spectral cooccurrence matrix and the feature calculation, a well-known classifiers can be used to classify multispectral textures. In *publication 1* and *publication 2* this method was applied to multispectral texture segmentation. The feature vectors calculated from the spectral cooccurrence matrices were classified by the k-nearest neighbor (k-NN) classifier [88] and by the multilayer perceptron (MLP) neural network [86]. In *publication 2* the spectral cooccurrence matrix itself was used as a feature by stacking it row by row into a vector. In this case the ordering of the spectral classes does not have so critical meaning when compared to Haralick's feature calculation. Figure 4.2 shows a schematic drawing including the steps of the proposed multispectral texture analysis method.

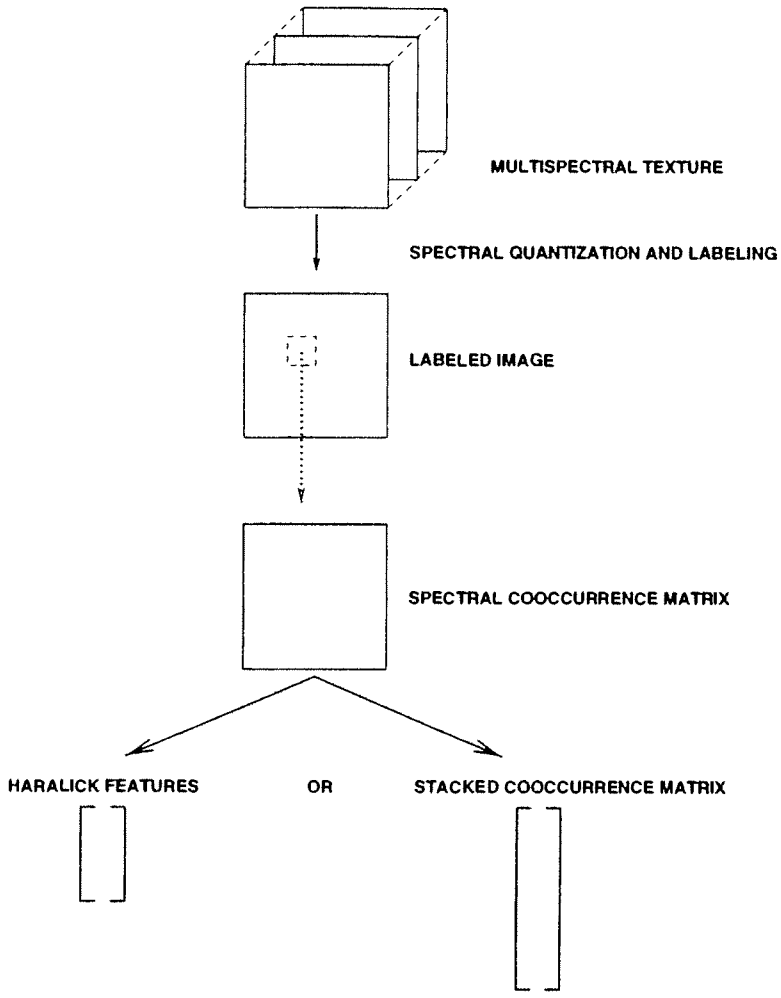

Figure 4.2: Schematic drawing of the multispectral texture representation.

CHAPTER V

Illumination Estimation

It was discussed in Chapter 2 that the measured spectral radiation τ is effected by the relative spectral power distribution $E(\lambda)$ of the illuminant. The measured spectral images are usually post-processed to eliminate the effect of the used illumination during the measurement. This can be done, for example, by measuring the spectrum of a standard reference white under the same illumination as used in the image measurement and then dividing the image data by the spectrum of the reference white. The result of this is object's spectrum $S(\lambda)$, which is derived from the equation $\tau(\lambda) = S(\lambda)E(\lambda)$.

However, it is also possible that only the measurements τ are available. If the same object with spectra $S(\lambda)$ is measured under a different illuminations, then the measured spectral images will be different, even if the same object is examined. In this case the machine vision system based recognition procedure usually treats the objects as different objects and therefore the recognition will fail.

The problem described above is under a great deal of attention in the color image analysis based on the three-dimensional color representations. In controlled laboratory experiments, by the use of standard light sources with known illumination spectra, it is possible to recognize the color of an object under different illuminations. However, in most real world applications only the digital RGB color image information is available. In this case the illumination changes can cause serious problems in machine vision based color image recognition. This phenomenon is known as the problem of color constancy.

5.1 Color constancy

In Ref. [39] Hunt defines the color constancy as follows: *The color constancy is an effect of visual adaptation whereby the appearance of colors remains approximately constant when the level and color of the illuminant are changed.* The human visual system can successfully compensate changes in the intensity, hue, and saturation and therefore the object's color tends to be interpreted as constant under changing illumination conditions. Color constancy has been widely studied in the field of color analysis [4, 13, 14, 15, 17, 18, 19, 20, 38, 109], but in the real world applications a satisfactory solution for the machine vision based color constancy is still an open question.

Color constancy deals with separating the influence of the illumination and the spectral characteristics of the object. In previous studies of color constancy the colors are usually represented in the three-dimensional color coordinate systems, in which the transformation induced by the changing illumination can be sometimes quite complicated. In this thesis a spectral based illumination estimation procedure is proposed.

5.2 Estimating the illumination spectrum

In *publication 3* we developed a spectral based illumination estimation method. The proposed method can be used to estimate the illumination from the three-dimensional color images and from the multispectral images. Possible applications of the method are, for example, color image normalization and color based search in color image databases.

First, we assume that all possible colors in a color image are described by a set of a large database of color spectra. For this purpose we use the Munsell spectral database and the spectral database measured from the NCS-system [30], which are described more detailed in Chapter 2, section 2.3. These high-resolution reflectance spectra measured from the color chips were combined into a spectral database containing 2782 spectra sampled from 400nm to 700nm at 5nm intervals. This spectral database can be represented accurately by a few basis vectors from the Karhunen-Loève expansion based subspace method. In *publication 3* we showed that also the logarithmic spectral database can be described accurately by a few basis vectors calculated from the logarithmic spectral database. The spectral based illumination estimation can be described as follows.

The measured color spectrum τ in a pixel x is defined as

$$\tau(\lambda, x) = S(\lambda, x)E(\lambda), \tag{5.1}$$

where the illumination $E(\lambda)$ is assumed to be uniform across the investigated part of the image. By taking the logarithms and defining them as $\log(\tau(\lambda, x)) = m(\lambda, x)$, $\log(S(\lambda, x)) = s(\lambda, x)$, and $\log(E(\lambda)) = l(\lambda)$, the linear relation

$$m(\lambda, x) = s(\lambda, x) + l(\lambda) \tag{5.2}$$

is obtained. If the k-th eigenvector of the logarithmic spectral database is $b_k(\lambda)$, then the functions m, s and l can be written as expansions

$$m(\lambda, x) = \sum_k \mu_k(x) b_k(\lambda), \quad s(\lambda, x) = \sum_k \rho_k(x) b_k(\lambda), \quad l(\lambda) = \sum_k \alpha_k b_k(\lambda). \tag{5.3}$$

Thus, for a given k we obtain

$$\mu_k(x) = \rho_k(x) + \alpha_k, \tag{5.4}$$

where the effect of an illuminant is a location independent, constant shift. If only the measured spectra $\tau(\lambda, x)$ are available, then only the coefficients $\mu_k(x)$ are known, whereas the reflection coefficients $\rho_k(x)$ for the object's spectra $S(\lambda, x)$, and the constants α_k for the illumination $E(\lambda)$ are unknown.

We already assumed that all possible colors in a color image are described in a spectral database. By using this we also assume that the distribution of the reflection coefficients

$\rho_k(x)$ has the same statistical characteristics as the coefficients computed from the spectral database. Under this assumption the global shift parameters α_k can be estimated by comparing the two probability distributions of the measured spectral image and the spectral database. In *publication 3* the probability distributions were described by their modes, *i.e.* the most probable value. Mode is a robust location estimator, which we use to extract the center of the probability distributions [84]. From the modes for the distributions of the measurement coefficients μ_k and the modes computed for the spectral database coefficients ρ_k, the values for the global shift parameters α_k can be computed. From these α_k, the spectrum for the illuminant $E(\lambda)$ can be derived by exponentiation of the linear combination of the logarithmic basis vectors. The following is the algorithm for this procedure.

Algorithm 5.1: Spectral based illumination estimation.

begin
V = logarithm of the combined Munsell and NCS spectral database;
b_k = eigenvectors of the N-dimensional subspace for V;
ρ_k = coefficients for the eigenvectors b_k;
compute the modes for distribution ρ_k;
X = a small number of random locations from the spectral image;
forall locations $x \in X$
$m(\lambda, x)$ = logarithm of the spectrum $\tau(\lambda, x)$;
$\mu_k(x)$ = coefficients for $m(\lambda, x)$;
endfor
compute the modes for distribution μ_k;
α_k = difference between the modes for μ_k and ρ_k;
illumination spectrum $E(\lambda) = e^{\sum_{k=1}^{N} \alpha_k b_k}$;
end

The time complexity for the Algorithm 5.1 depends mostly on the number of randomly chosen locations x and therefore the time complexity of it belongs to class $O(n)$, where n is a small number of chosen locations. The more detailed description of this method can be found in *publication 3*. This method can be also used for the color images based on the three-dimensional color coordinate systems, for example for RGB images. In this case the RGB image must be first converted to spectral image. This conversion is an ill-defined problem since many different spectra may be mapped to the same three-dimensional color coordinate vector. This phenomenon is known as metamerism, which was discussed in Chapter 2. In *publication 3* the RGB image was converted to a spectral image using a color lookup-table technique based on the spectra from the database.

The shift parameters α_k characterize the global color distribution in an image and therefore it can be used in color image retrieval applications. By the use of α_k the color images can be normalized and the illumination spectrum can be estimated. The experimental results can be found in *publication 3*.

CHAPTER VI

Spectral Vision System

In the current machine vision applications, there are two basic approaches to measure two-dimensional spectral images. One approach is to acquire a two-dimensional image at different wavelengths at different times. Another approach is to acquire a line image with simultaneous measurement of spectra at different wavelengths, and by scanning the camera or an object along the spatial axis to acquire the two-dimensional spectral image. Table 6.1 shows examples of existing spectral imaging systems, which are categorized into dispersive and spectral sampling methods.

Table 6.1: Examples of existing spectral imaging systems.

Dispersive	Spectral sampling
Prism	Narrow band interference filters
Grating	Broad band filters
	Linear varible filter
Acousto-optic tunable filter (AOTF)	

The spectral imaging systems based on the spectral sampling are mostly based on the use of a CCD-camera with a set of narrow band interference filters and broad band filters [32, 65]. The narrow band interference filters can be placed on a rotating filter wheel in the front of CCD-camera [2]. The number of interference filters is usually more than 30 and the transmittance of them is fixed. Also the use of electronically controlled optical filters, for example, the acousto-optic tunable filter (AOTF) [24, 25] and liquid crystal spatial light modulator (LCSLM) [46], belong to this category. The acquisition times of the spectral images depends mostly on the setup time of the optical filter. For example, in the case of narrow band interference filters the acquisition time can be several minutes. In general these devices are suitable for static objects. An advantage is that the spatial domain of the spectral images is acquired accurately for each wavelength band. Another approach is based on the simultaneous measurement of the spectrum along the wavelength axis, but scanning is needed along the spatial axis. In Ref. [40] the dispersive prism-grating-prism (PGP) based add-on component for the CCD-camera

was proposed. This device is especially suitable for industrial applications, in which the moving objects are examined. There are also other techniques for acquiring spectral images, for example, the Fourier transform based interferometric spectral imaging [43]. A comprehensive review of the spectral imaging systems can be found in Ref. [43] by Itoh.

Most of the present spectral imaging systems produce a large amount of data to be stored or transmitted. The compression of the high-dimensional spectral data is important to make the storing and transmission convenient. There are two approaches to compress spectral images:

- to have the measured spectra and compress them by software [49, 100],
- to design the spectral imaging system so that we already acquire the low-dimensional component images for the spectral reconstruction [98].

In this thesis the main interest is in the low-dimensional spectral imaging systems. The purpose of the low-dimensional spectral imaging system is to acquire the optimal component images for the spectral reconstruction by the use of a few optical color filters. This can be done

- by filtering the reflecting or transmitting light from an object by color filters [65, 98] or
- by illuminating an object by the light, which has the spectral characteristics of the color filter.

In the both methods above, the component images can be detected by the monochrome CCD camera. The detected intensity image corresponds to the optically calculated inner product between the sample's spectra and color filter. From these inner products the spectra of the sample can be reconstructed by the use of a pseudoinverse matrix. Tominaga [98] proposed a multispectral imaging system based on the use of a CCD camera with 6 color filters. The color filters used in Ref. [98] were Kodak Wratten gelatin filters with a fixed transmittance. In this thesis the aim is to propose a spectral vision system, in which the transmittance of the optical color filters can be changed arbitrarily, according to the filter set needed in each application.

In Chapter 2 it was discussed that a large Munsell spectral database can be represented accurately by a few basis vectors calculated by the Karhunen-Lòeve expansion based subspace method. The basis vector set for the Munsell spectra can also represent natural colors with a sufficient accuracy [44]. Jaaskelainen *et al.* [46] implemented the learning subspace method optically. In Ref. [46] the liquid crystal spatial light modulator (LC-SLM) was used to implement the color filters corresponding to the basis vectors of the subspace method. Hayasaka *et al.* [34] developed the optical system described in [46] to analyze two-dimensional microscopic images.

The basis vector set produced by the subspace method is orthogonal and it usually contains negative coefficients, which cannot be directly implemented optically. In Refs. [34] and [46] the basis vector set produced by the subspace method was biased and multiplied

to make suitable filters for LCSLM. Some of these basis vectors have also complicated shapes and it is often difficult to implement them accurately by the use of LCSLM. In Ref. [34] an iterative feedback method was proposed to accurately implement the basis vectors with complicated shapes by the LCSLM.

Recently, the color filter design with a constraint of positive spectral values has been the focus of growing interest [56, 91, 104, 105]. In Refs. [59, 103, 104] the methods for choosing the optimized set of a commercially available Kodak Wratten gelatin color filter set were proposed. In Ref. [56] the positive color filters were found by optimizing an energy function, which uses second- and fourth-order statistical moments [74]. In Refs. [26] and [99] the simulated annealing based method was used to design positive color filters for recording artworks [26] and for the electronic endoscope [99]. The color filters in these studies were narrow band shaped. In *publication 4* we proposed a new computational method for designing broad band color filters with a constraint of positive spectral values. By our method, the color filters can be designed according to an application, and they can be directly implemented optically.

6.1 Color filter design

The aim was to find a method, which can cluster the spectra into a few clusters and after clustering the centers of clusters could be used as color filters. We investigated the clustering properties of competitive learning and self-organization methods [23, 35, 54] and decided to use an unsupervised competitive neural network with a learning algorithm basing on the Instar-algorithm by Grossberg [23]. We also incorporated Kohonen's [54] Self-Organizing Map with a Winner Take All (WTA) layer to our model.

The competitive learning is defined as follows. In each learning iteration the winner neuron w_c is the weight vector, which has the closest Euclidean distance to the input vector x. The updating process of the weight vectors is defined by

$$w_i(t+1) = \begin{cases} w_i(t) + \alpha(t)[x(t) - w_i(t)] & \text{, if } i = c, \\ w_i(t) & \text{, otherwise,} \end{cases} \tag{6.1}$$

where t is the iteration parameter and $\alpha(t)$ is a learning rate. The learning rate decreases exponentially during the learning. In each cycle of the learning process the training sample is taken randomly from the input data. The weights are initialized by the center vector (≥ 0) of the input data. Eq. (6.1) can be written as $w_i(t+1) = w_i(t)[1 - \alpha(t)] + \alpha(t)x(t)$, where $0 \leq \alpha(t) < 1$, $w_i(t) \geq 0$, $x(t) \geq 0$ and therefore the weights w are always positive. A detailed description of the competitive learning and self-organization can be found in Ref. [54]. The algorithm for the unsupervised competitive neural network with the WTA-layer is defined as follows.

Algorithm 6.1: Unsupervised competitive neural network (Instar).

begin
e = number of iterations;
normalize the input data to unit norm;
initialize the weights w by the center vector of the input data;
for $t = 1$ **to** e **do**
take randomly vector x from the input data;
find the winner w_c for x by Eq. (4.3);
update the weight w_i by Eq. (6.1);
decrease learning rate α;
endfor
end

In *publication 4* we experimented with the Munsell spectral database containing 1269 reflectance spectra. The learned filter set containing 8 color filters with positive coefficients is shown in Figure 6.1.

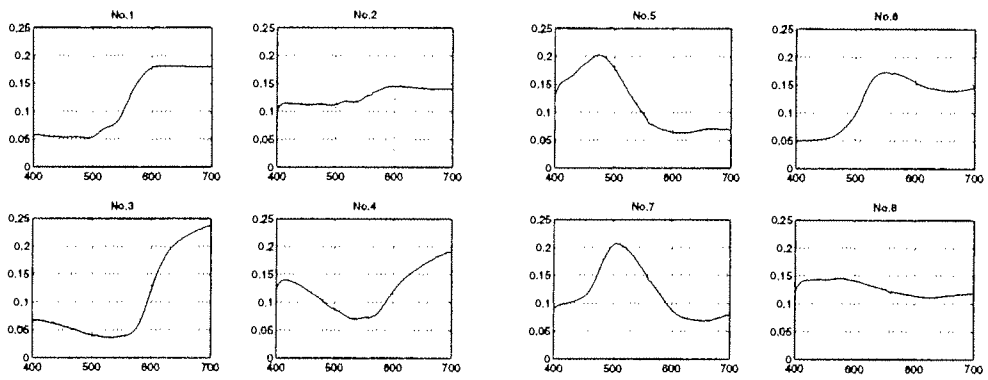

Figure 6.1: Learned color filters, a) No.1-4, b) No.5-8.

The learned filter set is non-orthogonal and the reconstruction τ' of the spectrum τ can be obtained by a pseudoinverse matrix

$$\tau' = W(W^T W)^{-1} W^T \tau, \tag{6.2}$$

where W is the filter set. In the optical implementation, $W(W^T W)^{-1}$ is known and the inner products, $W^T \tau$, between the color filter set W and spectrum τ are determined experimentally. In *publication 4* it was shown that the spectral reconstruction performance by the learned filter set is comparable to the eigenvectors of the subspace method.

6.2 Spectral imaging system

The color filters with positive coefficients were designed to be used in our spectral imaging system to calculate the inner products $W^T \tau$ in Eq. (6.2) optically. We will illuminate

the object by the light which has the spectral characteristics of the color filter. For this purpose we constructed a compact size optical setup for the spectral synthesizer, which is shown in Figure 6.2. In the spectral synthesizer, the light source is white light, which is filtered in the dispersion plane by the LCSLM, and the filtered light is mixed by the second grating to produce the output light.

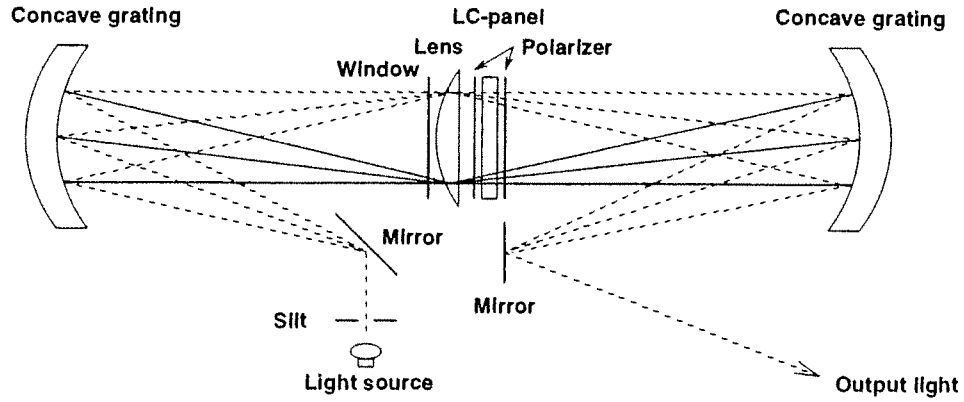

Figure 6.2: Optical setup for the spectral synthesizer.

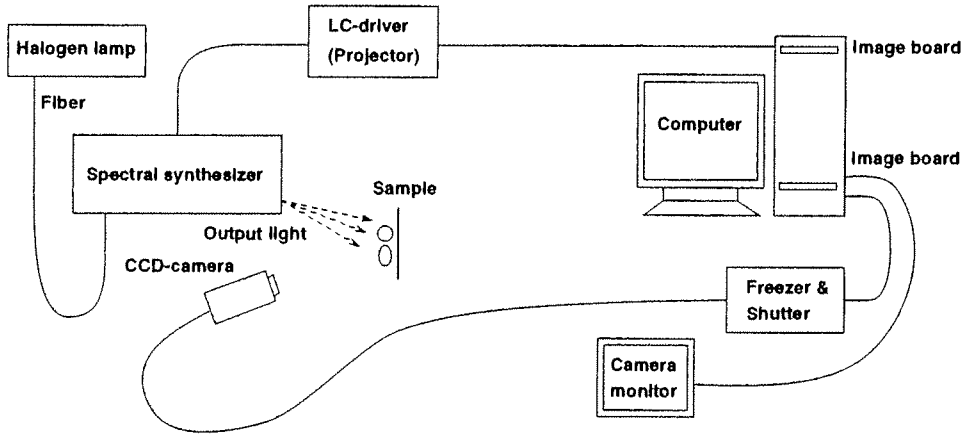

Figure 6.3: Spectral vision system.

The experimental setup for the spectral vision system is shown in Figure 6.3. The object is illuminated by the synthesized lights and the intensity images of the filtered object are detected by the CCD-camera. Note that the inner products are obtained parallel for every pixel. From these optically calculated inner products the object's spectra can be reconstructed by Eq. (6.2). In our experiments we noticed that a small error between the theoretic and optically calculated inner product caused sometimes large errors in the spectrum reconstruction. The investigations on this problem showed that the inverse matrix in Eq. (6.2) was in those cases near singular. In order to avoid the problem of

singularity, we used a regularization technique based on the truncated singular value decomposition (SVD) in the spectrum reconstruction. Recently, Hardeberg *et al.* [31] investigated the effect of noise in the spectrum reconstruction by computer simulations. The acquisition of the spectral image by our spectral vision system is performed by the following algorithm.

Algorithm 6.2: Spectral image acquisition.

begin
  n = number of filters;
  for $i = 1$ **to** n **do**
    illuminate the object by the synthesized light of w_i;
    detect inner product $w_i^T r$ by CCD-camera;
  endfor
  store or transmit the acquired data;
  if reconstruction = *true* **then**
    reconstruct the spectral image by Eq. (6.2) and
    if needed, use regularization;
  endif
end

The time complexity for the spectral image acquisition by our spectral vision system is $O(n)$, where n is the number color filters or the number of component images to be obtained. For one component image, the acquisition time complexity is $O(1)$. We use the low-dimensional color filter set designed by the unsupervised neural network, and therefore the value for n is small. For example, in *publication 5* four color filters were used.

Some of the present spectral imaging systems are based on the line scanning [40]. In these systems the spectra for one line are measured simultaneously along the wavelength axis, but along the spatial axis, the measurement device or the object must be scanned. The acquisition time complexity for each line is $O(1)$ and for the whole image $O(N)$, where N is the number of lines in an image. Extra care should be taken for acquisition of equilateral pixels when either the measurement device or the object is moving. In our spectral vision system, the spatial resolution of the image is defined by the CCD-array and one can obtain a two-dimensional image directly. The different spectral components are, however, acquired separately. For the time complexity $O(N)$ of our system and for the time complexity $O(N)$ of the line scanning based spectral camera, the following $O(n) \ll O(N)$ is true. Our belief is that the proposed system is easier to use and a better choice for static objects. For moving objects, the number of spectral components and the speed of image acquisition set limits of use. The most critical part is the set-up time of the LCSLM.

In *publication 5* we used 4 color filters to acquire the spectral image at the wavelength range from 400nm to 700nm at 10nm intervals. The data to be stored is only 4 monochrome images and they can be also used to transmit the spectral image. In our system, the inner products are calculated optically and therefore this system can be used in various optical pattern recognition tasks, in which the classification criterion contains the inner product calculation. *Publication 5* contains a detailed description of the spectral vision system and shows the results of the experiments with real world objects.

CHAPTER VII

Discussion

Since the first prototype for the multispectral imaging instrument developed in the beginning of 1970's, the spectral images have been mainly used in the field of remote sensing. However, due to the recent technological development in optics and computers, the spectral imaging has received a great deal of attention in the industrial machine vision applications. Due to the high accuracy, the spectral imaging is becoming an important quality factor in industrial processes.

In this thesis three areas of spectral imaging were investigated. The analysis of spectral textures, the illumination estimation, and the low-dimensional spectral imaging system are all important research areas in the field of machine vision based industrial applications. The results of this thesis can be further developed to be more suitable and accurate enough for machine vision. The usage of these techniques in industry are straightforward.

The multispectral texture analysis method was proposed basing on the gray level cooccurrence matrix. The use of gray level cooccurrence matrix is a simple method and it's accuracy still competes with the recent techniques in texture analysis. This was one of our motivations to generalize it for the multispectral texture analysis. It was shown that the proposed method can be used to represent multispectral textures. In *publication 2* this method was tested with natural spectral images and RGB images, and the segmentation accuracies with both images were approximately the same. The number of test images was small and therefore the generalization of the results needs to be investigated more deeply with larger data sets. Also the meaning of the location dependent Haralick features calculated from the spectral cooccurrence matrix depends on the order of the spectral classes and therefore the ordering of spectra needs to be studied more carefully. In this thesis the meaning of Haralick features for the spectral cooccurrence matrix was not studied in detailed, because of the nonuniquely defined order of the spectral classes.

The most important advantage of the proposed spectral cooccurrence matrix based method is that it can be used to recognize metameric textures, in which case the texture analysis done with three-dimensional color images will fail. The optical implementation of the spectral quantization is an interesting research topic in the future. In the Self-Organizing Map based spectral quantization, the characteristic vectors in the one-dimensional map are vectors with positive coefficients. Thus, by the optical setup described in *publication 5*, it is possible to calculate the optical inner products parallel

for the whole image in one shot. For the online use in industrial applications, a further investigation of the optical implementation is expected in future.

In machine vision the changing illumination conditions can cause serious problems for the automatic recognition procedure. This is a problem of color constancy, which is under a great deal of attention in the field of color research. In this thesis a new spectral based illumination procedure was proposed. The method gives an efficient approximation of the illumination spectrum on an image. It also describes the global color distribution in an image and therefore the use of it in color based search from color image database is straightforward. In general, the method can be used in color image normalization, which is a great help in applications with changing illumination conditions. In the case of RGB images, they must be first converted to spectral images, and after the illumination estimation, the spectral images must be converted back to RGB images for visual purposes. As discussed in *publication 3*, these conversions are ill-defined and need further study.

The spectral imaging is expected to increase in industrial use. Recently, the optical color filter design has been the focus of growing interest. There exists commercially available color filters, but they are usually expensive and with fixed transmittance, which cannot be changed according to the application. Also the production cost of color filter can be high. In *publication 4* we proposed an unsupervised competitive neural network based method to computationally design color filters. The color filters can be designed according to the application. In *publication 5* these filters were implemented optically by the LCSLM. Using LCSLM, we can easily rewrite color filters with arbitrary shape, *i.e.* we can reproduce optical color filters needed for a certain application. The construction cost of the spectral synthesizer is low compared to the production cost, for example, of the narrow band interference filters with a fixed transmittance.

The storing and transmission of the high-dimensional spectral data can be unconvenient. We proposed a prototype of the low-dimensional spectral imaging system, which can be used to reconstruct the spectral image from a few component images, with a sufficient accuracy. The experimental results in *publication 5* showed that our spectral vision system has potential, but it must be developed further in its color representation. The problem of near singularity in our experiments indicates that further study on the choice of the filter set is needed. Possible methods include, for example, the use of Independent Component Analysis (ICA) [57, 69]. In the spectrum reconstruction, the effect of the spectral sensitivity of the CCD camera [102], the possible system noise, and the highlights in images [53] need also further study. The spectral synthesizer can be used in various optical pattern recognition tasks, in which the classification criterion contains the inner product calculation.

The proposed spectral vision system is based on the use of the spectral synthesizer and therefore it is sensitive to other illumination. This means that it is limited mainly for indoor measurements. An interesting application could be to incorporate it to the electronic endoscope to measure spectral images for medical purposes. Recently, our group proposed a new spectral vision system [65], which is based on the use of the linear variable filter (LVF) and LCSLM. The new system filters the reflecting or transmitting light from an object by the rewritable optical transparent broad band filter, and it can be used also for the outdoor measurements.

In the future research, the following are planned to be investigated. In the multispectral texture analysis, the method will be tested with larger datasets and the optical implementation of the spectral quantization will be studied. In the spectral based illumination estimation, the conversion from RGB to spectra and *vice versa* will be improved. The optical color filter design will be studied further and the spectral vision system will be developed in its color representation.

[1] ALLAM S., ADEL M., AND RÉFRÉGIER P. Fast algorithm for texture discrimination by use of a separable orthonormal decomposition of the co-occurrence matrix. *Applied Optics 36*, 32 (1997), 8313–8321.

[2] BARONTI S., CASINI A., LOTTI F., AND PORCINAI S. Multispectral imaging system for the mapping of pigments in works of art by use of principal-component analysis. *Applied Optics 37*, 8 (1998), 1299–1309.

[3] BIJLSMA R. J. The characterization of natural vegetation using first-order and texture measurements in digitized, colour-infrared photography. *International Journal of Remote Sensing 14*, 8 (1993), 1547–1562.

[4] BRAINARD D. H., AND FREEMAN W. T. Bayesian color constancy. *Journal of the Optical Society of America A 14*, 7 (1997), 1393–1411.

[5] BRODATZ P. *Textures: A Photographic Album for Artists and Designers.* Reinhold, New York, 1968.

[6] CHANG C.-C., AND WANG L.-L. Color texture segmentation for clothing in a computer-aided fashion design system. *Image and Vision Computing 14*, 9 (1996), 685–702.

[7] CHEN P.-F., AND TRAN T. C. Hyperspectral imagery classification using a back-propagation neural network. In *Proceedings, International Conference on Neural Networks, Orlando, Florida, June 28 - July 2* (1994), vol. 5, pp. 2942–2947.

[8] CHOU J., WEGER R. C., LIGTENBERG J. M., KUO K.-S., WELCH R. M., AND BREEDEN P. Segmentation of polar scenes using multi-spectral texture measures and morphological filtering. *International Journal of Remote Sensing 15*, 5 (1994), 1019–1036.

[9] COHEN J. Dependency of the spectral reflectance curves of Munsell color chips. *Psychon. Sci. 1* (1964), 369–370.

[10] CUMANI A. Edge detection in multispectral images. *CVGIP: Graphical Models and Image Processing 53*, 1 (1991), 40–51.

[11] DÍAZ J. A., CHIRON A., AND VIÉNOT F. Tracing a metameric match to individual variations of color vision. *Color Research and Application 23*, 6 (1998), 379–389.

[12] DREW M. S., AND FUNT B. V. Natural metamers. *CVGIP: Image Understanding 56*, 2 (1992), 139–151.

[13] D'ZMURA M., AND IVERSON G. Color constancy. I. Basic theory of two-stage linear recovery of spectral descriptions for lights and surfaces. *Journal of the Optical Society of America A 10*, 10 (1993), 2148–2165.

[14] D'ZMURA M., AND IVERSON G. Color constancy. II. Results for two-stage linear recovery of spectral descriptions for lights and surfaces. *Journal of the Optical Society of America A 10*, 10 (1993), 2166–2180.

[15] D'ZMURA M., AND IVERSON G. Color constancy. III. General linear recovery of spectral descriptions for lights and surfaces. *Journal of the Optical Society of America A 11*, 9 (1994), 2389–2400.

[16] EKLUNDH J.-O., LANSNER A., AND WESSBLAD R. Classification of multispectral images using associative nets. In *Proceedings, 8th International Conference on Pattern Recognition, Paris, France, October 27-31* (1986), vol. 2, pp. 1240–1243.

[17] FINLAYSON G. D., DREW M. S., AND FUNT B. V. Color constancy: generalized diagonal transforms suffice. *Journal of the Optical Society of America A 11*, 11 (1994), 3011–3019.

[18] FINLAYSON G. D., AND FUNT B. V. Coefficients channels: Derivation and relationship to other theoretical studies. *Color Research and Application 21*, 2 (1996), 87–96.

[19] FUNT B., CARDEI V., AND BARNARD K. Neural network color constancy and specularly reflecting surfaces. In *Proceedings, 8th Congress of the International Colour Association, AIC Color 97, Kyoto, Japan, May 25-30* (1997), vol. 2, pp. 523–526.

[20] FUNT B. V., AND FINLAYSON G. D. Color constant color indexing. *IEEE Transactions on Pattern Analysis and Machine Intell. 17*, 5 (1995), 522–529.

[21] GALLOWAY M. Texture analysis using gray level run-lengths. *Computer Graphics and Image Processing 4* (1974), 172–199.

[22] GARCÍA-BELTRÁN A., NIEVES J. L., HERNÁNDEZ-ANDRÉS J., AND ROMERO J. Linear bases for spectral reflectance of acrylic paints. *Color Research and Application 23*, 1 (1998), 39–45.

[23] GROSSBERG S. *Studies of the Mind and Brain.* Reidel Press, Drodrecht, Holland, 1982.

[24] HALLIKAINEN J., PARKKINEN J., AND JAASKELAINEN T. An acousto-optic color spectrometer. *Review of Scientific Instruments 59*, 1 (1988), 81–83.

[25] HALLIKAINEN J., PARKKINEN J. P. S., AND JAASKELAINEN T. Color image processing with AOTF. In *Proceedings, 6th Scandinavian Conference on Image Analysis, SCIA'89, Oulu, Finland, June 19-22* (1989), pp. 294–300.

[26] HANEISHI H., HASEGAWA T., TSUMURA N., AND MIYAKE Y. Design of color filters for recording artworks. In *Proceedings, IS&T's 50th Annual Conference, Cambridge, Massachusetts, May 18-23* (1997), pp. 369–372.

[27] HANEISHI H., SHIOBARA T., AND MIYAKE Y. Color correction for colorimetric color reproduction in an electronic endoscope. *Optics Communications 114* (1995), 57–63.

[28] HARALICK R. M. Statistical and structural approaches to texture. *Proceedings of IEEE 67*, 5 (1979), 786–804.

[29] HARALICK R. M., SHANMUGAM K., AND DINSTEIN I. Textural features for image classification. *IEEE Trans. Syst. Man Cybern. SMC-3*, 6 (1973), 610–621.

[30] HÅRD A., SIVIK L., AND TONNQUIST G. Ncs, natural color system - from concepts to research and applications. *Color Research and Application 21*, 3 (1996), 180–205.

[31] HARDEBERG J. Y., BRETTEL H., AND SCHMITT F. Spectral characterisation of electronic cameras. In *Proceedings of SPIE, Electronic Imaging: Processing, Printing and Publishing in Color, Zürich, Switzerland, May 18-22* (1998), vol. 3409, pp. 100–109.

[32] HAUTA-KASARI M., MIYAZAWA K., TOYOOKA S., AND PARKKINEN J. Spectral vision system for color image analysis. In *Proceedings, 3rd International Symposium on Optics in Engineering, Kajaani, Finland, January 19-21* (1999).

[33] HAUTA-KASARI M., PARKKINEN J., JAASKELAINEN T., AND LENZ R. Spectral based analysis of color images. In *Proceedings, 8th Congress of the International Colour Association, AIC Color 97, Kyoto, Japan, May 25-30* (1997), vol. I, pp. 419–422.

[34] HAYASAKA N., TOYOOKA S., AND JAASKELAINEN T. Iterative feedback method to make a spatial filter on a liquid crystal spatial light modulator for 2D spectroscopic pattern recognition. *Optics Communications 119* (1995), 643–651.

[35] HAYKIN S. *Neural Networks.* Macmillan College Publishing Company, New York, 1994.

[36] HEALEY G., AND BENITES L. Linear models for spectral reflectance functions over the mid-wave and long-wave infrared. *Journal of the Optical Society of America A 15*, 8 (1998), 2216–2227.

[37] HEALEY G., AND WANG L. Illumination-invariant recognition of texture in color images. *Journal of the Optical Society of America A 12*, 9 (1995), 1877–1883.

[38] HO J., FUNT B. V., AND DREW M. S. Separating a color signal into illumination and surface reflectance components: Theory and applications. *IEEE Transactions on Pattern Analysis and Machine Intell. 12*, 10 (1990), 967–977.

[39] HUNT R. W. G. *Measuring Colour*, 2nd ed. Ellis Horwood, Chichester, England, 1991.

[40] HYVÄRINEN T., HERRALA E., AND DALL'AVA A. Direct sight imaging spectrograph: a unique add-on component brings spectral imaging to industrial applications. In *Proceedings, IS & T/SPIE's Symposium on Electronic Imaging: Science and Technology (EI98), San Jose, California, USA, January 25-30* (1998), vol. 3302-21.

[41] IMAI H. F., TSUMURA N., HANEISHI H., AND MIYAKE Y. Principal component analysis of skin color and its application to colorimetric color reproduction on CRT display and hardcopy. *Journal of Imaging Science and Technology 40*, 5 (1996), 422–430.

[42] IMAI H. F., TSUMURA N., HANEISHI H., AND MIYAKE Y. Prediction of color reproduction for skin color under different illuminants based on color appearance models. *Journal of Imaging Science and Technology 41*, 2 (1997), 166–173.

[43] ITOH K. Interferometric multispectral imaging. In *Progress in Optics XXXV*, E. Wolf, Ed. Elsevier Science, 1996, pp. 145–196.

[44] JAASKELAINEN T., PARKKINEN J., AND TOYOOKA S. Vector-subspace model for color representation. *Journal of the Optical Society of America A 7*, 4 (1990), 725–730.

[45] JAASKELAINEN T., SILVENNOINEN R., HILTUNEN J., AND PARKKINEN J. P. S. Classification of the reflectance spectra of pine, spruce, and birch. *Applied Optics 33*, 12 (1994), 2356–2362.

[46] JAASKELAINEN T., TOYOOKA S., IZAWA S., AND KADONO H. Color classification by vector subspace method and its optical implementation using liquid crystal spatial light modulator. *Optics Communications 89*, 1 (1992), 23–29.

[47] JAIN A. K. *Fundamentals of Digital Image Processing.* Prentice Hall, Englewood Cliffs, New Jersey, 1989.

[48] JUDD D. B., MACADAM D. L., AND WYSZECKI G. Spectral distribution of typical daylight as a function of correlated color temperature. *Journal of the Optical Society of America 54*, 8 (1964), 1031–1040.

[49] KAARNA A., ZEMCIK P., KÄLVIÄINEN H., AND PARKKINEN J. Multispectral image compression. In *Proceedings, 14th International Conference on Pattern Recognition, Brisbane, Australia, August 16-20* (1998), vol. 2, pp. 1264–1267.

[50] KAISER P. K., AND BOYNTON R. M. *Human Color Vision*, 2nd ed. Optical Society of America, Washington DC, 1996.

[51] KÄLVIÄINEN H., KUKKONEN S., HYVÄRINEN T., AND PARKKINEN J. Quality control in tile production. In *Proceedings, SPIE conference on intelligent Robots and Computer Vision XVII, Boston, Massachusetts, USA, November 2-3* (1998), vol. 3522, pp. 355–365.

[52] KAWATA S., SASAKI K., AND MINAMI S. Component analysis of spatial and spectral patterns in multispectral images. I. Basis. *Journal of the Optical Society of America A 4*, 11 (1987), 2101–2106.

[53] KLINKER G. J., SHAFER S. A., AND KANADE T. The measurement of highlights in color images. *International Journal of Computer Vision 2*, 1 (1988), 7–32.

[54] KOHONEN T. *The Self-Organizing Maps.* Springer-Verlag, Berlin Heidelberg, 1995.

[55] KONDEPUDY R., AND HEALEY G. Use of invariants for recognition of three-dimensional color textures. *Journal of the Optical Society of America A 11*, 11 (1994), 3037–3049.

[56] LENZ R., ÖSTERBERG M., HILTUNEN J., JAASKELAINEN T., AND PARKKINEN J. Unsupervised filtering of color spectra. *Journal of the Optical Society of America A 13*, 7 (1996), 1315–1324.

[57] LEPPÄJÄRVI S. *Image Segmentation and Analysis for Automatic Color Correction.* PhD thesis, Lappeenranta University of Technology, Lappeenranta, Finland, 1999.

[58] MACHUCA R., AND PHILLIPS K. Applications of vector fields to image processing. *IEEE Transactions on Pattern Analysis and Machine Intell. 5*, 3 (1983), 316–329.

[59] MAÎTRE H., SCHMITT F., CRETTEZ J.-P., WU Y., AND HARDEBERG J. Y. Spectrophotometric image analysis of fine art paintings. In *Proceedings, IS & T and SID's 4th Color Imaging Conference, Scottsdale, Arizona, USA, November* (1996), pp. 50–53.

[60] MALONEY L. T. Evaluation of linear models of surface spectral reflectance with small numbers of parameters. *Journal of the Optical Society of America A 3*, 10 (1986), 1673–1683.

[61] MALONEY L. T., AND WANDELL B. A. Color constancy: a method for recovering surface spectral reflectance. *Journal of the Optical Society of America A 3*, 1 (1986), 29–33.

[62] MANABE Y., SATO K., AND INOKUCHI S. An object recognition through continuous spectral images. In *Proceedings, 12th International Conference on Pattern Recognition, Jerusalem, Israel, October 9-13* (1994), vol. 1, pp. 858–860.

[63] MANTERE K., PARKKINEN J., AND JAASKELAINEN T. Simulation of white-light adaptation characteristics with use of nonlinear neural principal component analysis. *Journal of the Optical Society of America A 14*, 9 (1997), 2049–2056.

[64] MESSER K., AND KITTLER J. A comparison of colour texture attributes selected by statistical feature selection and neural networks methods. *Pattern Recognition Letters 18*, 13 (1997), 1241–1246.

[65] MIYAZAWA K., HAUTA-KASARI M., AND TOYOOKA S. Optical implementation of transparent broad-band filters for spectral image analysis. In *Proceedings, 3rd International Symposium on Optics in Engineering, Kajaani, Finland, January 19-21* (1999).

[66] *Munsell Book of Color, Matte Finish Collection.* Munsell Color, Baltimore, USA, 1976.

[67] OHANIAN P. P., AND DUBES R. C. Performance evaluation for four classes of textural features. *Pattern Recognition 25*, 8 (1992), 819–833.

[68] OJA E. *Subspace Methods of Pattern Recognition.* Research Studies Press, Letchworth, England, 1983.

[69] OJA E., KARHUNEN J., WANG L., AND VIGARIO R. Principal and independent components in neural networks - recent developments. In *Proceedings, VII Italian Workshop on Neural Nets (WIRN'95), Vietri sul Mare, Italy, May 18-20* (1995).

[70] OJA E., AND PARKKINEN J. Texture subspaces. In *Pattern Recognition Theory and Applications*, P. A. Devijver and J. Kittler, Eds. Springer-Verlag Berlin Heidelberg, 1987, pp. 21–33.

[71] OJA E., PARKKINEN J., SELKÄINAHO K., AND KÄRKI T. Regularity measurement, classification, and segmentation of textures. In *From Pixels to Features*, J. Simon, Ed. Elsevier Science Publishers B.V. (North-Holland), 1989, pp. 207–218.

[72] OJA E., AND VALKEALAHTI K. Co-occurrence map: Quantizing multidimensional texture histograms. *Pattern Recognition Letters 17*, 7 (1996), 723–730.

[73] OJALA T., PIETIKÄINEN M., AND HARWOOD D. A comparative study of texture measures with classification based on feature distributions. *Pattern Recognition 29*, 1 (1996), 51–59.

[74] ÖSTERBERG M. *Quality Functions for Parallel Selective Principal Component analysis.* PhD thesis, Linköping University, Linköping, Sweden, 1994.

[75] PANJWANI D. K., AND HEALEY G. Markov random field models for unsupervised segmentation of textured color images. *IEEE Transactions on Pattern Analysis and Machine Intell. 17*, 10 (1995), 939–954.

[76] PARKKINEN J., AND JAASKELAINEN T. Color representation using statistical pattern recognition. *Applied Optics 26*, 19 (1987), 4240–4245.

[77] PARKKINEN J. P. S., HALLIKAINEN J., AND JAASKELAINEN T. Characteristic spectra of Munsell colors. *Journal of the Optical Society of America A 6*, 2 (1989), 318–322.

[78] PÁRRAGA C., BRELSTAFF G., TROSCIANKO T., AND MOOREHEAD I. R. Color and luminance information in natural scenes. *Journal of the Optical Society of America A 15*, 3 (1998), 563–569.

[79] RAGHU P. P., POONGODI R., AND YEGNANARAYANA B. A combined neural network approach for texture classification. *Neural Networks 8*, 6 (1995), 975–987.

[80] RAMASAMY S. M., VENKATASUBRMANIAN V., AND ANBAZHAGAN S. Reflectance spectra of minerals and their discrimination using thematic mapper, irs and spot multi-spectral data. *International Journal of Remote Sensing 14*, 16 (1993), 2935–2970.

[81] RICHARDS J. A. *Remote Sensing Digital Image Processing.* Springer-Verlag, Berlin, 1993.

[82] ROCK B. N., VOGELMANN J. E., WILLIAMS D. L., VOGELMANN A. F., AND HOSHIZAKI T. Remote detection of forest damage: Plant responses to stress may have spectral "signatures" that could be used to map, monitor and measure forest damage. *BioScience 36*, 7 (1986), 439–445.

[83] ROSENFELD A., WANG C.-Y., AND WU A. Y. Multispectral texture. *IEEE Trans. Syst. Man Cybern. SMC-12* (1982), 79–84.

[84] ROUSSEEUW P. J., AND LEROY A. M. *Robust Regression & Outlier Detection.* Wiley, New York, 1987.

[85] RUDERMAN D. L., CRONIN T. W., AND CHIAO C.-C. Statistics of cone responses to natural images: implications for visual coding. *Journal of the Optical Society of America A 15*, 8 (1998), 2036–2045.

[86] RUMELHART D. E., HINTON G. E., AND WILLIAMS R. J. Learning internal representations by error propagation. In *Parallel Distributed Processing: Explorations in the Microstructures of Cognition*, D. Rumelhart and J. McClelland, Eds. MA: MIT Press, Cambridge, 1986, pp. 318–362.

[87] SABER E., AND TEKALP A. M. Integration of color, edge, shape, and texture features for automatic region-based image annotation and retrieval. *Journal of Electronic Imaging 7*, 3 (1998), 684–700.

[88] SCHALKOFF R. J. *Pattern Recognition: Statistical, Structural and Neural Approaches.* John Wiley & Sons, Inc., New York, 1992.

[89] SCHARCANSKI J., HOVIS J. K., AND SHEN H. C. Representing the color aspect of texture images. *Pattern Recognition Letters 15*, 2 (1994), 191–197.

[90] SCHETTINI R. A segmentation algorithm for color images. *Pattern Recognition Letters 14*, 6 (1993), 499–506.

[91] SHARMA G., TRUSSELL H. J., AND VRHEL M. J. Optimal nonnegative color scanning filters. *IEEE Transactions on Image Processing 7*, 1 (1998), 129–133.

[92] SHIOBARA T., ZHOU S., HANEISHI H., TSUMURA N., AND MIYAKE Y. Improved color reproduction of electronic endoscopes. *Journal of Imaging Science and Technology 40*, 6 (1996), 494–501.

[93] SLATER D., AND HEALEY G. Analyzing the spectral dimensionality of outdoor visible and near-infrared illumination functions. *Journal of the Optical Society of America A 15*, 11 (1998), 2913–2920.

[94] TAN T. S. C., AND KITTLER J. On colour texture representation and classification. In *Proceedings, 2nd International Conference on Image Processing, ICIP'92* (1992), pp. 390–395.

[95] TAN T. S. C., AND KITTLER J. Colour texture classification using features from colour histograms. In *Proceedings, 8th Scandinavian Conference on Image Analysis, SCIA'93, Tromso, Norway, May 25-28* (1993), vol. 2, pp. 807–813.

[96] TAN T. S. C., AND KITTLER J. Colour texture analysis using colour histogram. *IEE Proc.-Vis. Image Signal Process. 141*, 6 (1994), 403–412.

[97] THORTON W. S. How strong metamerism disturbs color spaces. *Color Research and Application 23*, 6 (1998), 402–407.

[98] TOMINAGA S. Multichannel vision system for estimating surface and illumination functions. *Journal of the Optical Society of America A 13*, 11 (1996), 2163–2173.

[99] TSUMURA N., TANAKA T., HANEISHI H., AND MIYAKE Y. Optimum spectral transmittance of color filters on single chip ccd for electronic endoscope. In *Proceedings, IS&T's 50th Annual Conference, Cambridge, Massachusetts, May 18-23* (1997), pp. 373–376.

[100] USUI S., NAKAUCHI S., AND NAKANO M. Reconstruction of Munsell color space by a five-layer neural network. *Journal of the Optical Society of America A 9*, 4 (1992), 516–520.

[101] VALKEALAHTI K., AND OJA E. Reduced multidimensional co-occurrence histograms in texture classification. *IEEE Transactions on Pattern Analysis and Machine Intell. 20*, 1 (1998), 90–94.

[102] VORA P. L., FARRELL J. E., TIETZ J. D., AND BRAINARD D. H. Linear models for digital cameras. In *Proceedings, IS&T's 50th Annual Conference, Cambridge, Massachusetts, May 18-23* (1997), pp. 377–382.

[103] VORA P. L., AND TRUSSELL H. J. Measure of goodness of a set of color-scanning filters. *Journal of the Optical Society of America A 10*, 7 (1993), 1499–1508.

[104] VORA P. L., AND TRUSSELL H. J. Mathematical methods for the design of color scanning filters. *IEEE Transactions on Image Processing 6*, 2 (1997), 312–320.

[105] VRHEL M. J., AND TRUSSELL H. J. Optimal color filters in the presence of noise. *IEEE Transactions on Image Processing 4*, 6 (1995), 814–823.

[106] WANDELL B. A. The synthesis and analysis of color images. *IEEE Transactions on Pattern Analysis and Machine Intell. PAMI-9*, 1 (1987), 2–13.

[107] WYSZECKI G., AND STILES W. S. *Color science : concepts and methods, quantitative data and formulae*, 2nd ed. Wiley, New York, 1982.

[108] YOUNG R. A. Principal-component analysis of macaque lateral geniculate nucleus chromatic data. *Journal of the Optical Society of America A 3*, 10 (1986), 1735–1741.

[109] ZAIDI Q. Identification of illuminant and object colors: heuristic-based algorithms. *Journal of the Optical Society of America A 15*, 7 (1998), 1767–1776.

Publications

Publication 1

HAUTA-KASARI M., PARKKINEN J., JAASKELAINEN T., AND LENZ R.,
Generalized Cooccurrence Matrix for Multispectral Texture Analysis,

Proceedings of the 13th International Conference on Pattern Recognition, (ICPR'96),
Vienna, Austria, August 25-29, 1996, Vol. II, pages 785-789.

Proceedings of the 13th International Conference on Pattern Recognition, (ICPR'96), Vienna, Austria, August 25-29, 1996, Vol. II, pages 785-789.

Generalized Cooccurrence Matrix for Multispectral Texture Analysis

M. Hauta-Kasari[1], J. Parkkinen[1], T. Jaaskelainen[2], and R. Lenz[3]

[1]Department of Information Technology, Lappeenranta University of Technology
P.O.Box 20, FIN-53851 Lappeenranta, FINLAND
Markku.Hauta-Kasari@lut.fi, Jussi.Parkkinen@lut.fi
[2] Väisälä Laboratory, University of Joensuu, P.O.Box 111, FIN-80101 Joensuu, FINLAND
jaaskelainen@joyl.joensuu.fi
[3] Image Processing Group, Department of Electrical Engineering
Linköping University, S-58183 Linköping, SWEDEN
reiner@isy.liu.se

Abstract

We present a new cooccurrence matrix based approach for multispectral texture analysis. The spectral and spatial domains of the multispectral textures are processed separately. The color space used in this study is represented by subspaces and it is classified by the averaged learning subspace method (ALSM). In the spatial domain we use a generalized cooccurrence matrix for vector valued pixels. The texture feature vectors are classified by the k-nearest neighbor (KNN) classifier and the multilayer perceptron (MLP) network. Experimental results of the multispectral texture segmentation are presented.

1. Introduction

The use of color in image analysis is growing and recently there has been a lot of interest in color textures. The most common color representations for color images are the RGB- and the Lab-model in industrial applications. Color textures with three-dimensional colorspace have been studied by Kittler et al. [16], Scharcanski et al. [14], Kondebudy et al. [7], Healey et al. [4] and by Panjwani et al. [10].

Methods of color image analysis are mainly based on RGB-images. The RGB-model can represent only that region of the electromagnetic spectrum (400-700 nm), which is visible to human. Furthermore, there is the problem of metamerism, i.e. several spectra may have the same RGB-values [2]. Therefore multispectral images can contain information that can not be detected in the corresponding gray-level or RGB-image [8]. Since all three-dimensional colorspaces have drawbacks, the whole spectrum is needed for accurate color representation.

Multispectral images and their analysis is receiving a great deal of attention, due to the technical development in imaging devices and computers. Multispectral images are used e.g. in remote sensing and industrial quality control. For example, in AVIRIS (Airborne Visible/ Infrared Imaging Spectrometer) imagery the images have 224 spectral bands (400-2450 nm) [17]. The new generation colorimeters based on the spectral representation of color are used in paper quality control at paper mills and the use of imaging spectrometers is increasing in the industry. The three-dimensional color coordinate systems are not accurate enough to meet all requirements in color analysis.

Color image segmentation has been studied e.g. in papers [10] and [15]. During segmentation, regions of interests are extracted from an image. There are two basic approaches to image segmentation: edge-based methods and region-based methods. The methods within these approaches in gray level images are not always straight forward expandable to multispectral images. Mathematically, one move from one dimensional space of gray values into a vector space of multispectral pixels. To define discontinuity or similarity in a vector space has not a unique solution.

Multispectral textures have two domains to be analyzed: the spectral domain and the spatial domain. In this study we use a two phase process for multispectral textures. The spectral domain is classified by the averaged learning subspace method. A widely used representation of second order statistics in texture analysis, cooccurrence matrix, is generalized for the multispectral images to analyze the spatial domain.

We produced multispectral images synthetically from the Brodatz textures [1]. Each gray level in these textures was

replaced by a natural color spectrum measured by the spectroradiometer from the canopy of pine, spruce and birch forest [6]. We made also experiments with a real multispectral image measured by the Finnish airborne spectrometer AISA (Airborne Imaging Spectrometer for Applications). The segmentation method described in this paper is region-based and the experimental results of multispectral texture segmentations are presented.

2. Classification of the spectral domain

The measured spectra span a high-dimensional pattern space, where the classes are represented by subspaces. The subspaces can be analyzed using the subspace method and the color coordinates are now the projections on these subspaces [5].

The definition for subspaces is based on the Karhunen-Loeve transformation. A measured spectrum $\tau(\lambda)$ can be represented as a vector $[\tau(\lambda_1), \tau(\lambda_2), \ldots, \tau(\lambda_n)]^T$, where λ is the wavelength and T denotes the transpose. To compute the characteristic vectors for the subspaces, we used the correlation matrix $R = \sum_{i=1}^{N_r} \tau_i(\lambda)\tau_i(\lambda)^T$, where the index i means ith spectrum in the set of N_r measured spectra. The characteristic vectors, i.e. the eigenvectors ϕ are the solutions of the equation $R\phi = \sigma\phi$, where σ is an eigenvalue of R. The first p eigenvectors form a basis for the subspace.

The subspace classification is based on the idea, that the classes are represented by the properly spanned subspaces and the unknown vectors are then classified into these classes according to the projection criterion. This supervised classification can be performed as follows: In the begin of the training phase, the color subspaces are formed from the color spectra with known classification. Then the training set is classified. If there are misclassifications in this phase, the subspaces are rotated by changing the correlation matrices [9] : $S_m^{(i)} = S_{m-1}^{(i)} + \sum_{j \neq i} a_{(i,j)} S_m^{(i,j)} - \sum_{j \neq i} b_{(i,j)} S_m^{(j,i)}$, where $S_{m-1}^{(i)}$ is the correlation matrix of a class $\omega^{(i)}$ at iteration $(m-1)$, a and b are small numbers defining the weighting for misclassification. $S_m^{(i,j)}$ is the autocorrelation matrix formed by the pattern vectors that belong to class $\omega^{(i)}$, but have been classified at iteration m to class $\omega^{(j)}$. Learning process continues until the results are correct or stable. This method is also known as the averaged learning subspace method (ALSM) [9]. The unknown measured vectors are then classified into these subspaces using the projection criterion.

3. A generalized cooccurrence matrix

The gray level cooccurrence matrix is defined as a sample estimate of the joint probability density of the gray levels of two pixels separated by a given displacement. In cartesian coordinates the displacement of the cooccurrence can be chosen as a vector $(\Delta x, \Delta y)$. The gray level cooccurrence matrix P is defined as

$$P(i,j) = \{\#\text{pair}(i,j) | \text{image}(x,y) = i \wedge \text{image}(x+\Delta x, y+\Delta y) = j\}, \quad (1)$$

where i, j are gray levels. Usually the cooccurrences are based on the natural lightness-based order of the pixels. In the multispectral images the pixel values are color spectra i.e. vectors and there is no natural order for the pixel values. Rosenfeld et al. [12] mentioned the cooccurrence matrix for vector valued pixels, but their model was computationally too expensive.

When each color spectrum in a multispectral image is classified to the color subspace, the result is an image where each pixel has a pointer to a certain color class. Now we can use this class value as a pixel value. From this image the generalized cooccurrence matrix can be computed. The element $(\omega^{(i)}, \omega^{(j)})$ is the number of pairs of pixels with displacement $(\Delta x, \Delta y)$, with a pair of color spectra belonging to color class $\omega^{(i)}$ and color class $\omega^{(j)}$, respectively. This generalized cooccurrence matrix is a joint probability function defined by pairs of color classes:

$$P(\omega^{(i)}, \omega^{(j)}) = \{\#\text{pair}(p,q) | p(x,y) \in \omega^{(i)} \wedge q(x+\Delta x, y+\Delta y) \in \omega^{(j)}\}, \quad (2)$$

where $\omega^{(i)}, \omega^{(j)}$ are color classes, p and q are color spectra associated to the pixels at the points (x, y) and $(x+\Delta x, y+\Delta y)$.

The problem now is to find out the proper subspaces representing each color. This means that the most suitable subspace representation can be chosen according to the application. When we are comparing a fixed set of textures with each other, e.g. in the texture segmentation problem, the color classes are not necessary to be ordered. However, if the cooccurrence matrices shall be repeatedly, uniquelly reconstructed, unique order for the color classes shall be found. The size of P is $G \times G$, where G denotes the number of gray levels or color classes. In order to avoid large cooccurrence matrices, the number of gray levels is usually compressed. Typical values for G in gray level images are from 4 to 32. The number of color classes depends on the number of the proper color subspaces for needed classification accuracy.

Haralick et al. [3] described fourteen features extracted from the cooccurrence matrix P. In this study we use the following five of them : energy, entropy, contrast, correlation and homogeneity.

4. Multispectral texture segmentation

The texture features calculated from the generalized cooccurrence matrix are classified by the multilayer percep-

tron neural network. Recently, Raghu et al. [11] used MLP to classify Gabor features in the gray level texture segmentation. The MLP used in this study consists of an input layer, one hidden layer and an output layer. Input vectors are now the texture feature vectors and outputs are desired classes. The network training is done by using the back-propagation algorithm [13].

Generalization is an important property of MLP which depends on the number of training epochs and the number of neurons in the hidden layer. Usually it is easy to get a low error rate for a training set when the training process is continued. However, this can lead to overtraining, i.e. the test set error may actually start to increase after a certain number of training steps. To avoid overtraining, the expected error of the network can be calculated using a test set that is independent of the training set. Training should be stopped when the error of this independent test set reaches its minimum.

The segmentation process is performed as follows. First the subspaces for spectral domain classification are constructed from the manually extracted training set. Next the training set for segmentation process is created by taking randomly image windows from each multispectral texture used in our experiment. Then the spectral domain is classified to subspaces by ALSM. Next the feature vectors are calculated from the generalized cooccurrence matrix constructed from each image window. The MLP is trained with these feature vectors with known classification.

In the beginning of the test image segmentation the spectral domain is classified. Next the image is segmented by gliding an image window from upper left corner to lower right corner over the multispectral image and in each window position the generalized cooccurrence matrix is computed, the feature vectors are calculated and classified by MLP. Each pixel in an image window is then marked to belong to a same class that is the output of the MLP for the image window feature vector.

5. Experiments

5.1. Multispectral texture image

First we made experiments with the synthetically produced multispectral textures. The spectral data used in this experiment was measured by the spectroradiometer from the canopy of growing trees (Scots pine, Norway spruce and birch) [6]. Each set of spectra consists of 300 spectra sampled from 400 to 700 nm at 5 nm intervals, i.e. 61 reflectance values. Fig. 1 shows the average spectra from each set. It can be seen that the curve for pine is almost equal to the curve for spruce.

A multispectral texture mosaic was made synthetically combining the spectra measured from growing trees with

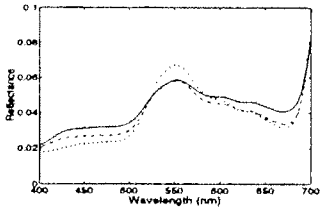

Figure 1. The averaged reflectance spectra from the pine (solid curve), spruce (dot-dashed) and birch (dotted) spectra sets.

the Brodatz textures. The original textures (D28 and D33) were 512 × 512 images with 256 gray levels, which were first compressed to 2 gray levels. Six spectral textures were then made as follows. First gray level 0 in both textures was replaced by the black spectrum. Then gray level 1 in both textures was replaced by 100 randomly selected spectra from pine. Next two textures were made by replacing gray level 1 by 100 randomly selected spectra from spruce and the third texture pair was made by replacing gray level 1 by 100 randomly selected spectra from birch.

Fig. 3 a) shows the gray level transformed multispectral texture mosaic. The multispectral 512 × 512 texture mosaic was formed from six textures so that in the left column is the texture D28 and in the right column is the texture D33. At the top of the image is the spectra from pine, in the middle from spruce and at the bottom from birch. Now the segmentation problem is to divide the multispectral texture mosaic into six regions. This is the same kind of problem as to segment the forest region into thick and sparse forest in real aerial images.

5.2. Gray level texture segmentation

First we segmented using only information from the spatial domain. The corresponding gray level image was constructed by replacing each spectrum in the multispectral image by its CIE 1976 lightness (L^*) value. These were compressed to 4 lightness values. The training data for the spatial domain classification was extracted from six multispectral textures, which made up the texture mosaic. These six textures were transformed to gray level images same way as the texture mosaic. From each of these textures 40 randomly located 20 × 20 texture windows were taken as training data.

Next the gray level cooccurrence matrices were computed from the training samples. The displacement of the cooccurrence matrix was the right neighbor in horizontal direction. The feature vectors were constructed by calculating energy, entropy, contrast, correlation and homogeneity features. The feature vectors were normalized to unity. With

3 inputs, 7 hidden neurons and 6 outputs (6 classes). The MLP was trained using the backpropagation algorithm and the training was stopped when the sum squared error (SSE) of the independent test set was at its minimum.

The gray level texture mosaic was segmented by gliding a 20 × 20 window from upper left corner to lower right corner. In each window position the cooccurrence matrix was calculated, the feature vector was constructed and normalized to unity, and classified by MLP. Then each pixel inside this window was replaced by the feature vector's classification value. Fig. 3 b) shows the segmentation result in pure spatial domain. The percentage of the correctly classified pixels is 60 %.

5.3. Multispectral texture segmentation

The spectral domain of the multispectral image was classified by ALSM with a training set of 150 arbitrarily chosen spectra from each tree. From the training data we constructed 3 subspaces of 11 dimensions. Three hundred spectra used in test image were classified into these subspaces giving a pointer from each spectrum into a color class. Percentages of correct classification were 62%, 69% and 89% for pine, spruce and birch, respectively.

From each of the six multispectral textures that made up the multispectral texture mosaic, 40 randomly located 20 × 20 texture windows were taken as a training data. The spectral domain of each training window was classified to the subspaces, the generalized cooccurrence matrices were computed and the feature vectors were calculated and normalized to unity.

The multispectral texture mosaic was segmented by gliding the 20 × 20 window over the image, as in the previous test. In each window position the generalized cooccurrence matrix was calculated, the feature vector was constructed and normalized to unity, and classified to the training set by the k-nearest neighbor (KNN) classifier. Fig. 3 c) shows the segmented image.

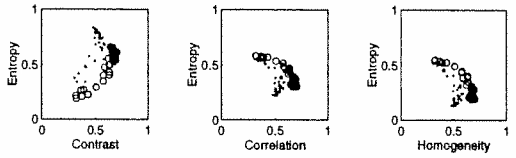

Figure 2. Examples of the feature spaces of two classes. Dot marks: upper left corner texture, circles: middle left texture.

Fig. 2 shows the example of the feature spaces extracted from the training data. Dot marks correspond to the upper left corner texture and circles correspond to the middle left correlation and homogeneity features shows that the curved class boundaries are needed in the feature space. The MLP with nonlinear activation function is especially suitable for this kind of data. We used the logistic sigmoidal activation functions in the hidden and in the output layer neurons.

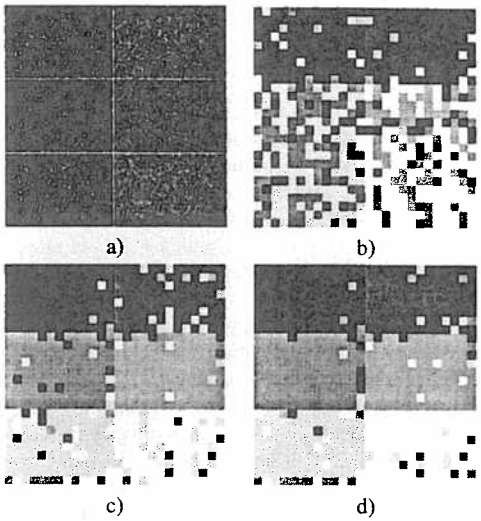

Figure 3. a) Multispectral texture mosaic (the white lines show the edges between the regions). Segmented multispectral texture b) in pure spatial domain c) by KNN d) by MLP.

The MLP was trained as in the gray level segmentation. The training data was the same as in the KNN-based segmentation. The test image was segmented with the 20 × 20 window. In each window position the generalized cooccurrence matrix was calculated, feature vector was constructed and normalized to unity, and classified by MLP. Fig. 3 d) shows the segmented image. In Table 1 are the percentages of the correctly classified pixels in KNN- and MLP-based segmentation.

Table 1. The percentages of the correctly classified pixels in the multispectral segmentation by KNN and MLP. Region 1 : upper left corner, region 6 : lower right corner.

Region	KNN	MLP
1	92.57 %	92.10 %
2	77.36 %	86.52 %
3	87.90 %	92.89 %
4	91.65 %	90.74 %
5	77.04 %	83.31 %
6	76.31 %	87.17 %
Average	83.81 %	88.79 %

Next we made experiments with the multispectral image measured by the Finnish airborne spectrometer AISA (Airborne Imaging Spectrometer for Applications). The image contains terrain regions such as forest, grassland and areas with buildings. Each pixel has a 25-component spectrum measured between 649.9 nm to 747.4 nm. Figure 4 a) shows the 356×700 AISA-image gray level transformed.

The spectral domain of the AISA-image was classified by ALSM. The training set was manually extracted containing data from each of the four desired terrain categories. The regions of interests were forest, grassland 1 (darkest region in upper left), grassland 2 (dark region in middle) and road. Training set sizes were from 132 to 840 pixels. From the training data we constructed 4 subspaces of 8 dimensions. Next each pixel (i.e. spectrum) of the multispectral image was classified to these subspaces. Figure 4 b) shows segmented AISA-image. The gray levels correspond to the spectral subspaces.

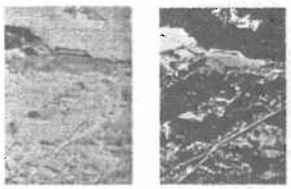

a) b)

Figure 4. a) AISA-image, b) result of the spectral domain segmentation.

The segmentation result shows that the terrain regions are clearly segmented in the spectral domain alone. However, if we want to segment the forest region (i.e. region with same spectra) into thick and sparse forest (i.e. different texture), then the spatial domain must also be analyzed. In this experiment we pass the spatial domain analysis because there was no ground truth for the textured regions in the AISA-image.

6. Discussion

We have presented a new method for multispectral texture analysis, which is based on the generalized cooccurrence matrix for vector valued pixels. The color space was represented by subspaces and for this application we trained the subspaces accurately for the natural spectra measured from the canopy of trees.

The multispectral texture segmentation results show that this method can recognize textures that have the same color and a different structure, or the same structure and a different color. The use of MLP in feature classification was suitable, because the curved class boundaries were needed in the feature space. We showed that the spectral and spatial domains processed together give good results in the multispectral texture segmentation compared to the segmentation

With the synthetic and real multispectral images we have shown that this method can be used in multispectral texture analysis. This study can be seen as a step towards the real multispectral texture analysis. In the future we will test this method with the real images.

Acknowledgement: We thank Pentti Pylkkö for the AISA-image.

References

[1] P. Brodatz. *Textures: A Photographic Album for Artists and Designers*. Reinhold, New York, 1968.

[2] M. S. Drew and B. V. Funt. Natural metamers. *CVGIP: Image Understanding*, 56:139–151, 1992.

[3] R. M. Haralick, K. Shanmugam, and I. Dinstein. Textural features for image classification. *IEEE Trans. Syst. Man Cybern.*, SMC-3:610–621, 1973.

[4] G. Healey and L. Wang. Illumination-invariant recognition of texture in color images. *J. Opt. Soc. Am. A.*, 12:1877–1883, 1995.

[5] T. Jaaskelainen, J. Parkkinen, and S. Toyooka. Vector-subspace model for color representation. *J. Opt. Soc. Am. A.*, 7:725–730, 1990.

[6] T. Jaaskelainen, R. Silvennoinen, J. Hiltunen, and J. P. S. Parkkinen. Classification of the reflectance spectra of pine, spruce, and birch. *Applied Optics*, 33:2356–2362, 1994.

[7] R. Kondepudy and G. Healey. Use of invariants for recognition of three-dimensional color textures. *J. Opt. Soc. Am. A.*, 11:3037–3049, 1994.

[8] Y. Manabe, K. Sato, and S. Inokuchi. An object recognition through continuous spectral images. In *Proceedings, 12th International Conference on Pattern Recognition, Jerusalem, Israel*, pages 858–860, 1994.

[9] E. Oja. *Subspace Methods of Pattern Recognition*. Research Studies Press, Letchworth, England, 1983.

[10] D. K. Panjwani and G. Healey. Markov random field for unsupervised segmentation of textured color images. *IEEE Trans. Pattern Anal. Mach. Intell.*, 17:939–954, 1995.

[11] P. P. Raghu, R. Poongodi, and B. Yegnanarayana. A combined neural network approach for texture classification. *Neural Networks*, 8:975–987, 1995.

[12] A. Rosenfeld, C.-Y. Wang, and A. Y. Wu. Multispectral texture. *IEEE Trans. Syst. Man Cybern.*, SMC-12:79–84, 1982.

[13] D. E. Rumelhart, G. E. Hinton, and R. J. Williams. Learning internal representations by error propagation. In D. Rumelhart and J. McClelland, editors, *Parallel Distributed Processing: Explorations in the Microstructures of Cognition*, pages 318–362. MA: MIT Press, Cambridge, 1986.

[14] J. Scharcanski, J. K. Hovis, and H. C. Shen. Representing the color aspect of texture images. *Pattern Recognition Letters*, 15:191–197, 1994.

[15] R. Schettini. A segmentation algorithm for color images. *Pattern Recognition Letters*, 14:499–506, 1993.

[16] T. S. C. Tan and J. Kittler. Colour texture analysis using colour histogram. *IEE Proc.-Vis. Image Signal Process.*, 141:403–412, 1994.

[17] World wide web-page, ftp://ophelia.jpl.nasa.gov/pub/docs/html/aboutav.htm.

Publication 2

HAUTA-KASARI M., PARKKINEN J., JAASKELAINEN T., AND LENZ R.,
Multi-spectral Texture Segmentation Based on the Spectral Cooccurrence Matrix,

In Press.

Multi-spectral Texture Segmentation Based on the Spectral Cooccurrence Matrix

Markku Hauta-Kasari [1], Jussi Parkkinen [2], Timo Jaaskelainen [3], and Reiner Lenz [4]

[1] Department of Information Technology
Lappeenranta University of Technology
P.O.Box 20, FIN-53851 Lappeenranta, FINLAND
Email: Markku.Hauta-Kasari@lut.fi

[2] Department of Computer Science
University of Joensuu
P.O.Box 111, FIN-80101 Joensuu, FINLAND
Email: Jussi.Parkkinen@cs.joensuu.fi

[3] Väisälä Laboratory
University of Joensuu
P.O.Box 111, FIN-80101 Joensuu, FINLAND
Email: Timo.Jaaskelainen@joensuu.fi

[4] Department of Science and Engineering
Campus Norrköping, Linköping University
SE-60174 Norrköping, SWEDEN
Email: reile@itn.liu.se

Short running head: Multi-spectral Texture Segmentation

Correspondence to be sent:

Markku Hauta-Kasari
Department of Information Technology
Lappeenranta University of Technology
P.O.Box 20, FIN-53851 Lappeenranta, FINLAND
Phone: +358 5 624 3430
Fax: +358 5 621 3456
Email: Markku.Hauta-Kasari@lut.fi

Multi-spectral Texture Segmentation Based on the Spectral Cooccurrence Matrix

Abstract

Multi-spectral images are becoming more common in industrial inspection tasks where the colour is used as a quality measure. In this paper we propose a spectral cooccurrence matrix based method to analyse multi-spectral texture images, in which every pixel contains a measured colour spectrum. We first quantise the spectral domain of the multi-spectral images using the Self-Organising Map (SOM). Next we label the spectral domain according to the quantised spectra. In the spatial domain, we represent a multi-spectral texture using the spectral cooccurrence matrix, which we calculate from the labelled image. In the experimental part of this paper, we present the results of segmenting natural multi-spectral textures. We compared the k-nearest neighbour (k-NN) classifier and the multilayer perceptron (MLP) neural network-based segmentation results of the multi-spectral and RGB colour textures.

Keywords

Colour; Cooccurrence matrix; Multi-spectral imaging; Multi-spectral texture; Segmentation; Texture

List of Symbols

Symbol	Definition
Lab	CIELAB colour coordinate system
Luv	CIELUV colour coordinate system
RGB	Red-Green-Blue colour coordinate system
i,j,x,y	Indexes
x	Input vector for SOM
N_c	Neighbourhood in SOM
m	weight vector
α	Learning rate
t	Iteration parameter
$P(i,j)$	Cooccurrence matrix
μ_x	mean
σ_x	Standard deviation
p,q	Pixel spectra in the multi-spectral image
$\Delta x, \Delta y$	Displacement in x- and y-direction
G	Number of grey levels

1. INTRODUCTION

Multi-spectral image analysis is receiving a great deal of attention due to technical developments in imaging devices [1]. In industrial inspection tasks, such as in quality control of products, the importance of colour as a quality measure is growing. Usually, the colour is measured through a few filters, and the colour analysis is made using colour coordinates, which are based on the CIE tristimulus values [2, 3]. In industrial applications, common three-dimensional colour coordinate systems are the Lab-model and the Luv-model, and in colour image representation, the RGB-model is used. The colour analysis based on the three-dimensional colourspaces can sometimes be too restrictive for accurate colour representation. In these cases, the entire colour spectrum is needed to obtain the highest accuracy.

Recently, there has been a lot of interest in colour textures. Tan and Kittler [4] proposed a supervised colour texture classification method, which uses eight Discrete Cosine Transform (DCT) texture features extracted from each of the three RGB colour channels. They have also proposed a method where the three-dimensional colour information and texture information are processed separately [5]. Eight DCT features were calculated [5] from the intensity image, and six colour features were derived from the colour histogram. Recent studies in the field of colour textures of their group can be found in elsewhere [6,7]. Scharcanski, Hovis and Shen [8] used colour codebooks to represent the colour aspect of the colour textures. Kondebudy and Healey [9], Healey and Wang [10] and Panjwani and Healey [11] used Markov models and spatial correlation functions for modelling colour textures.

All of these methods based on the three-dimensional colourspaces give a computationally effective way to process colour images, and their accuracy is enough for many applications. However, there are some restrictions in these models. They can represent only that region of the electromagnetic spectrum (380-780 nm), which is visible to humans. Sometimes, for example, the interesting part of the measurement can be in the near infrared or infrared region of the electromagnetic spectrum. Furthermore, there is a problem of metamerism, where several different spectra may have the same three-dimensional colour coordinate values [12]. In this case, it is possible that humans cannot see the difference between the colour of two metameric objects under a certain illumination, but when the illumination is changed, the difference between the colours of the objects can be seen. Due to these drawbacks of the three-dimensional colour representation, sometimes the whole colour spectrum is needed for accurate colour representation.

The use of imaging spectrometers is growing in remote sensing [13,14], and in industrial quality control [1]. An imaging spectrometer allows accurate measurements of the spectral reflectances over the visible and infrared regions. Such a multi-spectral image has a large number of spectral channels, and can contain information that is not available in the corresponding grey level or RGB image [15]. In AVIRIS-imagery (Airborne Visible/Infrared Imaging Spectrometer), one multi-spectral image consists of 224 spectral channels (400-2450 nm) [16,17]. Also, the industrial use of imaging spectrometers has received growing interest recently [1], and Baronti et al [18] used a visible-infrared multi-spectral imaging system to

analyse works of art. If the multi-spectral imaging system is tuned to measure the visible light in the wavelength range from 380-780 nm, then the measured image represents a high-quality colour image where every pixel contains a colour spectrum. Multi-spectral images are, however, not restricted to the visible band of the electromagnetic spectrum. Other techniques for obtaining images with more accurate colour information are also possible: Tominaga [19] proposed a multi-channel vision system based on the use of a CCD-camera and a few colour filters covering the spectral range from 400-700 nm.

During segmentation, Regions Of Interests (ROI) are extracted from an image. There are two basic approaches to image segmentation. The first approach is based on the discontinuities in an image (edge-based methods), while the second approach is based on the similarities in an image (region-based methods). These methods are usually used for grey level images, and their generalisation for multi-spectral images is not always straightforward. Mathematically, one moves from a one-dimensional space into a multi-dimensional vector space, and discontinuity or similarity in a vector space is not uniquelly defined [20,21]. Examples of RGB image segmentation can be found elsewhere [11,22].

Multi-spectral images have two domains to be analysed: the spectral domain and the spatial domain. In this study, we use a two-phase process to analyse multi-spectral texture images. First we quantise the spectral domain by the use of the Self-Organising Map (SOM) of Kohonen [23]. Next we label the spectral domain according to the quantised spectra. In the spatial domain, a widely used grey level texture representation, a grey level cooccurrence matrix by Haralick, Shanmugan and Dinstein [24], is used for the labelled image to analyse the spatial domain. In our proposed method, the cooccurrence matrix describes the spatial dependency of the quantised spectral domain, and therefore we call it as a spectral cooccurrence matrix. The multi-spectral texture features are constructed by calculating five Haralick features from the cooccurrence matrices. Furthermore we use the spectral cooccurrence matrices themselves as a feature vector [25]. Chang and Wang [26] used the colour cooccurrence matrix-based method to analyse three-dimensional colour textures. They first quantised the colours in an image, labelled the colour domain according to the quantised colours, and then used the colour cooccurrence matrix-based method for the labelled image.

We made experiments with the natural multi-spectral images measured by Parraga et al [27]. In our experiments, we segmented the natural multi-spectral textures by the use of the k-nearest neighbour (k-NN) classifier and the multilayer perceptron (MLP) neural network. The segmentation method described in this paper is region-based, and the experimental results of the natural multi-spectral texture segmentations show that the proposed method can be used to analyse multi-spectral texture images. The results are compared with the segmentation results of the RGB colour textures.

The paper is organised as follows. Section 2 gives a description of quantising the spectral domain. The spectral cooccurrence matrix is described in Section 3, and the segmentation method in Section 4. The experimental results are presented in Section 5. Finally, discussion is given in Section 6.

2. QUANTISATION OF THE SPECTRAL DOMAIN

The spectra of the multi-spectral images are vectors in a high-dimensional pattern space. In our method, we first quantise the spectra into fewer spectra using the SOM [23]. The Self-Organising Maps are based on unsupervised competitive learning, which can be used to cluster the input data. We quantise the spectral domain by training a one-dimensional map, where each weight vector contains a spectrum representing the spectral cluster in the spectral domain. The unsupervised learning can be described as follows. At each learning iteration the winner m_c is a weight vector, which has the closest Euclidean distance to the input vector x:

$$\|x - m_c\| = \min_i \{\|x - m_i\|\}, \tag{1}$$

where i is the index of the weight vectors. The winner m_c is also called a best-matching unit for the input vector x. Next the winner m_c and its topological neighbourhood N_c are updated as follows

$$m_i(t+1) = \begin{cases} m_i(t) + \alpha(t)[x(t) - m_i(t)] & \text{,if } i \in N_c(t) \\ m_i(t) & \text{,otherwise,} \end{cases} \tag{2}$$

where t is the iteration parameter and $\alpha(t)$ is a learning rate, $0 \le \alpha(t) \le 1$. The input data is first normalised to unit norm, and the map is initialised by the centre vector of the input data. In each learning iteration, the training sample is taken randomly from the input data and the learning rate decreases exponentially. The size of the neighbourhood N_c also decreases during learning.

The result of the self-organising process is a map, where the weight vectors m are adapted towards to the characteristic vectors of the spectral clusters in the spectral domain. After learning, the spectral domain is classified using the self-organised map by finding the best-matching unit from the map for each spectrum in the spectral domain.

3. A SPECTRAL COOCCURRENCE MATRIX

The grey level cooccurrence matrix is defined as a joint distribution of the grey levels of two pixels separated by a given displacement [24]. In cartesian coordinates, the displacement of the cooccurrence can be chosen as a vector $(\Delta x, \Delta y)$. The grey level cooccurrence matrix P is defined as

$$P(i,j) = \{\#\,\text{pair}(i,j) \mid \text{image}(x,y) = i \wedge \text{image}(x+\Delta x, y+\Delta y) = j\}\,, \tag{3}$$

where i and j are grey levels. Usually, the cooccurrences are based on the natural lightness-based order of the grey levels. In the multi-spectral images, the pixel values are measured spectra, i.e. vectors, and there is no natural order for them. Rosenfeld, Wang and Wu [28] have proposed a multi-spectral texture analysis method, which is based on two-band features for the textures with vector-valued pixels. Recently, Oja and Valkealahti [29] used multi-dimensional cooccurrence histograms to classify three-dimensional colour textures.

In this paper, the spectral domain of the multi-spectral images is quantised into fewer spectra by the SOM, and then the spectral domain is labelled according to the quantised spectra. In the labeling process, each spectrum in the multi-spectral image is classified to the spectral cluster. As a result, we have an image where each pixel is a scalar value describing the number of the spectral class. The order of the spectral classes is defined as the index number of the weight vectors in the one-dimensional SOM from left to right.

From the labelled image a spectral cooccurrence matrix can be computed. The element (i,j) is now the number of pixel pairs of spectra belonging to spectral class i and j, with a displacement $(\Delta x,\Delta y)$:

$$P(i,j) = \{\#\,\text{pair}(p,q) \mid p(x,y) \in i \wedge q(x+\Delta x, y+\Delta y) \in j\}, \tag{4}$$

where p and q are spectra associated with the pixels at spatial locations (x,y) and $(x+\Delta x,y+\Delta y)$. The spectral cooccurrence matrix contains information on the spatial dependency of the spectral classes in the multi-spectral image. In this study, the unsymmetric spectral cooccurrence matrices are used.

The size of the cooccurrence matrix P is $G \times G$, where G denotes the number of grey levels or spectral classes. To avoid large cooccurrence matrices, the number of grey levels is usually compressed. Typical values for G in grey level texture analysis are from 4 to 32. The number of spectral classes depends upon the quantisation degree, which can be chosen according to the accuracy needed for each application. Haralick, Shanmugam and Dinstein [24] described 14 features extracted from the grey level cooccurrence matrix P. In this study, we use the following five of them:

$$\begin{aligned}
\text{Energy} &= \sum_i \sum_j P^2(i,j), \\
\text{Entropy} &= -\sum_i \sum_j P(i,j) \log P(i,j), \\
\text{Contrast} &= \sum_i \sum_j (i-j)^2 P(i,j), \\
\text{Correlation} &= \sum_i \sum_j \frac{1}{\sigma_x \sigma_y}(i-\mu_x)(j-\mu_y)P(i,j), \\
\text{Homogeneity} &= \sum_i \sum_j \frac{P(i,j)}{1+|i-j|},
\end{aligned} \tag{5}$$

where μ_x, μ_y, σ_x and σ_y are the means and the standard deviations of the rows and columns of P, respectively. The cooccurrence matrices can be computed with different displacements, and the features of these matrices can be combined for the classification process.

The features described in Eq. (5) have been defined to represent the grey level cooccurrence matrix. In the case of the spectral cooccurrence matrix, the meaning of some features in Eq. (5) is different. The most critical features are contrast, correlation and homogeneity, where the feature calculation depends upon the ordering of indices i and j. Grey levels have natural lightness based ordering, but there is no natural ordering for the measured spectra. However,

the order of the spectral clusters produced by the SOM is self-organised, and it may be a promising method for ordering the spectral type data.

The cooccurrence matrix itself can be used as a feature vector by stacking it row by row into a vector [25]. This feature vector represents the second-order statistics of the texture, and there is only a little loss of information when going from raw image data to the texture representation. In the case of a stacked spectral cooccurrence matrix, the ordering of the spectral classes does not have so critical a meaning when compared to the feature calculation in Eq. (5).

4. MULTI-SPECTRAL TEXTURE SEGMENTATION

In our experiments, the texture features extracted from the spectral cooccurrence matrix are classified by the k-nearest neighbour (k-NN) classifier, and by the multilayer perceptron (MLP) neural network. Raghu, Poongodi and Yednanarayana [30] have used the MLP to classify Gabor features in the grey level texture segmentation. The MLP used in our study consists of an input layer, one hidden layer and an output layer. Input vectors are texture feature vectors and outputs are desired classes. The network training is done by the backpropagation algorithm [31]. In feature classification, the aim is to divide the input feature space into regions. We use the MLP to classify the input feature space, and therefore the use of one hidden layer was chosen. In the hidden layer and in the output layer, the logistic sigmoidal activation functions were used. The number of neurons in the hidden layer was decided by analysing the number of training samples versus the number of free parameters in the MLP.

Generalisation is an important property of MLP which depends upon the number of training epochs and the number of neurons in the hidden layer. Usually, it is easy to get a low error rate for a training set when the training process is continued. However, this can lead to overtraining, i.e. the test set error may actually start to increase after a certain number of training steps. To avoid overtraining, we approximate the early stopping of the training process by the cross-validation method [32].

The training process is performed as follows. First, the training set is created by randomly taking image windows from each multi-spectral texture used in our experiments. Then the spectral domain is quantised by the SOM, the spectra is classified to spectral clusters, and the spectral domain is labelled. Next the feature vectors are calculated from the spectral cooccurrence matrices, which are constructed for each training image window. The MLP is trained with these feature vectors with known classification.

At the beginning of the multi-spectral texture segmentation, the spectral domain of the test image is labelled according to the spectral quantisation, which was performed in the training phase. Next, the test image is segmented by gliding an image window from the left upper corner to the right lower corner, and in each window position the spectral cooccurrence matrix is computed, and the feature vector is calculated and classified by the MLP. Each pixel inside an image window is marked to belong to the same class.

The training process based on the stacked spectral cooccurrence matrix includes the training set extraction and the spectral domain quantisation of the multi-spectral texture, which are done as before. The texture feature vectors are now constructed by stacking the spectral cooccurrence matrix of each training texture row by row into a vector. The segmentation phase is done as before, except that the stacked spectral cooccurrence matrices are used as multi-spectral texture features.

5. EXPERIMENTS

5.1. Natural Multi-spectral Images

We experimented with the natural multi-spectral image database measured by Parraga et al [27]. The database consists of 29 multi-spectral images measured by a hyperspectral camera system from the natural scenes including plants, flowers, trunks, branches, grass, leaves, trees, bushes, rocks and sky. The multi-spectral images are measured using 31 narrow-band interference filters, which cover the visible wavelength range from 400-700 nm at 10nm intervals. Each multi-spectral image contains a total of 31 monochrome 256×256 pixel images, where the spectral reflectances are stored as 8 bits/pixel format. The database also contains the same natural images as RGB colour images. A detailed description of the hyperspectral database can be found elsewhere [27].

From the database we extracted four 128×128 pixel multi-spectral images, which contained textured regions of green grass, trunk, rock and green grass with yellow leaves. We combined these parts into one 256×256 multi-spectral texture mosaic, which is shown as an RGB-image in Fig. 1. Every pixel in the multi-spectral texture mosaic contains a 31-component colour spectrum in the wavelength range from 400-700nm at 10nm intervals. The segmentation problem is to divide the multi-spectral texture mosaic into four regions.

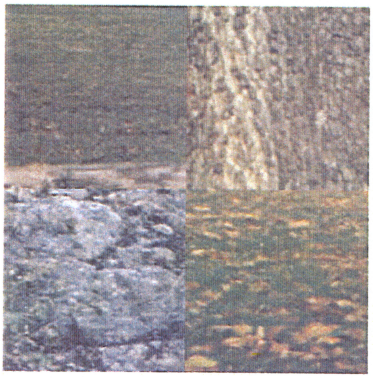

Fig. 1. Multi-spectral texture mosaic as a RGB image.

5.2. Segmentation

A. Training Data

From each of the 128 × 128 pixel multi-spectral images that were used to make the multi-spectral texture mosaic, 30 randomly located 16 × 16 multi-spectral texture windows were taken as training data. The window size of 16 × 16 pixels was decided empirically according to the appearance of the texture in the images. It is possible to extract 64 non-overlapping 16 × 16 windows from the 128 × 128 pixel image, but because we extract the training data from the same images that will be segmented, the locations were chosen randomly to avoid a strong correlation between the training and test data. The number of windows was chosen as 30 to avoid serious overlapping of the randomly selected windows.

B. Spectral Domain Quantisation

These multi-spectral texture windows contained a total of 30,720 spectra of 31 components in each spectrum. The 30,720 spectra were normalised to unit norm, and quantised by the one-dimensional SOM. In the SOM we used 10 units, which means that the spectral domain is quantised into 10 levels. The size of the SOM was decided to be small enough to avoid large spectral cooccurrence matrices. We used 40,000 iterations to train the Self-Organising Map. The learning rate was decreasing exponentially from the initial value of 1 towards 0. Also, the size of the topological neighbourhood of the best-matching unit was decreasing exponentially from a value of 9 so that after 4000 iterations it was 1. In the series of experiments, we noticed that the map was approximately organised after 20,000 iterations, but we fine-tuned the map until 40,000 iterations to obtain the final map organisation.

After unsupervised learning, the weight vectors of the SOM are the characteristic vectors for the spectral clusters. Next, the spectral domain of the training samples was classified into the spectral clusters by the use of the self-organised map by finding the best-matching unit from the map for each spectrum in the spectral domain. The spectral domain was labelled according to the index numbers of the best-matching units in SOM. The spectral domain of the multi-spectral texture mosaic was classified and labelled in the same way. Figure 2 (a) shows the result of the spectral domain quantisation as a grey level image with 10 grey levels. We also compared the results with the RGB colour-based quantisation results. The same textures were loaded as RGB colour images, and the training data was extracted at the same locations as before. Then a total of 30,720 RGB colour coordinates were quantised into a one-dimensional SOM, and the colour domain of the RGB texture mosaic was classified and labelled. Figure 2 (b) shows the result of the colour domain quantisation of the RGB texture mosaic as a grey level image with 10 grey levels.

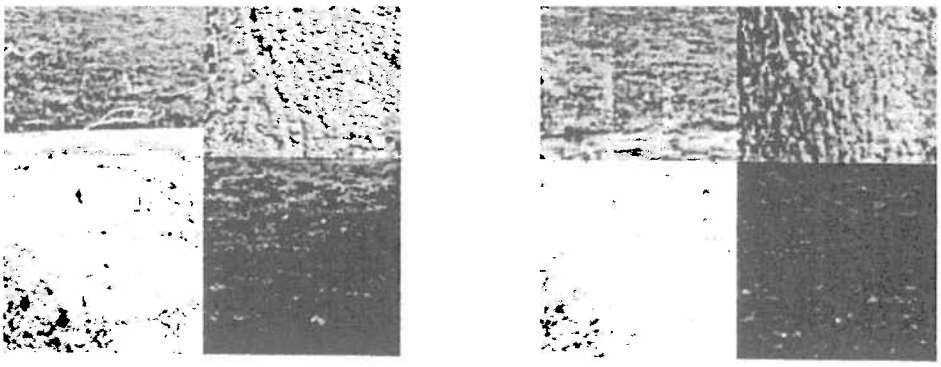

a) b)

Fig. 2. Quantisation results of the spectral domain. (a) Multi-spectral texture mosaic, (b) RGB texture mosaic.

C. Feature Extraction and Segmentation

Next the 10×10 spectral cooccurrence matrices were calculated from each of 120 multi-spectral textures used in the training data. Several displacements of the spectral cooccurrence matrix were tested, and the right neighbour in the horizontal direction was selected. The feature vectors for each spectral cooccurrence matrix were constructed by calculating five Haralick features described in Eq. (5). The feature vectors were normalised to unit norm. Then the multi-spectral texture mosaic was segmented by gliding the 16×16 window over the image at 4 pixel intervals. In each window position, the 10×10 spectral cooccurrence matrix was computed, five Haralick features were calculated, and the feature vector was normalised to unit norm. The feature vector was classified by the use of the k-nearest neighbour (k-NN) classifier. We found that the feature classes were chain-shaped in the feature space, and therefore the value of $k = 1$ was used. Figure 3 (a) shows the k-NN classifier based segmentation result of the multi-spectral texture mosaic. The percentage of the correctly classified pixels is 62.6 %.

The same was done for the RGB colour textures. The training textures were the same as before, and the features were calculated from the colour cooccurrence matrices, which are defined as a joint distribution of the quantised RGB colour clusters of two pixels separated by a given displacement. Also in this experiment, the image was segmented by gliding the 16×16 pixel segmentation window over the image at 4 pixel intervals. Figure 3 (b) shows the k-NN classifier-based segmentation result of the RGB texture mosaic. The percentage of the correctly classified pixels is 66.0 %.

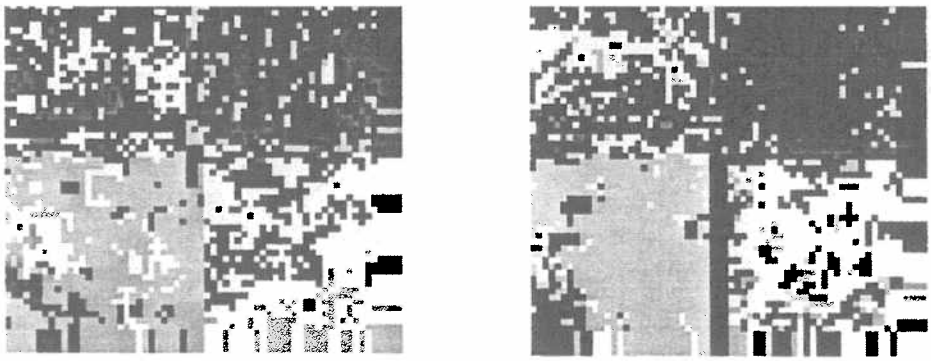

a) b)

Fig. 3. Segmentation results by the use of a 1-NN classifier. (a) Multi-spectral texture mosaic, (b) RGB texture mosaic.

Then we segmented the multi-spectral and RGB texture mosaics using MLP. The MLP was trained with the same training data that was used in the previous experiment. The MLP had five inputs, seven hidden neurons and four outputs (four classes). The number of free parameters in the MLP is now 74, and the number of equations (training samples) is 120. It is possible that more hidden neurons can give better results, but when the number of free parameters in the MLP is increased, it can lead to overtraining. The MLP was trained by the backpropagation algorithm, where the number of suitable training iterations was analysed by the cross-validation method. In the cross-validation we divided the training data randomly into a training set and a cross-validation set. The training set, which contained 80 samples, was trained by the MLP, and in each iteration step the neural network was tested by the cross-validation set, which contained 40 samples. The error for the cross-validation set started to grow after 1500 iterations, while the error of the training set was still decreasing. This means that the neural network was overlearning after 1500 iterations, and this iteration value was used to stop the training of the MLP.

The multi-spectral texture mosaic was segmented by gliding the 16×16 window over the image at 4 pixel intervals. In each window position, the 10×10 spectral cooccurrence matrix was computed, five Haralick features were calculated, and the feature vectors were normalised to unit norm. The feature vector was classified by the MLP, and each pixel inside an image window was marked as belonging to the same class. Figure 4 (a) shows the segmentation result of the multi-spectral texture mosaic. The percentage of correctly classified pixels is 67.1 %. Next, the same MLP was trained for the RGB data, and the RGB texture mosaic was segmented by gliding the 16×16 pixels window over the image at 4 pixel intervals. The number of iterations used in the training was analysed by cross-validation, and the value of 6500 iterations was used. Figure 4 (b) shows the MLP based segmentation result of the RGB texture mosaic. The percentage of correctly classified pixels is 69.0 %.

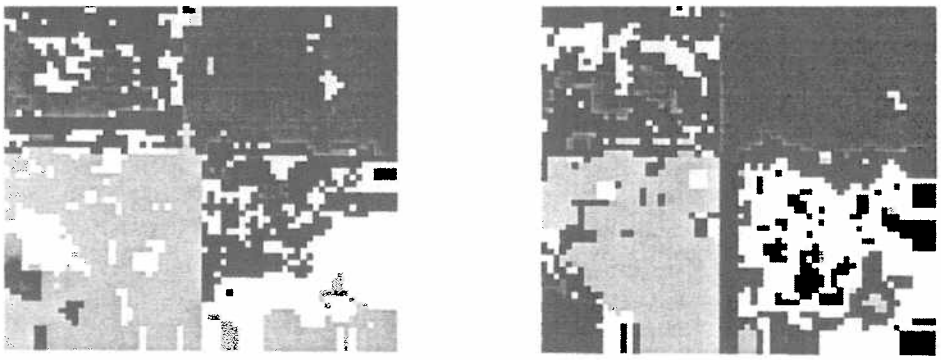

a) b)

Fig. 4. Segmentation results by the use of the MLP. (a) Multi-spectral texture mosaic, (b) RGB texture mosaic.

Finally, we carried out experiments by using the spectral cooccurrence matrix itself as a feature. The training textures were the same as in the previous experiments. The segmentations were done as in the previous tests, except that the 10×10 spectral cooccurrence matrices were stacked row by row into a 100×1 vector, and these were normalised to unit norm. Figure 5 (a) shows the 1-NN-based segmentation result of the multi-spectral texture mosaic, when the spectral cooccurrence matrix itself was used as a feature. In this result, the percentage of correctly classified pixels is 92.9 %.The same was done for the RGB textures. Now the 10×10 colour cooccurrence matrices were stacked row by row into a 100×1 vector, and the segmentation was done by the 1-NN classifier. Figure 5 (b) shows the result of the 1-NN-based segmentation of the RGB texture mosaic. The percentage of the correctly classified pixels is 91.6 %.

We collected the results of the experiments in Table 1. It shows the percentages of the correctly classified pixels in each experiment. A discussion on the results is given in the next section.

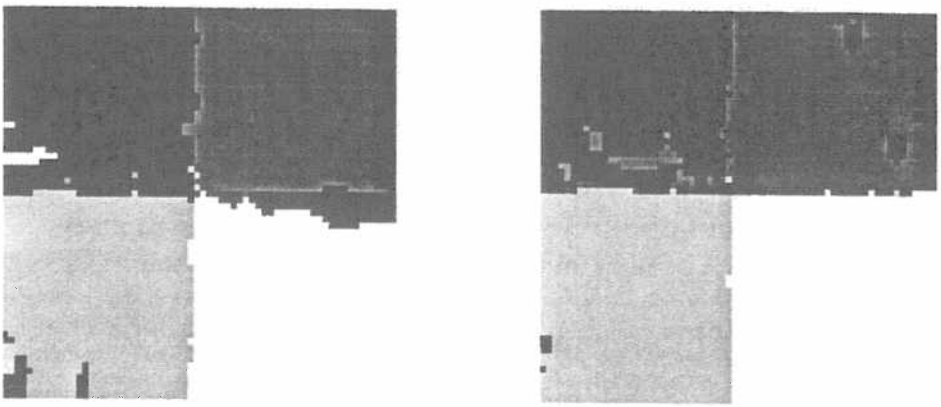

a) b)

Fig. 5. Segmentation results by the use of a 1-NN classifier, stacked cooccurrence matrices were used. (a) Multi-spectral texture mosaic, (b) RGB texture mosaic.

Table 1. Percentages of correctly classified pixels in the RGB colour texture segmentation and in the multi-spectral texture segmentation.

Method	RGB colour texture	Multi-spectral texture
1-NN, Haralick features	66.0 %	62.6 %
MLP, Haralick features	69.0 %	67.1 %
1-NN, stacked cooccurrence matrices	91.6 %	92.9 %

6. DISCUSSION

We have proposed a method for multi-spectral texture segmentation which is based on the spectral cooccurrence matrix. This matrix contains information about the spectral and spatial domains, and it can be used to analyse textures with vector valued pixels. The use of this method in colour image processing and in remote sensing is straightforward.

The grey level cooccurrence matrix of a grey level image captures the second order statistics of the original pixels based on their grey values. According to the approach of this paper, the grey values can be seen as spectral classes of the multi-spectral image. The spectral cooccur-

rence matrix has been expanded to represent the high-dimensional spectral data. Between the grey levels and the quantised spectral classes there is a clear difference. The grey levels have a natural order, but in the case of the spectral classes, the order is not so clear. In the proposed method we used the Self-Organising Map to quantise the spectral domain. The order of the weight vectors in SOM is self-organised, and therefore it may be a promising method to approximate the natural order of the spectral type data.

After quantisation of the spectra, which were normalised to unit norm, the image was labelled according to the quantised spectra. The labelled images are shown in Fig. 2, where the labels of the spectral classes are shown as grey levels. From the spectral domain quantisation results shown in Fig. 2, an interesting phenomenon can be seen. The quantised spectral domain of the multi-spectral texture mosaic in Fig. 2 (a) shows some objects which are difficult to recognise from the original colour image shown in Fig. 1. For example, the branches lying on a grass field in the left upper texture can be seen clearly from the quantised image. Also, the right upper texture of a trunk seems to be histogram equalised. In the original colour image shown in Fig. 1, the left part of the trunk is much brighter than the right part, but the quantised image has a smooth variance over the image. From the RGB colour texture mosaic quantisation results shown in Fig. 2 (b) the same phenomenon cannot be seen.

The multi-spectral texture features were constructed by calculating five Haralick features, and also the cooccurrence matrix itself was used as a feature. The disadvantage of our Haralick feature-based texture segmentation is that the classification is performed in the feature space constructed by energy, entropy, contrast, correlation and homogeneity features. Some of these location-dependent features have a different meaning in the case of the spectral cooccurrence matrix, because of the non-uniquely defined ordering of the spectral clusters. If the spectral cooccurrence matrix itself is used as a feature vector, without calculating the Haralick features, then the feature space contains more information about the spatial dependency of the spectral clusters. In this case, the order of the spectral clusters does not have as critical a meaning as in the case of Haralick's features. Especially in the segmentation problem, if the cooccurrence matrix has to be computed from a small texture window, and also if the dimension of the cooccurrence matrix is small, then the sparse cooccurrence matrix itself has more information than the five Haralick features computed from the cooccurrence matrix. However, when the dimension of the cooccurrence matrix is large, it is more suitable to use Haralick's features, because the dimension of the stacked cooccurrence matrix can be too large for the computationally effective segmentation process.

We compared the texture segmentations with the k-NN and MLP-based methods. Both of them were suitable for our method. The segmentation results between the RGB colour textures and multi-spectral textures were similar. The results were improved by using the spectral cooccurrence matrix itself as a feature, without calculating the Haralick features. The segmentation window was moved by 4 pixel intervals, which was chosen empirically. In general, if the curved edges between the regions in an image are needed, then the segmentation window must be moved by a few pixel intervals, while in the case of horizontal and vertical edges, the segmentation window can be moved by larger steps. Figure 2 shows that the spectral image contains more information than the RGB image. This advantage of accurate colour information seems to be partly lost in spatial analysis by the cooccurrence matrix in our test

images. In the images that are similar to each other, the difference between the methods is expected to be larger. The quantised multi-spectral image shows very detailed regions of the spectral image, but in the texture analysis we cannot say anything about one single pixel; a larger region is always needed for the appearance of the texture.

The real-time performance of the proposed method is important in industrial tasks. Our method can be partly implemented optically: after training the SOM, the spectral domain quantisation can be calculated optically using a Liquid Crystal Spatial Light Modulator (LCSLM) [33]. Recently, Allam, Adel and Refregier [34] proposed a fast implementation to discriminate textures by the use of an orthonormal decomposition of the cooccurrence matrix.

From our investigations, we conclude that in the natural colour textures used in this study, the appearance of the texture was not strongly dependent upon the accuracy of the colour representation used. However, in the pure colour analysis, the clear advantage of the spectral information can be seen from Fig. 2 (a). There are still unanswered questions in this paper which need further study: experiments with a larger set of multi-spectral textures and with possible metameric textures should be done. Also, the spectral cooccurrence matrices could be computed with different displacements, and their features could be combined for the classification process. The choice of the correct number of colour classes and the segmentation window size, which both have an effect on the cooccurrence matrix statistics, should also be investigated more carefully. In this study, we used multi-spectral images in the visible range so that the segmentation results can be compared with RGB images. In the future research, the images measured outside the visible light area will be experimented on. The main results of the proposed spectral cooccurrence matrix based method compared to the three-dimensional colour texture analysis methods are that the proposed method can be used to recognise metameric colour textures and multi-spectral textured images, which are measured outside the visible part of the electromagnetic spectrum.

References

[1] Hyvarinen T, Herrala E, Dall'Ava A. Direct sight imaging spectrograph: an unique add-on component brings spectral imaging to industrial applications. Proceedings of the IS&T/SPIE's Symposium on Electronic Imaging: Science and Technology, 1998; 3302-21

[2] Kaiser PK, Boynton RM, Human Color Vision (2nd ed). Optical Society of America, Washington DC, 1996

[3] Wyszecki G, Stiles WS, Color Science : Concepts and Methods, quantitative data and formulae, Wiley, New York, 1982

[4] Tan TSC, Kittler J. On colour texture representation and classification. Proceedings 2nd International Conference on Image Processing, 1992; 390-395

[5] Tan TSC, Kittler J. Colour texture classification using features from colour histograms. Proceedings 8th Scandinavian Conference on Image Analysis, 1993; 807-813

[6] Tan TSC, Kittler J. Colour texture analysis using colour histogram. IEE Proc Vis. Image Signal Process 1994; 141(6): 403-412

[7] Messer K, Kittler J. A comparison of colour texture attributes selected by statistical feature selection and neural networks methods. Pattern Recognition Lett 1997; 18(13): 1241-1246

[8] Scharcanski J, Hovis JK, Shen HC. Representing the color aspect of texture images. Pattern Recognition Lett 1994; 15(2): 191-197

[9] Kondepudy R, Healey G. Use of invariants for recognition of three-dimensional color textures. J Optical Society of America A 1994; 11(11): 3037-3049

[10] Healey G, Wang L. Illumination-invariant recognition of texture in color images. J Optical Society of America A 1995; 12(9):1877-1883

[11] Panjwani DK, Healey G. Markov random field for unsupervised segmentation of textured color images. IEEE Trans Pattern Analysis and Machine Intelligence 1995; 17(10): 939-954

[12] Drew MS, Funt BV. Natural metamers. CVGIP: Image Understanding 1992; 56(2): 139-151

[13] Ramasamy SM, Venkatasubrmanian V, Anbazhagan S. Reflectance spectra of minerals and their discrimination using Thematic Mapper, IRS and SPOT multi-spectral data. Int J Remote Sensing 1993; 14(16): 2935-2970

[14] Richards JA. Remote Sensing Digital Image Analysis: An introduction. Springer-Verlag, Berlin, 1993

[15] Manabe Y, Sato K, Inokuchi S. An object recognition through continuous spectral images. Proceedings 12th International Conference on Pattern Recognition 1994; 1: 858-860

[16] World Wide Web: ftp://ophelia.jpl.nasa.gov/pub/docs/html/aboutAV.htm

[17] Chen PF, Tran TC. Hyperspectral imagery classification using a backpropagation neural network. Proceedings International Conference on Neural Networks 1994; 1: 2942-2947

[18] Baronti S, Casini A, Lotti F, Porcinai S. Multispectral imaging system for the mapping of pigments in works of art by use of principal component analysis. Applied Optics 1998; 37(8): 1299-1309

[19] Tominaga S. Multichannel vision system for estimating surface and illumination functions. J Optical Society of America A 1996; 13(11): 2163-2173

[20] Machuca R, Phillips K. Applications of vector fields to image processing. IEEE Trans Pattern Analysis and Machine Intelligence 1983; 5(3): 316-329

[21] Cumani A. Edge detection in multi-spectral images. CVGIP: Graphical Models and Image Processing 1991; 53(1): 40-51

[22] Schettini R. A segmentation algorithm for color images. Pattern Recognition Lett 1993; 14(6): 499-506

[23] Kohonen T. The Self-Organizing Maps, Springer-Verlag, Berlin, Heidelberg, 1995

[24] Haralick RM, Shanmugam K, Dinstein I. Textural features for image classification. IEEE Trans Systems, Man, and Cybernetics 1973; SMC-3(6): 610-621

[25] Oja E, Parkkinen J. Texture subspaces. In: Devijver PA, Kittler J (eds). Pattern Recognition Theory and Applications. Springer-Verlag, Berlin, Heidelberg, 1987; 21-27

[26] Chang CC, Wang LL. Color texture segmentation for clothing in a computer-aided fashion design system. Image and Vision Computing 1996; 14(9): 685-702

[27] Parraga CA, Brelstaff G, Troscianko T, Moorehead IR. Color and luminance information in natural scenes. J Optical Society of America A 1998;15(3): 563-569

[28] Rosenfeld A, Wang CY, Wu AY. Multi-spectral texture, IEEE Trans Systems, Man, and Cybernetics 1982; SMC-12(1): 79-84

[29] Oja E, Valkealahti K. Co-occurrence map: Quantising multidimensional texture histograms. Pattern Recognition Lett 1996;17(9): 723-730

[30] Raghu PP, Poongodi R, Yednanarayana B. A combined neural network approach for texture classification. Neural Networks 1995; 8(6): 975-987

[31] Rumelhart DE, Hinton GE, and Williams RJ. Learning internal representations by error propagation. In: Rumelhart DE, McClelland JL (eds). Parallel Distributed Processing: Explorations in the Microstructures of Cognition, Vol. 1. MIT Press, Cambridge, MA, 1986; 318-362

[32] Haykin S, Neural Networks, Macmillan, New York, 1994

[33] Jaaskelainen T, Toyooka S, Izawa S, Kadono H. Color classification by vector subspace method and its optical implementation using liquid crystal spatial light modulator. Optics Comm 1992; 89(1): 23-29

[34] Allam S, Adel M, Refregier P. Fast algorithm for texture discrimination by use of a separable orthonormal decomposition of the co-occurrence matrix. Applied Optics 1997; 36(32): 8313-8321.

Biographies

Markku Hauta-Kasari was born in 1970 in Sukeva, Finland. He received a MSc degree in computer science from the University of Kuopio in 1994. Since 1995 he has been working at the Department of Information Technology, Lappeenranta University of Technology, Finland, as an assistant. He is a postgraduate student on the doctor-course. From 1996 to 1998, he was a visiting researcher at the Optical Sensing Laboratory, Graduate School of Science and Engineering, Saitama University, Japan. His research interests include colour research, computer vision, pattern recognition, neural networks and optical pattern recognition. He is a member of the Optical Society of Japan and Pattern Recognition Society of Finland.

Jussi Parkkinen was born in 1953 in Mikkeli, Finland. He received his MSc in medical physics in 1982 and his PhD in mathematics in 1989, from the University of Kuopio, Finland. From 1989 to 1990 he was with the University of Iowa, USA as visiting researcher. In 1990-1992 he was with the University of Kuopio as a research scientist and acting professor. From 1992 to 1998 he was with the Lappeenranta University of Technology, Finland as associate professor and professor. Presently, he is a professor in computer science at the University of Joensuu, Finland. His research interests include colour image analysis, pattern recognition and molecular computing.

Timo Jaaskelainen was born in 1953 in Luumäki, Finland. He received the PhD degree in 1981 in physics from the University of Joensuu, Finland. From 1981 to 1991 he was working at the University of Kuopio as a chief assistant, and acting associate professor. In 1987-1989 he was visiting research scientist at the Saitama University, Japan. In 1991, he joined the Department of Physics, University of Joensuu, Finland, as an associate professor. Since 1994 he has been a professor at the same department. He is also the head of department. His research interests include optical materials research, optical metrology, colour research and information optics. Professor Jaaskelainen has published about 100 articles. He is a member of Optical Society of America.

Reiner Lenz is associate professor in the media group at the Department of Science and Technology, Campus Norrköping, Linköping University, Sweden. He received a diploma in mathematics from the University in Göttingen, Germany and a PhD degree in computer engineering from Linköping University. From 1979 to 1982 he was with the Image Processing Group at the University in Stuttgart, Germany, and from 1983 to 1997 with the Image Processing Laboratory at Linköping University. He held visiting appointments at the ZEISS Central Research and Development Department, Oberkochen, Germany, the Advanced Telecommunications Research (ATR) Institute, Kyoto, Japan, the Mechanical Engineering Laboratory, Tsukuba, Japan, and at Rutgers University, USA. He received an honorable mention for the Pattern Recognition Society Award and the SAAB-Combitech award for his work in image processing. He is interested in the application of group theoretical methods in signal processing and colour and multi-spectral image processing.

Publication 3

LENZ R., MEER P., AND HAUTA-KASARI M.,
Spectral-Based Illumination Estimation and Color Correction,

COLOR

research and application

Endorsed by Inter-Society Color Council

The Colour Group (Great Britain)

Color Science Association of Japan

Dutch Society for the Study of Color

The Swedish Colour Centre Foundation

Colour Society of Australia

Centre Français de la Couleur

VOLUME 24 NUMBER 2 APRIL 1999

WILEY
Publishers Since 1807

ISSN 0361-2317
CREADU 24(2) (1999)

Spectral-Based Illumination Estimation and Color Correction

Reiner Lenz,[1]* Peter Meer,[2] Markku Hauta-Kasari[3†]

[1] Image Processing Laboratory, Dept. Electrical Engineering, Linköping University, S-58183 Linköping, Sweden

[2] Dept. Electrical and Computer Engineering, Rutgers University, Piscataway, New Jersey 08855-0909

[3] Graduate School of Science and Engineering, Saitama University, 255 Shimo-okubo, Urawa, Saitama 338, Japan

Received 13 November 1997; revised 30 April 1998; accepted 8 September 1998

Abstract: We present a statistical technique to characterize the global color distribution in an image. The result can be used for color correction of a single image and for comparison of different images. It is assumed that the object colors are similar to those in a set of colors for which spectral reflectances are available (in our experiments we use spectral measurements of the Munsell and NCS color chips). The logarithm of the spectra can be approximated by finite linear combinations of a small number of basis vectors. We characterize the distributions of the expansion coefficients in an image by their modes (the most probable values). This description does not require the assumption of a special class of probability distributions and it is insensitive to outliers and other perturbations of the distributions. A change of illumination results in a global shift of the expansion coefficients and, thus, also their modes. The recovery of the illuminant is thus reduced to estimating these shift parameters. The calculated light distribution is only an estimate of the true spectral distribution of the illuminant. Direct inverse filtering for normalization may lead to undesirable results, since these processes are often ill-defined. Therefore, we apply regularization techniques in applications (such as automatic color correction) where visual appearance is important. We also demonstrate how to use this characterization of the global color distribution in an image as a tool in color-based search in image databases. © 1999 John Wiley & Sons, Inc. Col Res Appl, 24, 98–111, 1999

Key words: color correction; color constancy; principal components; robust statistics

INTRODUCTION

A color image is always the result of a complex interaction between three different components: the optical properties of the scene, the illumination sources, and the sensors. Estimating the influence of these three factors on the measured signals is one of the main goals of color image analysis. The influence of the sensors is usually known, and the remaining problem is to separate the effects of the scene properties and the influence of the illumination. The human visual system can approximately solve this problem, a phenomenon known as color constancy (see Ref. 1 for an introduction and references). The problem is also actively pursued in computer vision and image processing, but a satisfactory solution for real world conditions is yet to be found.[2–18]

In this article, we describe the overall color distribution in an image (or an image-patch) as follows. First the color of a single point in an image is defined by the logarithm of its spectrum. This log-spectrum is then approximated by the first few terms in a series expansion. The coefficients are computed for all points under consideration and for each

[†]Current address: Department of Information Technology, Lappeenranta University of Technology, P.O. Box 20, Fin-53851 Lappeenranta, Finland

* Correspondence to: R. Lenz, Department of Science and Engineering, Campus Norrköping, Norrköping University, SE-60174 Norrköping, Sweden

Contract grant sponsor: National Science Foundation; Contract grant number: IRI-9530546

Contract grant sponsor: Swedish Institute International Research Fellowship

Contract grant sponsor: Swedish Research Council for Engineering Sciences

Contract grant sponsor: Wihuri Foundation

Contract grant sponsor: Finnish Cultural Foundation/South Karelia Foundation

TABLE I. The relative mean approximation error.

Order N	Error $\hat{E}_N$	Error log coordinates E_N
1	28.7639	34.5235
2	13.5956	15.9981
3	6.6864	7.9114
4	4.7054	6.3125
5	3.4572	5.2342
6	2.9545	4.4786
7	2.4831	3.6910
8	2.1312	3.3019
9	1.6335	3.0091
10	1.2080	2.3878
11	0.9910	2.2866
12	0.7635	1.6729
13	0.6565	1.6152
14	0.5690	1.5403
15	0.4471	0.9986

coefficient the statistical distribution is characterized by its mode, i.e., its most probable value. The properties and the performance of the description will be demonstrated with some examples, where we apply it to color image normalization and color texture characterization.

In our image formation model, we assume that the spectral distribution $M(\lambda, x)$, measured at location x in the image can be written as $M(\lambda, x) = R(\lambda, x) \cdot L(\lambda)$, where $R(\lambda, x)$ is the reflectance function at that location and $L(\lambda)$ the spectrum of the light-source. Using the logarithm, a linear relation, $m(\lambda, x) = r(\lambda, x) + l(\lambda)$, is obtained. Note that the lighting is assumed to be uniform across the investigated part of the image. Here we do not model more complicated interactions between the scene, the illumination, and the sensors such as body-reflection or fluorescence.[19,20] Expressing the functions m, r and l in the same coordinate system spanned by functions $b_k(\lambda)$, we obtain the following series expansions:

$$m(\lambda, x) = \sum_k \mu_k(x) b_k(\lambda),$$

$$r(\lambda, x) = \sum_k \rho_k(x) b_k(\lambda), \quad l(\lambda) = \sum_k \alpha_k b_k(\lambda). \quad (1)$$

Thus, for a given k we obtain

$$\mu_k(x) = \rho_k(x) + \alpha_k, \quad (2)$$

i.e., the effect of the illuminant on the k-th expansion coefficient of the log-reflectance function is a location independent, constant shift. The coordinate system used in this article is based on an eigenvector expansion and will be described later.

In our applications, we will not use Eq. (2) pointwise, i.e., for individual positions x, but we will use the fact that the probability distributions of the coefficients $\mu_k(x)$ and $\rho_k(x)$ are related by the shift coefficient α_k. The value of α_k can, thus, be estimated by comparing the two probability distributions or parameters derived from them. In this article, we choose to describe probability distributions by their modes, i.e., their most probable value. The use of the mode is motivated by the need for a robust location estimator. We want to extract the "center" of the distribution for each coefficient. Using maximum likelihood would implicitly assume that the underlying distribution is normal, which is probably not the case for real data. The mode is insensitive to both skew and more, importantly, long tails (outliers) of the distribution. Note that the median (another robust location estimator) will be biased for a skewed or long tailed distribution. Modeling such distributions as a mixture of Gaussians makes the analysis cumbersome. The mode, on the other hand, can be computed by a simple algorithm, essentially a window sliding over the data. It can be shown that for unimodal distributions the result remains correct even when almost half the data is distributed along one of the tails. The mode is a maximum *a posteriori* (MAP) estimator, since it corresponds to the maximum of the p.d.f. of the given data.

Among the possible applications of Eq. (2) we mention the following:

- Color constancy: If the modes of the distributions of the coefficients μ_k and ρ_k are known, then the value of α_k and, thus, an estimation of the light source spectrum $L(\lambda)$ can be computed. The modes of the ρ_k distributions might be known from previous experience or, in the case of a dynamically changing illumination, they could be known from an estimation computed from a previous image.
- Image normalization: A desired global color impression of a color-corrected image can be obtained through a definition of the modes of ρ_k.
- Color description: In image database searches, it is often useful to find images with a given overall color impression. In this case, the modes of the ρ_k distributions are used as origin and the values of α_k characterize the color distribution in the image. We will later introduce the

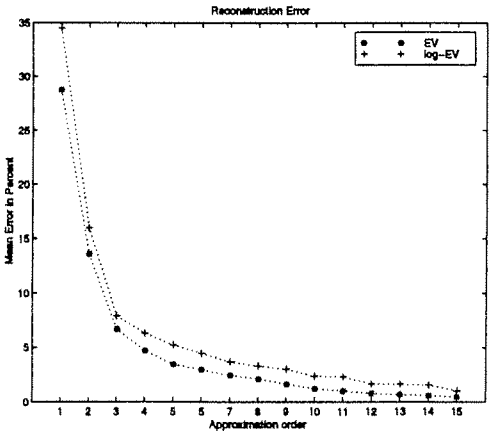

FIG. 1. Error function of the approximation order.

TABLE II. Modes from database and gray world assumption.

Eigenvector number	Mode database	Coefficient gray world
1	−9.1353	−9.7295
2	1.3931	1.0771
3	−0.5151	−0.2446
4	−0.0130	−0.1857
5	−0.1320	−0.0849
6	−0.1106	−0.0093
7	−0.2579	−0.0509
8	0.1048	0.0767
9	0.1099	0.0799
10	−0.2045	−0.1047
11	−0.0394	−0.0105
12	0.1370	0.0806
13	0.0134	0.0096
14	−0.0439	−0.0110
15	0.1156	0.0508

concept of a relative illuminant and describe how to use it for color image retrieval.

The rest of the article is organized as follows: In Section 2, we describe how the basis functions $b_k(\lambda)$ are computed and we investigate the properties of the resulting coordinate system. In almost all applications, the spectral description of the color at a point in an image is not available. A conversion from the given color system to the spectral description is, therefore, necessary before the basic algorithm can be applied. In Section 3, we discuss this conversion for the case where the pixels are RGB-vectors. Section 4 describes the estimation of the illumination light spectrum, and Section 5 its application in the restoration or compensation of the color shift. Section 6 discusses some useful postprocessing techniques, and the last section illustrates the results of some experiments.

BASIC ALGORITHM

Since human color perception is based on three different receptor types in the retina, the traditional approach towards color is to use three-dimensional coordinate systems. Each of these systems was designed for a certain type of application, and a substantial part of color science deals with the study of their properties and the conversion procedures among them. Examples are color monitors (RGB), color printing (CMY), computer vision and computer graphics (IHS), and the colorimetry (CIE-systems) such as Lab, Luv, etc. For exact definitions and descriptions see Refs. 21 and 22. None of the systems is especially suited for investigation of color constancy algorithms, because a change in the spectral characteristics of the illumination source often leads to complicated transformations in the 3-D coordinate space.

Our approach is based on the assumption that the space of electro-magnetic spectra, which is relevant for human color vision, can be described by a set of the order of a few

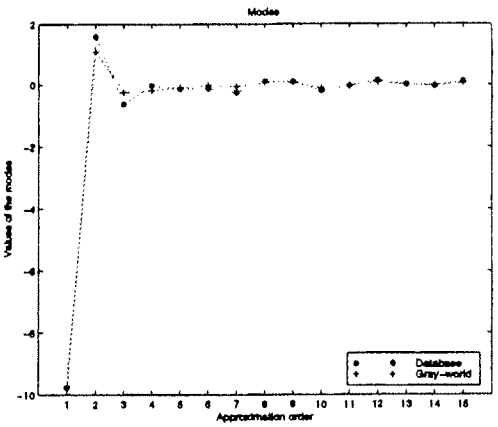

FIG. 2. Modes computed from the database and the "gray world" hypothesis.

thousand representative colors.[23] The representative colors are chosen based on perceptual criteria, i.e., they incorporate the subjectiveness of human color perception. The most well-known color-appearance systems are the Munsell system[24] and the Natural Color System (NCS).[25]

High-resolution measurements of the spectra of color chips for these representative colors are now available.* For each of the 1269 chips of the Munsell System, their spectra was measured from 380–800 nm at 1-nm steps, while the 1513 samples from the NCS system were measured from 380–780 nm at 5-nm intervals. These measurements were

* The Munsell spectra are available from the Information Technology Dept., Lappeenranta University of Technology, Lappeenranta, Finland. The NCS spectra were obtained from the Scandinavian Color Institute in Stockholm courtesy of B. Kruse.

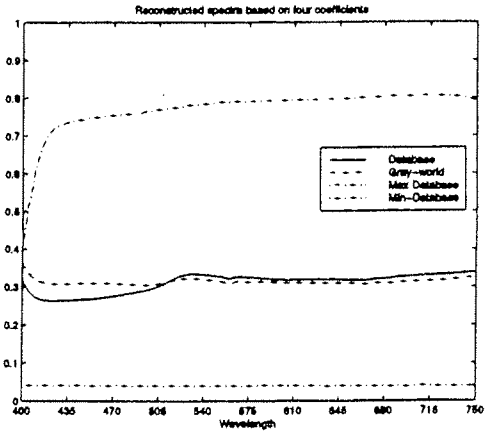

FIG. 3. Spectra computed from the database and the "gray world" hypothesis.

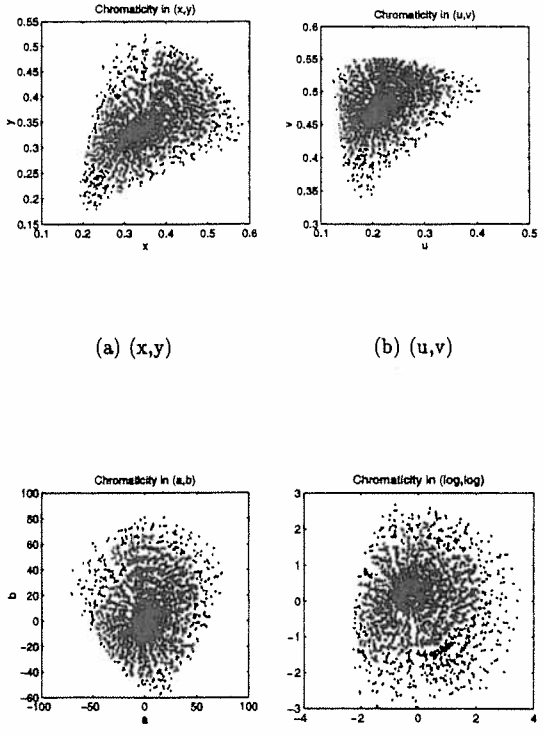

(a) (x,y) (b) (u,v)

(c) (a,b) (d) (log,log)

FIG. 4. Chromaticity coordinates of the database spectra.

combined in one set consisting of 2782 spectra (usually sampled in 5-nm steps from 400–750 nm). In the following we refer to this set of spectra as the spectral database.

These spectra are, of course, the spectra of the pigments used in the production of the color chips, they are not spectra of real world objects. The usage of these spectra is, however, necessary, because (to our knowledge) no equally comprehensible, representative set of natural spectra is available. Furthermore, we are only interested in some statistical properties of larger collections of colors, and the assumption that these properties are very similar for the color chips and the natural colors seems to be reasonable.

Most approaches to computational color constancy are based on the assumption that the reflectance spectra can be described by a low-dimensional model.[26–29] Usually, the coefficients in the eigenvector expansion of the spectra are used as variables. In this article, we do not approximate the spectra themselves by linear combinations of eigenvectors, but we use an expansion in logarithmic coordinates instead. We compute first the eigenvectors of the logarithmic spectra in the spectral database. Then we approximate the logarithm of a given spectrum by a linear combination of the first few eigenvectors. From this the original spectrum can be recovered by exponentiation. This expansion has always a higher minimum-mean-squared-error than the eigenvector expansion, but we found that the differences for approximation orders higher than two are small.

If $S(\lambda)$ is a positive function of the wavelength variable λ, then $s(\lambda) = \ln(S(\lambda))$ is the logarithm of this function. Lowercase letters always denote the logarithm of the capital symbols. By $\hat{b}_n(\lambda)$, we denote the eigenvectors computed from the original spectral database, and $b_n(\lambda)$ is the n-th eigenvector computed from the logarithm of the spectra in the same spectral database. The number of eigenvectors used in the approximation is N. The N-term approximation of the vector $S(\lambda)$ in the $\hat{b}_n(\lambda)$ system is given by $\hat{S}_N$, and the corresponding approximation in the $b_n(\lambda)$ system by S_N:

$$\hat{S}_N = \sum_{k=1}^{N} \alpha_k \hat{b}_k \text{ and } S_N = e^{\sum_{k=1}^{N} \beta_k b_k}. \tag{3}$$

The mean approximation errors are computed as

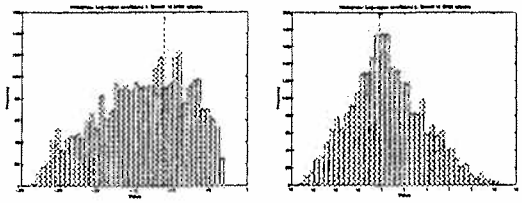

First Coefficient Second Coefficient

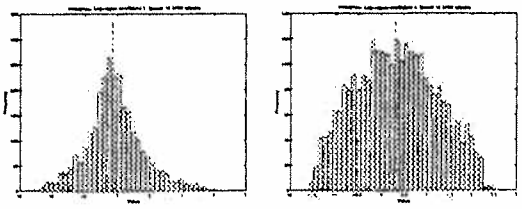

Third Coefficient Fourth Coefficient

FIG. 5. Histograms for log-database.

$$E_N = 100 \times \frac{\text{mean}\|S - S_M\|}{\text{mean}\|S\|}$$
$$\hat{E}_N = 100 \times \frac{\text{mean}\,\|S - \hat{S}_M\|}{\text{mean}\,\|S\|}, \qquad (4)$$

where the mean is computed over all spectra in the database.

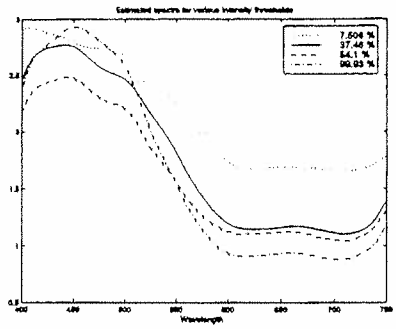

FIG. 6. Estimated spectrum as a function of the intensity threshold.

In Table I and Fig. 1, these errors are summarized. In our image formation model 1, we will always use the eigenvectors computed from the log-spectra.

In most applications, only a few measurements derived from the spectrum $M(\lambda, x)$ (such as the tristimulus values) will be available. In this case, the spectrum has to be estimated from the measurements. One way this can be done is described in the next section. Even when the whole spectrum is known, we see from Eq. (2) that only the distributions of the coefficients $\mu_k(x)$ are available, whereas the distributions of the reflection coefficients $\rho_k(x)$ and the constants α_k are unknown.

In such a case, we have to make some assumptions about the distributions of the coefficients r_k or α_k, or both. This is similar to the Bayesian framework used by Brainard and Freeman.[2] In our calculations, these assumptions will, however, enter only as the values of the modes of the distributions of the coefficients. We do not need to specify the complete distribution as in the Bayesian approach. Statisti-

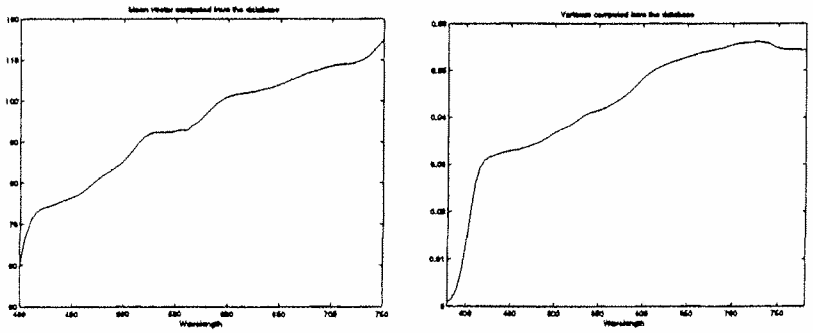

(a) (b)

FIG. 7. The mean- $A(\lambda)$ (a) and variance-function $B^2(\lambda)$ (b) computed from the database.

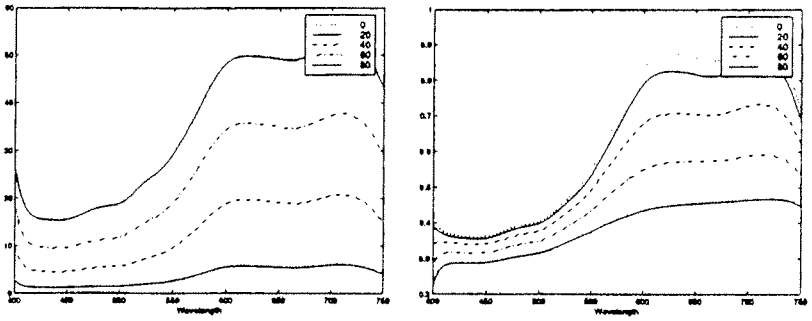

(a) (b)

FIG. 8. The multiplicative (a) and additive (b) restoration functions $a_v(\lambda)$ and $b_v(\lambda)$ for various regularization levels.

cal properties of the set of possible illumination spectra (like the daylight spectra[22]) can also be incorporated, but they will not be used in the following.

One hypothesis that we will often use is the assumption that the distribution of the reflection coefficients ρ_k has the same modes as the coefficients computed from the spectral database. This is certainly not the case in reality, since the spectra in the database appear with different probabilities in real scenes. Better estimates of the modes of the ρ_k distributions can be obtained by incorporating further knowledge about the image formation process. A simple way to compensate the different probabilities of the colors is by counting each color only once.

Another guess about the values of the modes of the distributions of the ρ_k coefficients can be obtained via the "gray world hypothesis" (see Ref. 2, p. 512). This assumption states that the mean over all reflectance functions is independent of λ:

$$\text{mean}_x\, r(x,\lambda) = \gamma. \tag{5}$$

In our experiments, we select λ in the range from 400–750 nm and choose the value of the constant γ such that the norm of the resulting constant vector has norm equal to the mean norm of the vectors in the spectral database. The logarithm of this function is approximated by the eigenvector expansion, and the coefficients in this expansion are listed in the second column of Table II. The first column of Table II contains the modes of the distributions of the expansion coefficients computed from the log-spectra in the database. Figure 2 shows these values in a diagram, and Fig. 3 shows the corresponding spectra computed from the modes of the first four coefficients (the upper and lower spectra are the spectra from the database, which have the highest and lowest norm, respectively). Apart from a small deviation in the shorter wavelength region, the two assumptions lead to nearly identical spectra.

From the modes of the distributions of the measurement coefficients μ_k and the modes computed from the spectral database (column one in Table II or the expansion coefficients in the second column of Table II), the values of the shift parameters α_k can be computed. From these α_k, a spectrum can be derived by exponentiation of the linear combination of the log-eigenspectra. This spectrum will be called a relative illuminant. In the case where the hypothesis

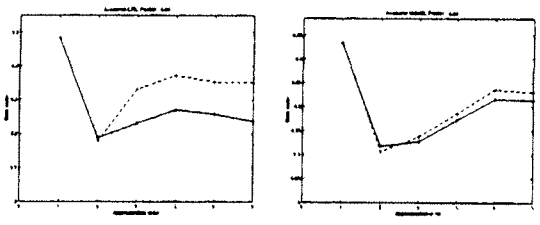

(a) LTS (b) LMedS

FIG. 9. Error distributions for two different images and A-source.

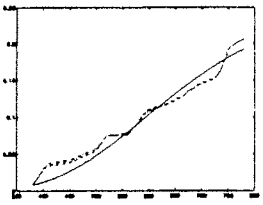

FIG. 10. A-source spectrum and its estimators.

about the statistical properties of the coefficients is true, the relative illuminant is an approximation of the true illuminant. For images in general, we can interpret the shift parameters α_k as a characterization of the global color distribution of the image. The parameter vector (α_k) has then the role of a coordinate vector, which can be used in color-image retrieval applications.

RGB TO SPECTRUM CONVERSION

True multispectral imaging is today only used in a few application areas such as remote sensing. The vast majority of color images is, however, stored in one of the three-dimensional color systems such as RGB, or CIE-related systems like Lab.[1,22,30]

A conversion from these descriptions to the spectral domain is needed before the algorithm can be applied. This is an ill-defined problem, since many different spectra will be mapped to the same coordinate vector in a three-dimensional coordinate system, an effect known as metamerism.

In the following, we assume that we are given a digital color image in RGB-format. Given the RGB vector at position x in an image, we have to estimate which spectral vector $m(\lambda, x)$ corresponds to this RGB-vector. The simplest estimation computes the RGB-coordinates for all elements in the spectral database and defines the spectrum $m(\lambda, x)$ as the nearest neighbor in RGB-space. This is unreliable due to the noneuclidean structure of the RGB-space. In the experiments described below, we first separate the intensity and the chromaticity properties of the RGB-vector and then we find the database spectrum with the best matching chromaticity values.

One motivation for this separation lies in the different ways that these values are obtained. The range of the RGB values (usually 0 . . . 255) is given by the hardware requirements of the digital image processing hardware, whereas the scaling of the spectral measurements in the database is determined by the physics of the measurement process.

Which spectrum is selected for a given RGB-vector depends on the coordinate system used in the chromaticity space. We experimented with the four different systems as follows: a given RGB-vector is first converted to *XYZ*-coordinates using the linear transformation specified by the CIE-1931 RGB- and *XYZ*-systems (Ref. 1, p. 139). For the spectra in the database, the *XYZ*-coordinates are computed using the CIE primary stimuli X, Y, and Z.[1] From the (X, Y, Z) vector, the chromaticity vector (x, y, z) is computed as

$$(x, y, z) = \frac{(X, Y, Z)}{(X + Y + Z)} \tag{6}$$

In the following, denote the chromaticity vectors of the image RGB-vector and the database spectrum by $C_i = (X_i, Y_i, Z_i)$ and $C_s(X_s, Y_s, Z_s)$, respectively. The following methods to compute the distance between C_i and C_s were used:

(x, y): The distance between C_i and C_s is the l^1 norm of the (x, y)-part, i.e.:

$$\text{dist}_{xy}(C_i, C_s) = |x_i - x_s| + |y_i - y_s|. \tag{7}$$

(u, v): This metric is the l^1 norm in the coordinates: $u = 4 * X/(X + 15 * Y + 3 * Z)$ and $v = 9 * Y/(X + 15 * + 3 * Z)$ resulting in

$$\text{dist}_{uv}(C_i, C_s) = |u_i - u_s| + |v_i - v_s|. \tag{8}$$

(a, b): The chromaticity coordinates are defined as: $a = 500 * (X^{1/3} - Y^{1/3})$, $b = 200 * (Y^{1/3} - Z^{1/3})$ and

$$\text{dist}_{ab}(C_i, C_s) = |a_i - a_s| + |b_i - b_s|. \tag{9}$$

(This is essentially the La^*b^* system, where reference white has (X, Y, Z) coordinates (1, 1, 1) and large enough intensity values.)

(log, log): Since we would like to use a table-lookup based conversion, we want the converted chromaticity vectors of the database spectra to fill a rectangle as evenly as possible. Therefore, we introduced the following conversion of the (X, Y, Z) vectors: First we compute: $(\xi, \eta) = (\log(X) - \log(Y), \log(Y) - \log(Z))$, which is similar to the Lab conversion. Then we shift and scale them as $((\xi - E(\xi))/S(\xi), (\eta - E(\eta))/S(\eta))$ (where E and S denote the expectation and the standard deviation), and finally a 45° rotation is applied. The chromatic distance between C_i and C_s is now the l^1 norm of the difference in these new coordinates.

For each element in the spectral database, we computed its coordinates in each of the four coordinate systems described above. In Fig. 4, the distributions of the resulting position vectors are shown for the four coordinate systems.

ESTIMATING THE ILLUMINATION LIGHT SPECTRUM

Using the table lookup described in the previous section gives, for each selected RGB-vector in the image, the spectrum in the database with the most similar chromaticity properties. The norm of this spectrum vector is then multiplied with a normalizing factor, which compensates the intensity differences between the image RGB-vector and the database spectrum. Expanding the logarithm of this spec-

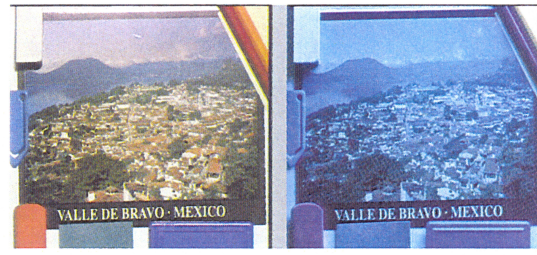

(a) (b)

FIG. 11. Postcard image: (a) indoor illumination; (b) blue light.

trum in eigenvectors of the set of log-database spectra results in the values $\mu_k(x)$ introduced in Eq. (1).

The distribution of the expansion coefficients can be very diverse. This can be seen in Fig. 5, which shows the distribution of the first four components ρ_k, $k = 1 \ldots 3$ computed from the spectral database.

To estimate the mode (the most probable value) for each coefficient, a robust mode estimator has to be employed. In a Bayesian framework, the mode is a MAP estimator, which minimizes the uniform error cost function [Ref. 31, p. 210]. In robust statistics several mode estimators were developed. We used the least trimmed squares (LTS) and the least median of squares (LMedS) estimators.[32] The same mode estimator is used to find the

(a) (b)

FIG. 12. Spectral normalization intensity threshold using (a) 37.46% vs. (b) 99.93% of the pixels.

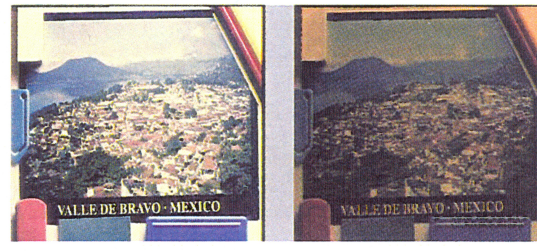

(a) (b)

FIG. 13. Spectral normalization based on 99.93% of the pixels: (a) with and (b) without histogram equalization.

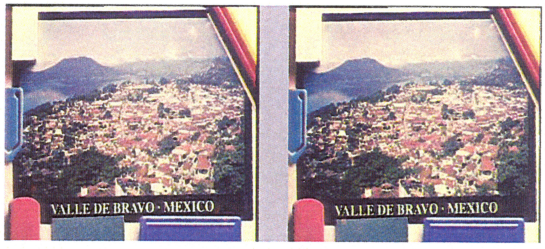

(a) (b)

FIG. 14. (a) Spectral normalization vs. (b) RGB normalization.

most probable value of the measurement coefficients $\mu_k(x)$ and the database coefficients $\rho_k(x)$. The value of the shift parameter α_k is given by the difference between the two modes.

In our experiments, we also found that, in the computation of the estimated relative illumination spectrum, one should take into account the intensity values at various positions. We include only the pixels with gray values above a given threshold in the estimation process. Figure 6 shows how the estimated spectrum depends on this threshold. (The numbers show the percentage of all pixels that were incorporated into the estimation.)

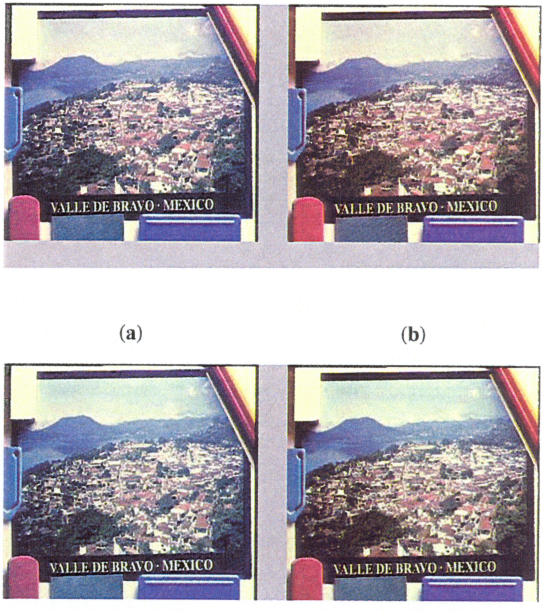

(a) (b)

(c) (d)

FIG. 15. Regularization: (a) threshold 2, regularization 0; (b) threshold 2, regularization 60; (c) threshold 5, regularization 0; (d) threshold 5, regularization 60.

(a) (b)

FIG. 16. Image of the same scene captured with (a) normal lens and (b) telephoto lens.

CORRECTION

In the case where the image formation model $M = R \cdot L$ is correct and the estimated light source $\tilde{L}$ is equal to the true source L, the reflection function can be computed as $R = M/L$. In reality, the spectrum $\tilde{L}$ computed from the image is only an estimation of the true illumination characteristic. This is a typical ill-posed problem in which small estimation errors may lead to large errors in the final result. Regularization is a standard technique to avoid these effects. We applied it as follows.

In the original model: $M(\lambda, x) = R(\lambda, x) \cdot L(\lambda)$ the reflectance $R(\lambda, x)$ is regarded as a random variable with mean $A(\lambda)$ and variance $B^2(\lambda)$. The values of A and B^2 are estimated from the database spectra.

The differences between the real imaging process and its simplified model are collected in the random variable ϵ with mean zero and variance ν^2. This leads to $M(\lambda, x) = L(\lambda) \cdot R(\lambda, x) + \epsilon$.

The best linear estimator of the centered variable $R(\lambda, x) - A(\lambda)$ is [Ref. 33, Section 4.4.2]

$$\frac{L(\lambda)\, B^2(\lambda)(M(\lambda,x) - A(\lambda))}{L^2(\lambda)\, B^2(\lambda) + \nu^2}. \tag{10}$$

For the original variable R, this leads after some algebraic manipulations to the estimator

$$\begin{aligned} R(\lambda,x) &\approx \frac{L(\lambda)\, B^2(\lambda)\, M(\lambda,x)}{L^2(\lambda)\, B^2(\lambda) + \nu^2} \\ &\quad + \frac{([L^2(\lambda) - L(\lambda)]\, B^2(\lambda) + \nu^2)\, A(\lambda)}{L^2(\lambda)\, B^2(\lambda) + \nu^2} \\ &= M(\lambda,x) \cdot a_\nu(\lambda) + b_\nu(\lambda). \end{aligned} \tag{11}$$

This is the restoration formula used in the implementation. The values of A and B are estimated from the database, and the value of ν^2 is a free parameter that describes the confi-

FIG. 17. Result of RGB normalization experiments.

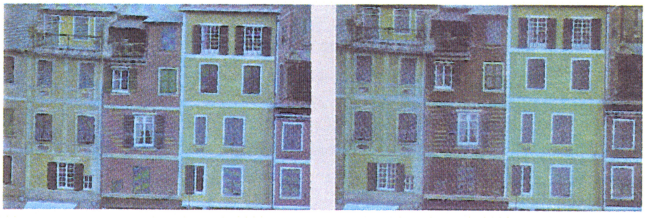

FIG. 18. Result of spectral-based normalization experiments.

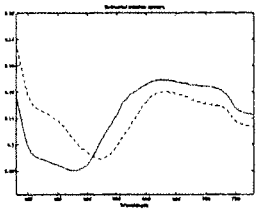

FIG. 19. Estimated illumination spectra from street images: (solid) normal lens; (dashed) telephoto lens.

dence in the estimate. (Note that ν^2 is global, while A and B depend on the wavelength.)

The distribution of the variance $B^2(\lambda)$ as computed from the spectral database is shown in Fig. 7. It shows that for short wavelengths λ the restored value of $R(\lambda, x)$ mainly depends on the average value $A(\lambda)$, whereas the measured value $M(\lambda)$ is dominating for the long wavelength region. Examples of the form of the functions $a_\nu(\lambda)$ and $b_\nu(\lambda)$ for various values of the regularization parameter ν are shown in Fig. 8.

In many correction problems, an input RGB-image has to be converted into an output RGB-image. For such applications it is often unnecessary to compute the nonlinear spectral-based correction pixel-by-pixel. A computationally more attractive approach is to replace the nonlinear estimation [like the one described in Eq. (11)] by the linear approximation

$$r_c = A \cdot r_o + b, \tag{12}$$

where r_c is the corrected output RGB-vector, r_o is the original RGB-vector, A is a 3×3 matrix, and b is a vector. For the zero vector b, this is one of the most often used methods for color correction (see Ref. 8 and Section 5.12 in Ref. 22).

One general method to find a suitable matrix A and a vector b for a given relative illuminant spectrum L is the following. In the first step, it is assumed that the estimated illuminant L is correct, and the spectra in the database are multiplied with the illuminant L to find a representative collection of reflected spectra. These spectra are then converted to RGB coordinates. The result is a matrix F containing the RGB-vectors of the spectra under the assumed illumination. In the second step, the desired inversion procedure (as in Ref. 8) is applied to these simulated illuminated object reflectance spectra given the corrected spectra. These corrected spectra are also converted to RGB resulting in a matrix G of RGB-vectors. Now the matrix A and the vector b are computed as solutions of the matrix equation $A \cdot F + b = G$. This equation can then be solved by familiar methods like the least-squares or total-least-squares. In our experiments, these two methods always produced comparable results, and the resulting RGB-images were visually more or less identical to the images obtained by the spectral-based correction images.

POSTPROCESSING

Using the spectral-based normalization method results in a restored spectrum $R(\lambda, x)$, which is an estimation of the reflectance properties of the object. It can, therefore, be used to compute the appearance of the object under any other illumination, simply by pointwise multiplication of the estimated spectrum and the spectrum of the light source.

For a conversion from the spectral domain to a three-dimensional coordinate system, like RGB, to be meaningful, the spectrum must lie in the gamut of the output device. This is not automatically the case, if we restore the spectrum with the procedure described above. In practice it is, therefore, often necessary to apply some postprocessing to the estimated spectra. In our current implementation, we first convert the spectra to RGB vectors and then we apply intensity-based postprocessing methods. Usually we truncate negative RGB values and we apply a gray-value based histogram-equalization to the corrected image. This is usually necessary, since the raw-restoration usually leads to a greatly reduced contrast in the image.

EXPERIMENTS

In the first series of experiments, we simulated the estimation of a known light source as follows. First, the RGB input image is converted to a multispectral image. Then pointwise multiplication with a known light source gives the simulated multispectral measurement image. The input to the algorithm is this RGB-converted multispectral image. From this RGB image, the illumination spectrum is estimated and compared with the true spectrum.

In the series of experiments we investigated the role of several factors:

1. 4 different input images
2. 1–6 eigenvectors to approximate the log-spectra
3. LTS and LMedS mode detectors
4. Four CIE light sources A, B, C, and D65
5. (x, y) and (log, log) chromaticity metric

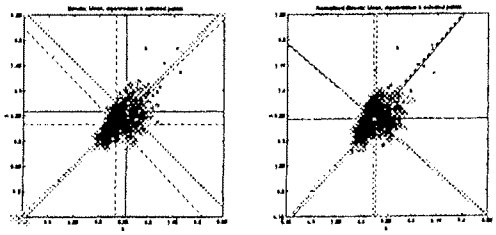

(a) (b)

FIG. 20. Chromaticity distributions of normal and telephoto images: (a) original images; (b) after normalization.

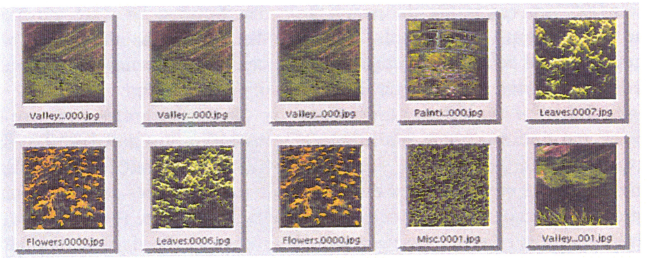

FIG. 21. Color-based search in image database.

The main conclusions from these experiments is that the LMedS and the LTS estimators nearly always gave identical results. The (log, log) metric was always slightly better than the (x, y) metric, only in one case [Fig. 9(a), solid line based on (log, log) and dashed line based on (x, y)] was this difference significantly higher. Using three eigenvectors to approximate the log-spectrum usually gave the lowest error. The error distribution for one of the images illuminated by the A-source (which has the strongest effect on the image colors) is shown in Fig. 9(b). The spectrum of the A-source and the estimated spectral distributions computed from the same image as in Fig. 9(b) is shown in Fig. 10. Here three eigenvectors and the LMedS and LTS-estimators were used.

The next experiment used more realistic conditions. A simple scene was captured under two different illuminations. In Fig. 11(a), normal indoor light conditions were used, whereas in Fig. 11(b) the light box 2412 of the Aristo Grid Lamp Products, Inc. provided a mostly blue illumination. In Figs. 12–15 some of the results with these images are summarized.

Figure 12 shows the result of the direct spectral normalization procedure [regularization parameter $\nu = 0$ in Eq. (11)] based on the spectra estimated from 37.46% and 99.93% of the input pixels (see Fig. 6 for the estimated spectra).

Figure 13 illustrates the effect of the gray-value based histogram equalization on the final image. Figure 14 compares the result of the normalization in the spectral domain with the normalization based on the RGB-to-RGB conversion method described in Eq. (12). Both normalization procedures are combined with the gray-value histogram-equalization. The resulting images are more or less identical.

The images in Fig. 15 finally show the effect of the regularization parameter ν in Eq. (11). In the upper row [images (a) and (b)], 37.46% of the pixels were used in

FIG. 22. Color-based search in image database.

FIG. 23. Color-based search in image database.

the estimation, whereas 66.39% entered in the computation of the images in the lower row [(c) and (d)]. In the computation of the images in the left column [(a) and (c)] no regularization is used, whereas for the right images [(b) and (d)] the regularization value 60 was used. (See Fig. 8 for the form of the multiplicative and additive restoration functions a_ν and b_ν.)

Beside the well-known dependence on the spectral composition of the illuminant (e.g., the recorded colors change significantly when the illumination changes from daylight to indoor incandescent light), an image can also appear significantly different when recorded in differently calibrated systems (photographic and/or electronic).

In Fig. 16, two color images of the same scene are shown, scanned in from Ref. 34, pp. 90–91. The image in Fig. 16(a) was taken from 50 m, while the image in Figure 16(b) was taken with a telephoto lens from 1000 m. In the latter, all the colors appear less saturated and the gray tones dominate. Note that the final result of the scanning process is not a photometrically correct description of the scanned image, since commercial scanners usually apply color transformations to produce visually more pleasing results.

We then investigated the normalization of the street images in Fig. 16. First, the illuminants relative to the complete Munsell/NCS system were computed. This information characterizes the chromatic properties of the images and can be used for indexing into a database. They are shown in Fig. 19. Note that the less saturated telephoto image leads to a flatter estimated spectrum.

For each of the two images, its estimated relative illuminant was then used to adjust the global color distribution of the image to the distribution of the Munsell/NCS system. Using both the spectral- and the RGB-normalization procedures we obtained two normalized images. The results of these experiments are shown in Fig. 17 for the RGB-based normalization and in Fig. 18 for the spectral based normalization.

The top row shows the original images as in Fig. 16. In the middle row are the results from the RGB-normalization, and in the bottom row the results for the spectral normalization.

A more quantitative description of the normalization effects can also be obtained. In Fig. 20, the chromaticity distributions (in CIE-xy space) of the two images (a) before and (b) after normalization are shown. The distributions are based on the chromaticity vectors of the same, 1000 randomly selected pixels. The points originating in the normal lens images (original and processed) are marked with a +, while the points from the telephoto images with a o. For all four images it was assumed that the images are viewed under D65 daylight and the chromaticity coordinates were computed accordingly.

The directions of the two eigenvectors of each chromaticity distribution were then computed, and are shown with solid lines for the normal lens images and dashed lines for the telephoto images. The centers of these eigenvector coordinate systems are located at the means of the chromaticity distributions. They are shown with the solid line cursor for the normal lens images, and with the dashed cursor for the telephoto images. The effect of the normalization is clearly revealed.

In the last experiment, we use the relative illuminant to locate images in a database. The database used consisted of the 473 color texture images in the VISTEX database.* For each of the images in the database we compute first the relative illuminant as described before. In the experiments below, we used 6 eigenvectors and we estimated the relative illuminant from 5000 randomly selected pixels in each image. Once these spectra are computed, they can be used to search in the database for images that have a certain global color distribution. In Figs. 21–23, we illustrate some of the results. In these experiments, we select first one image in the database as a prototype image and then we find those images in the database with the most similar color distribution. For this we normalize first all relative illuminant spectra to norm one to eliminate the influence of intensity variations, and then we use the scalar product of the two normalized relative illuminants as similarity measure for the global color distributions of these two images. Intensity properties of the images are ignored, because only normalized spectra enter the similarity computations. Figures 21–23 show the prototype image in the upper-left corner of the image. The other nine images are the most similar images found in the database (where the images are sorted from left to right, top to bottom with falling similarity values). Note that the database contains several images of the same texture at different resolutions and, therefore, the same texture may appear more than once.

Figures 21 and 22 show that the matching results are reasonable for homogeneous textures, whereas the results are less intuitive for images with different textures such as Fig. 23.

DISCUSSION AND CONCLUSIONS

We have shown that the log-eigenvector expansion of color spectra defines a coordinate system that allows an efficient solution to problems related to color constancy. Combining the log-spectral space with color-appearance systems (which are based on human color vision) allows a reliable estimation of the global color characteristics of a color image. The conversion procedures between this and other color systems however, need, further study.

The interpolation procedures used to convert RGB-vectors to spectra were sufficient in our application, because only statistical properties of a large number of spectra were needed. More difficult was the conversion from the spectral representation to quantized three-dimensional color representations like RGB. Here we found that a number of practical problems influenced the final results in a funda-

* http://www-white.media.mit.edu/vismod/imagery/VisionTexture/vistex.html.

mental way. Problems that had to be considered included: the handling of spectra that are outside the gamut of the chosen output device, and quantization methods that use the available number of colors efficiently and that at the same time preserve the structure in the spectral space.

ACKNOWLEDGMENTS

Markku Hauta-Kasari is on leave from the Department of Information Technology, Lappeenranta University of Technology, Lappeenranta, Finland.

The spectra in the Munsell database were measured at the Department Physics, Joensuu University, Finland and are available from the Department Information Technology, Lappeenranta University of Technology, Lappeenranta, Finland.

The NCS-database was obtained from the Scandinavian Color Institute in Stockholm and provided by B. Kruse.

1. Kaiser PK, Boynton RM. Human color vision. Washington, DC: OSA; 1996.
2. Brainard DH, Freeman WT. Bayesian color constancy. J Opt Soc Am A 1997;14:1393–1411.
3. D'Zmura M, Iverson G. Color constancy. i. basic theory of two-stage linear recovery of spectral descriptions for lights and surfaces. J Opt Soc Am A 1993;10:2148–2165.
4. D'Zmura M, Iverson G. Color constancy. ii. results for two-stage linear recovery of spectral descriptions for lights and surfaces. J Opt Soc Am A 1993;10:2166–2180.
5. D'Zmura M, Iverson G. Color constancy. iii: General linear recovery of spectral descriptions for lights and surfaces. J Opt Soc Am A 1994;11:2389–2400.
6. Finlayson GD. Color constancy in diagonal chromaticity space. In: Proc Int Conf Computer Vision. IEEE; 1995. p 218–223.
7. Finlayson GD, Drew MS, Funt BV. Color constancy: generalized diagonal transforms suffice. J Opt Soc Am A 1994;11:3011–3019.
8. Finlayson GD, Funt BV. Coefficient channels: derivation and relationship to other theoretical studies. Col Res Appl 1996;21:87–96.
9. Finlayson GD, Funt BV, Barnard K. Color constancy under varying illumination. In: Proc Int Conf Computer Vision. IEEE; 1995. p 720–725.
10. Forsyth DA. A novel algorithm for color constancy. Int J Computer Vision 1990;5:5–36.
11. Funt B, Cardei V, Barnard K. Neural network colour constancy and specularly reflecting surfaces. In: Proc AIC Colour 97. AIC; 1997.
12. Funt BV, Cardei V, Barnard K. Learning color constancy. In: IS&T fifth color imaging conference; 1996.
13. Funt BV, Finlaysson GD. Color constant color indexing. IEEE Trans Pattern Anal Mach 1995;17:522–529.
14. Finlayson GD. Color in perspective. IEEE Trans Pattern Anal Mach 1996;18:1034–1038.
15. Luong QT. Color in computer vision. In: Chen CH, et al., editors. Handbook of pattern recognition and computer vision. World Scientific; 1993. p 311–368.
16. Maloney LT, Wandell BA. Color constancy: a method for recovering surface spectral reflectance. J Opt Soc Am A 1986;3:29–33.
17. Sharma G, Trussell HJ. Digital color imaging. IEEE Trans Im Proc 1997;6:901–932.
18. Webster MA. Human color perception and its adaptation. Network: Comp Neur Sys 1996;7:587–634.
19. Klinker GJ, Shafer SA, Kanade T. The measurement of highlights in color images. Int J Computer Vision 1988;2:7–32.
20. Hecht E. Optics. Reading, MA: Addison-Wesley; 1987.
21. Ballard DB, Brown CM. Computer vision. Englewood Cliffs, NJ: Prentice Hall; 1982.
22. Wyszecki G, Stiles WS. Color science. 2nd Ed. London: Wiley & Sons; 1982.
23. Derefeldt G. Colour appearance systems. In: Gouras P, editor. The perception of colour. New York: CRC Press; 1991. p 218–261.
24. Munsell Book of Color, Matte Finish Collection. Baltimore: Munsell Color; 1976.
25. Hård A, Sivik L, Tonnquist G. NCS, natural color system—from concepts to research and applications. Col Res Appl 1996;21:180–205.
26. Brainard DH. Colorimetry. In: Bass M, editor. Handbook of optics. Vol. 1. New York: McGraw-Hill; 1995. p 26.1–26.54.
27. Jaaskelainen T, Parkkinen J, Toyooka S. Vector subspace model for color representation. J Opt Soc Am A 1990;7:725–730.
28. Maloney LT. Evaluation of linear models of surface spectral reflectance with small numbers of parameters. J Opt Soc Am A 1986;3:1673–1683.
29. Parkkinen JPS, Hallikainen J, Jaaskelainen T. Characteristic spectra of Munsell colors. J Opt Soc Am A 1989;6:318–322.
30. The science of color. Washington DC: Opt Soc Am; 1973.
31. Mendel JM. Lessons in estimation theory for signal processing, communications, and control. Engelwood Cliffs, NJ: Prentice Hall; 1995.
32. Rousseeuw PJ, Leroy AM. Robust regression & outlier detection. New York: Wiley; 1987.
33. Louis AK. Inverse und schlecht gestellte Probleme. Stuttgart: Teubner Verlag; 1989.
34. De Grandis L. Theory and use of color. Englewood Cliffs, NJ: Prentice Hall; 1986.

Publication 4

HAUTA-KASARI M., WANG W., TOYOOKA S., PARKKINEN J., AND LENZ R.,
Unsupervised Filtering of Munsell Spectra,

Lecture Notes in Computer Science 135

Roland Chin Ting-Chuen Pong (Eds.)

Computer Vision – ACCV'98

Third Asian Conference on Computer Vision
Hong Kong, China, January 1998
Proceedings, Volume I

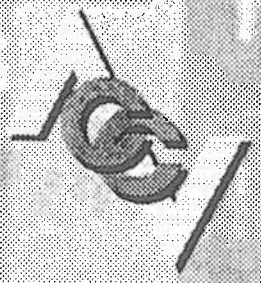

Springer

Proceedings of the 3rd Asian Conference on Computer Vision, (ACCV'98), Hong Kong, January 8-10, 1998, Vol. I of *Lecture Notes in Computer Science 1351*, R. Chin and T.-C. Pong, Eds., Springer 1998, pages 248-255.

Unsupervised Filtering of Munsell Spectra

M. Hauta-Kasari[1], W. Wang[1], S. Toyooka[1], J. Parkkinen[2], and R. Lenz[3]

[1] Department of Environmental Science and Human Engineering,
Graduate School of Science and Engineering, Saitama University,
255 Shimo-okubo, Urawa, Saitama, 338 JAPAN
Email: mhk@mickey.mech.saitama-u.ac.jp
[2] Department of Information Technology, Lappeenranta University of Technology,
P.O.Box 20, FIN-53851 Lappeenranta, FINLAND
[3] Image Processing Laboratory, Department of Electrical Engineering,
Linköping University, S-58183 Linköping, SWEDEN

Abstract. We present a new method for producing color filters with positive coefficients to represent color reflectance spectra. The subspace method which is based on the KL-expansion can be used to define a basis to describe the spectral data accurately. However, due the orthogonality of the eigenvectors, the corresponding color filters usually contain negative coefficients and cannot be used in optical components directly. Our method finds the set of vectors which span a very similar color space as the subspace method does. These color filters contain only positive coefficients and can be directly used in optical implementations. We used an unsupervised competitive neural network (Instar) to find a set of positive color filters. The experiments with the Munsell spectra show that the filters produced by the neural network span a color space very similar to the color space spanned by the eigenvectors of the subspace method.

1 Introduction

Color is an important factor in many computer vision-, pattern recognition-, and industrial quality control applications. Usually the color analysis is based on three-dimensional color coordinate systems, like CIE xyY-, Lab- and Luv-color spaces. These three-dimensional color spaces are related to human color vision system, in which there are three different types of photoreceptors [1, 2].

The color of an object is a sensation, which is produced in the brain [1] and it is thus hard to define color. Color can however be defined indirectly through the cause of the sensation. This is called color spectrum, which can be measured physically: the electromagnetic spectrum in the wavelength range from 380 nm to 780 nm. Using the spectrum itself as color representation avoids problems such as metamerism [3], where several spectra have the same three-dimensional color coordinates.

In the subspace method the color coordinates are projections, i.e. the values of inner products between the color spectrum and the basis. This avoids the problem of metamerism and the accuracy is high [4, 5]. The Munsell [6] color spectra database can be described by a few basis vectors, and this basis can be also used for describing natural colors [5]. Usui et al. [7] described a multilayer

perceptron based system where the weights in the hidden layer were used to reconstruct Munsell data from the three-dimensional color space representation.

The optical implementation of the subspace method gives the possibility of faster calculation, which is needed in many industrial applications. The basis produced by the subspace method is orthogonal and therefore usually contains negative coefficients. These cannot be directly implemented in optical components. For example, the liquid crystal spatial light modulator (LCSLM), which has been used to calculate the optical inner product [8, 9], takes only filters with positive coefficients. In Refs. [8, 9], the basis vector set produced by the subspace method was biased and multiplied to make suitable filters for LCSLM. It is also possible to divide the basis vectors to the positive and negative parts, and handle these parts separately, but this leads to more complicated optical systems. The aim of this study is to produce a vector set with positive coefficients, which can be directly used in optical pattern recognition. This problem was also addressed in [10]. There the positive color filters are found by optimizing an energy function based on second- and fourth-order statistical moments [11].

In this paper we present an unsupervised neural network based method to find filters with positive coefficients. The competitive neural network finds the centers of color clusters in the color space. After learning, the weight vectors of the neural network are used as filters, which span a color space very similar to the color space spanned by the eigenvectors of the subspace. Our experiments show that the Munsell color spectra can be described very accurately by these filters. The obtained filter systems are compared with the results reported in [10].

2 Subspace Method

In [4, 5] it is shown that the color space for the color spectra can be described accurately by the subspace method. A measured spectrum $s(\lambda)$ can be represented as a column vector $s(\lambda) = [s(\lambda_1), s(\lambda_2), \ldots, s(\lambda_n)]^T$, where λ is the wavelength and T denotes the transpose. Next we compute the eigenvectors of the correlation matrix $R = \sum_{i=1}^{N} s_i(\lambda) s_i(\lambda)^T$, where the index i indicates the ith spectrum in the set of N measured spectra. The eigenvectors ϕ are the solutions of the equation $R\phi = \sigma\phi$, where σ is an eigenvalue of R. The first n eigenvectors form a basis for the subspace. The subspaces can be designed for several different color regions in parallel [12]. In this study we formed only one subspace representing the whole Munsell color space.

The information content, i.e. the fidelity value k of the first n eigenvectors can be defined as $k = \sum_{i=1}^{n} \sigma_i / \sum_{i=1}^{N} \sigma_i$, where k is ratio of the information on the first n largest eigenvalues over the information on all N eigenvalues. In Ref. [4], eight basis vectors were needed for describing the Munsell database accurately.

The basis vector set for the Munsell spectra is orthogonal and the vectors contain negative coefficients. For optical pattern recognition, a small vector set with only positive coefficients spanning the color space as accurately as possible should be found. Since the subspace method produces systems with minimal squared error, it can be used as a reference.

3 Unsupervised Neural Network

Color filters suitable for optical pattern recognition should fulfill the following requirements: *1) the filters should contain only positive coefficients, 2) the filters should span the color space as accurately as possible, 3) the filters should be separated from each other.* To fulfill these conditions, we investigated the clustering properties of competitive learning and self-organization methods [13–15]. The main problem was if it is possible to cluster the input color spectra and use the centers of these clusters for a representation of the whole color space. The method we decided to use is based on competitive learning, which clusters the input data without any knowledge of the right cluster distributions.

In our experiments we used an unsupervised competitive neural network with a learning algorithm based on the Instar-algorithm by Grossberg [13]. We also incorporated Kohonen's [14] self-organizing map with a winner take all layer (WTA). The competitive neural network clusters the input data so that the weight vectors are the centers of these clusters [15]. In our study the input data are the measured color spectra containing only positive coefficients. Thus the weight vectors, i.e. the color filters are also positive. These weight vectors should span the color space like the eigenvectors of the subspace method. In the competitive neural network only the winner neuron learns during each learning cycle, which means that the filters are separated from each other.

The winner w_c is the weight vector, which has the closest euclidean distance to the input vector x. Next, the updating process of the weight vectors is defined as follows

$$w_i(t+1) = \begin{cases} w_i(t) + \alpha(t)[x(t) - w_i(t)] & \text{, if } i = c, \\ w_i(t) & \text{, otherwise,} \end{cases} \tag{1}$$

where t is the iteration parameter and $\alpha(t)$ is a learning rate. The learning rate is decreasing exponentially during the learning. In each cycle of the learning process the training sample is taken randomly from the input data. The weights are initialized by the average vector (≥ 0) of the input data. Equation 1 can be written as $w_i(t+1) = w_i(t)[1 - \alpha(t)] + \alpha(t)x(t)$, where $0 \leq \alpha(t) < 1$, $w_i(t) \geq 0$, $x(t) \geq 0$ and therefore the weights w are always positive. A detailed description of the competitive learning and self-organization can be found in Ref. [14].

4 Filtering the Spectral Database

To measure the accuracy of the produced color filters we reconstructed the Munsell database and compared the results to the subspace method. The reconstruction procedure is as follows:

If the basis vector set is orthonormal, the reconstructed spectrum s' can be calculated from the equation $s' = BB^T s$, where s is the original spectrum and B is the basis vector set.

In the nonorthonormal case, as in the case of filters with positive coefficients, the reconstruction is obtained by the generalized inverse matrix:

$s' = W(W^TW)^{-1}W^Ts$, where W is the filter set. In the optical implementation $W(W^TW)^{-1}$ is known and W^Ts is determined experimentally.

We calculate the relative error as the norm of spectrum's reconstruction error divided by the norm of original spectrum: error $= 100 \times \|s' - s\|/\|s\|$ (%).

5 Experiments

In our experiments the Munsell database was used. It consists of 1269 color spectra measured by a spectrophotometer from the *Munsell Book of Color* [6]. We used the wavelength range from 400 nm to 700 nm, at 5nm intervals, i.e. each spectrum contained 61 components. Fig. 1 shows the first eight basis vectors of the subspace method. The fidelity value for the first eight eigenvalues is 99.99%.

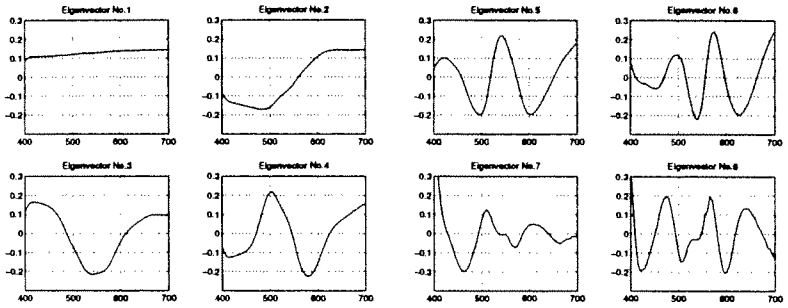

a) b)

Fig. 1. Eigenvectors of the subspace method a) No.1-4, b) No.5-8.

5.1 Filter Design

The input data, i.e. the whole Munsell data was processed by the competitive neural network, with an included WTA-layer. The number of neurons was 8 and the total number of learning cycles was 50000. The learning data was first normalized to unit norm, the weights were initialized by the average vector of the input data and the learning rate was decreasing exponentially from 0.9 towards 0 during learning. The learned filter functions are shown in Fig. 2. The filters produced by the competitive neural network are the centers of color clusters in the color space. Fig. 2 shows that they represent regularly the spectral range from 400 nm to 700 nm. Fig. 3 visualizes the Munsell data and the filters in two-dimensional CIE 1931 xy-diagram. CIE 1931 xy-coordinates were calculated under daylight illumination D65. The xy-coordinates are only used for visualization, but not used in the experiments. Fig. 3 a) shows the xy-color coordinates of Munsell data and Fig. 3 b) shows the xy-coordinates of filters. The numbers in Fig. 3 b) correspond to the filter numbers shown in Fig. 2. It can

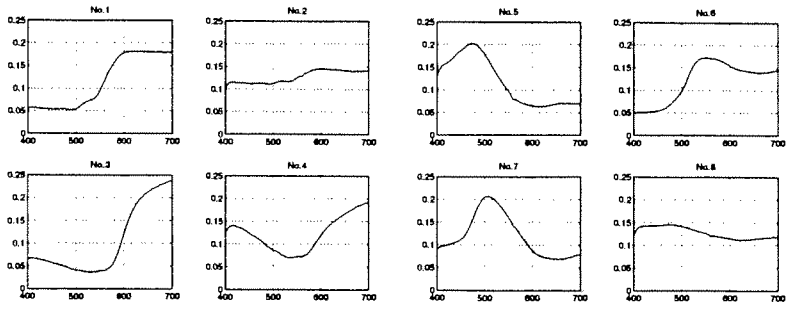

a) b)

Fig. 2. Learned filter functions a) No.1-4, b) No.5-8.

be seen that the CIE xy-coordinates of the filter set have approximately equal distances between each other. These filters are the centers of eight color clusters of the Munsell database. The CIE 1931 xy-diagram shows that two filters, no.2 and no.8 are near the xy-values $x = 0.33$, $y = 0.33$. This is the area of Munsell colors with high value- and low chroma-components, near white. Each color page in Munsell book has this color and therefore it is natural that the competitive learning represents this highly populated area by two filters.

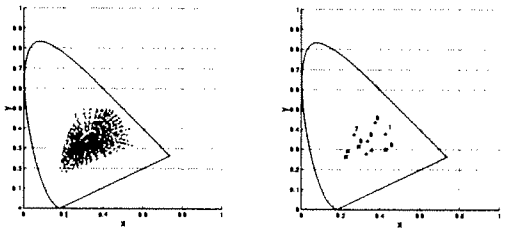

a) b)

Fig. 3. CIE 1931 xy-diagram of a) Munsell-data, b) filters.

Next the learned filter set was orthogonalized by the singular value decomposition (SVD) method. The orthogonalized filters are highly correlated to the basis vectors of the subspace method shown in Fig. 1. The numerical correlations between the eigenvectors of subspace method and orthogonalized filters are 0.999, −0.974, −0.966, 0.984, −0.901, −0.551, −0.361, and −0.096, respectively. The anticorrelation in the 2nd, 3rd and 5th correlation values is not problem, since if ϕ is an eigenvector of R then also $-\phi$ is an eigenvector of R [4]. In the orthogonalized filter set, the last three filters are less correlated to the eigenvectors and they also contained some noise. The information content of these last three vectors is very small, since the fidelity value for the first five eigenvalues is 99.93%. The orthogonalized filter set was only used for showing the similarity to the eigenvectors of the subspace method and it was not used in filtering.

5.2 Filtering the Munsell Database

To obtain a detailed error analysis the Munsell database was first reconstructed by the subspace method using the basis vectors shown in Fig. 1. The reconstruction error of each Munsell spectrum is shown in Fig. 4 a). Next the database was reconstructed by the learned filters shown in Fig. 2. The reconstruction was done using generalized inverse matrix method and Fig. 4 b) shows the reconstruction error obtained. In Table 1, the correspondence between sample number and Munsell color category is tabulated.

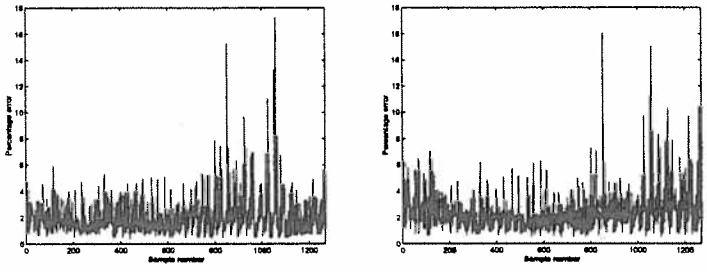

a) b)

Fig. 4. The Munsell database reconstruction errors, using a) subspace method, b) learned filters.

Table 1. Correspondence between sample number and Munsell color category.

Sample number range	Munsell color category
1-139	Red (R)
140-261	Yellow-Red (YR)
262-404	Yellow (Y)
405-531	Green-Yellow (GY)
532-646	Green (G)
647-752	Blue-Green (BG)
753-864	Blue (B)
865-1001	Purple-Blue (PB)
1002-1132	Purple (P)
1133-1269	Red-Purple (RP)

The largest error for the learned filters (16.0%), (sample 853, blue (B), Hue 10, Value 2.5, Chroma 4), is lower than for the subspace method (17.3%), (sample 1058, purple (P), Hue 5, Value 2.5, Chroma 6). The average reconstruction error for the subspace method is 1.9% and for the learned filters 2.3%.

Fig. 4 shows that the high error peaks are repeated after every 10-20 samples. We found that the corresponding spectra had low intensity information. The learned filters don't have enough information for these low intensity spectra. In the Munsell book, every color page has this kind of spectrum and because of

the sampling order in the measurement the error peaks are repeated after every 10-20 samples. Fig. 5 a) and b) shows the spectra with the largest reconstruction errors. Fig. 5 c) shows the typical spectrum for the average reconstruction error using learned filters (sample 465, Green-Yellow (GY), Hue 5, Value 8, Chroma 8).

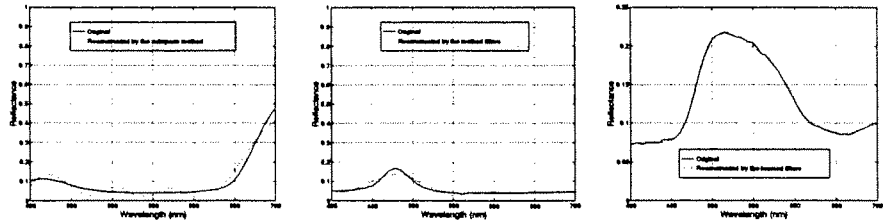

a) b) c)

Fig. 5. Spectra with the largest errors, reconstructed by a) subspace method (plate 5P V2.5 C6), b) learned filters (plate 10B V2.5 C4). In c) is the typical spectrum with average reconstruction error using learned filters (plate 5GY V8 C8).

Finally we made a numerical comparison with the filters in Ref. [10]. To be comparable, we used the Munsell data at the wavelength area from 381 nm to 776 nm, at 5 nm intervals. We trained 6 filters and reconstructed the whole Munsell database with them. The Munsell database was also reconstructed by the filters produced in [10]. The average percentage error for our filters was 4.6% and for the filters in Ref. [10] the error was 6.1%.

6 Conclusions

In this study we presented a new unsupervised method to produce color filters for optical pattern recognition. The competitive neural network found the centers of color clusters in color space. The weight vectors from the neural network were used as color filters.

The experimental part of this paper showed that the learned filters are comparable to the basis vectors of the subspace method. Both of them span similar color spaces and the reconstruction errors with the Munsell data were small. It can be seen that the largest reconstruction errors in Fig. 4 are in the sample range 800-1269. The subspace method has largest errors in sample range 800-1050, containing the purple-blue (PB) and purple (P) colors in the Munsell color category. For the learned filters the largest errors are in the sample range 1050-1269, i.e. purple (P) and red-purple (RP) colors in the Munsell color category. Purple color spectra have usually a very flat region in the wavelength range 500-600nm and then a narrow peak or peaks in blue and red region. Both methods have problems to recover flat spectra in the range 500-600nm, as can be seen in Fig. 5. The reason is that both the basis vectors and learned filters vary in the wavelength range 500-600nm and therefore they cannot represent this flat region accurately.

For a smaller spectral region than the Munsell colors the number of filters can be decreased. In this case the number of learning cycles needed in the learning phase can also be decreased. In this study we produced filters for the Munsell spectra. The strategy of our method is general and can be used for special applications in which the filters have to be designed for a special class of spectra.

The learned filters with positive coefficients can be directly used in optical components, like in liquid crystal spatial light modulators. The optical implementation of these filters is under investigation.

Acknowledgements: M. Hauta-Kasari and W. Wang were financially supported by the Monbusho (Japanese Ministry of Education, Science, Sports and Culture). M. Hauta-Kasari was also supported by grants from Emil Aaltonen Foundation and Wihuri Foundation. He is on leave from the Department of Information Technology, Lappeenranta University of Technology, Finland. The spectral database is available at the www-server of Lappeenranta University of Technology, `http://www.it.lut.fi/research/color/lutcs_database.html`.

References

1. P.K. Kaiser and R.M. Boynton, *Human Color Vision, Second Edition*, Optical Society of America, Washington DC, 1996.
2. G. Wyszecki and W.S. Stiles, *Color science : concepts and methods, quantitative data and formulae*, Wiley, New York, 1982.
3. M.S. Drew and B.V. Funt, Natural Metamers, *CVGIP: Image Understanding* **56**, 1992, 139-151.
4. J.P.S. Parkkinen, J. Hallikainen, and T. Jaaskelainen, Characteristic spectra of Munsell colors, *J. Opt. Soc. Am. A.* **6**, 1989, 318-322.
5. T. Jaaskelainen, J. Parkkinen, and S. Toyooka, Vector-subspace model for color representation, *J. Opt. Soc. Am. A.* **7**, 1990, 725-730.
6. *Munsell Book of Color, Matte Finish Collection*, Munsell Color, Baltimore, USA, (1976).
7. S. Usui, S. Nakauchi, and M. Nakano, Reconstruction of Munsell color space by a five-layer neural network, *J. Opt. Soc. Am. A.* **9**, 1992, 516-520.
8. T. Jaaskelainen, S. Toyooka, S. Izawa, and H. Kadono, Color classification by vector subspace method and its optical implementation using liquid crystal spatial light modulator, *Optics Communications* **89**, 1992, 23-29.
9. N. Hayasaka, S. Toyooka, and T. Jaaskelainen, Iterative feedback method to make a spatial filter on a liquid crystal spatial light modulator for 2D spectroscopic pattern recognition, *Optics Communications* **119**, 1995, 643-651.
10. R. Lenz, M. Österberg, J. Hiltunen, T. Jaaskelainen, and J. Parkkinen, Unsupervised filtering of color spectra, *J. Opt. Soc. Am. A.* **13**, 1996, 1315-1324.
11. M. Österberg, *Quality Functions for Parallel Selective Principal Component analysis*, Ph.D. dissertation, Linköping University, Linköping, Sweden, 1994.
12. E. Oja, *Subspace Methods of Pattern Recognition*, Research Studies Press, Letchworth, England, 1983.
13. S. Grossberg, *Studies of the Mind and Brain*, Reidel Press, Drodrecht, Holland, 1982.
14. T. Kohonen, *The Self-Organizing Maps*, Springer-Verlag, Berlin Heidelberg, 1995.
15. S. Haykin, *Neural Networks*, Macmillan College Publishing Company, New York, 1994.

Publication 5

HAUTA-KASARI M., MIYAZAWA K., TOYOOKA S., AND PARKKINEN J.,
A Prototype of the Spectral Vision System,

In Press.

Proceedings of the 11th Scandinavian Conference on Image Analysis, (SCIA'99), Greenland, June 7-11, 1999.

A Prototype of the Spectral Vision System

Markku Hauta-Kasari
Department of Information Technology,
Lappeenranta University of Technology,
P.O.Box 20, FIN-53851 Lappeenranta, FINLAND
Email: *Markku.Hauta-Kasari@lut.fi*

Kanae Miyazawa, Satoru Toyooka
Graduate School of Science and Engineering,
Saitama University,
255 Shimo-okubo, Urawa, Saitama 338-8570, JAPAN

Jussi Parkkinen
Department of Computer Science,
University of Joensuu,
P.O.Box 111, FIN-80101 Joensuu, FINLAND

Abstract

In this study we present a spectral vision system, which can be used to measure a color spectrum and two-dimensional spectral images. First, the low-dimensional color filter set was designed by an unsupervised neural network. Then the compact size optical setup for the spectral synthesizer was constructed to synthesize the light which corresponds to the spectral characteristics of the color filter. In the optical setup a liquid crystal spatial light modulator (LCSLM) was used to implement color filters. The sample was illuminated by synthesized lights and the intensity images which correspond to the inner products between the color filter and the sample were detected by CCD-camera. From the detected inner products the sample's color spectra were reconstructed using a pseudoinverse matrix. Experimental results of measuring a single color spectrum and spectral images are presented.

1 Introduction

Multispectral imaging has received a great deal of attention recently. Spectral measurements are used, for example, in the field of remote sensing [1], computer vision and industrial applications [2]. Because of the high accuracy of spectral information, it has become an important quality factor in many industrial processes.

In color research, the color is usually represented using three-dimensional color coordinate systems like CIE xyY, CIELAB, CIELUV, and RGB colorspaces. In the human color vision system there are three different types of photoreceptors [3, 4] and for this reason these three-dimensional color coordinate systems are usually used as a color representation. These models are computationally effective and suffice for many purposes, but they have problems such as metamerism [5], where the same three-dimensional color coordinate corresponds to several different spectra. If the measured color spectrum covering the visible spectral region from 380nm to 780nm itself is used as the color representation, then metamerism is avoided and accuracy is high. When the spectral imaging system is tuned to measure the visible light, then the acquired image represents a high quality color image, where every pixel contains a color spectrum.

To measure a color spectrum, devices such as a monochromator, a radiometer, or a spectrophotometer are usually used. Spectral images can be measured, for example, by CCD-camera with narrow band interference filters [6], by acousto-optical tunable filter [7] or by Fourier transform based methods [8]. These devices are usually expensive and a large amount of image data must be processed and stored. The spectra are generally measured from 1nm to 10nm intervals, and therefore, for example, the spectral image measured in the wavelength range from 400nm to 700nm contains from 301 to 31 component images, respectively. Transmission of the spectral image obtained using these conventional methods is difficult, because of the large amount of data to be transmitted.

It has been shown that low-dimensional representation of spectra can reproduce the original spectrum accurately. One approach used to compress spectra is to have the measured spectra and compress them by software [9, 10]. Another approach is to design the low-

dimensional multispectral imaging system so, that we already acquire optimal component images for spectral reconstruction.

Recently, low-dimensional multispectral imaging systems have been the focus of growing interest. Tominaga [11] proposed a multichannel vision system based on the use of a CCD-camera and six color filters. The system was used to reconstruct the surface-spectral reflectance and illuminant spectral-power distribution from the image data. Baronti *et al.* [12] used a multispectral imaging system with 29 filters to analyze works of art in a wavelength range from 420nm to 1550nm. Haneishi *et al.* [13] designed five color filters for archiving spectral images of artworks. Lenz *et al.* [14] designed low-dimensional color filter sets for color spectra by optimizing an energy function based on second- and fourth-order statistical moments.

Spectra of natural color samples are smooth and correlate highly with each other. Parkkinen *et al.* [9] showed that a spectral database containing 1257 samples measured from the Munsell book of color [15] can be represented accurately by a few basis vectors produced using a subspace method. These basis vectors can also be used to describe natural color spectra [16]. Jaaskelainen *et al.* [17] implemented the learning subspace method optically. They used a liquid crystal spatial light modulator (LCSLM) to implement the color filters corresponding to the basis vectors. Hayasaka *et al.* [18] developed the system described in [17] to analyze two-dimensional microscopic images.

In our previous study [19] we designed a low-dimensional color filter set by an unsupervised neural network for 1269 color spectra measured from the Munsell book of color. In this paper we propose a low-dimensional filtering method which can be used to measure a color spectrum and two-dimensional spectral color images. The proposed method is fast and the amount of data obtained from the filtering process is small and, therefore, convenient for storing and transmitting the spectral image.

The paper is organized as follows. In Section 2 we briefly review the color filter design from our previous study. Then in Section 3 we introduce the optical setup for the spectral synthesizer. In Section 4 we show the experimental results of our measurements and in Section 5 we give a discussion.

2 Color Filter Design

The subspace method [20], which is based on the Karhunen-Loève expansion, can be used to define a basis to describe the spectral data accurately. The color spectra measured from the Munsell book of color can accurately be represented from 3 to 8 basis vectors produced by the subspace method [9]. The basis vector set for the Munsell color spectra is orthogonal and contains negative coefficients, which cannot be directly implemented optically. In Refs. [17, 18] the basis vector set was biased and multiplied to make it suitable for optical implementation. In Ref. [19] we designed, using an unsupervised neural network, a low-dimensional color filter set with a constraint of positive spectral values for the 1269 Munsell spectra. The competitive learning algorithm was based on the Instar-algorithm by Grossberg [21], which was incorporated by Kohonen's [22] self-organizing map with the winner take all (WTA) layer. The neural network clusters the color spectra, and after learning, the centers of the clusters are used as color filters. A detailed description of competitive learning and self-organization can be found in Refs. [21, 22, 23]. In [19] we showed that the Munsell spectral database was reconstructed by the designed color filters with sufficient accuracy and the reconstruction accuracy was comparable to the subspace method.

The designed color filter set is non-orthogonal and to use it to reconstruct a spectrum s, a pseudoinverse matrix can be used:

$$s' = W(W^T W)^{-1} W^T s, \tag{1}$$

where W is the filter set. In the optical implementation, $W(W^T W)^{-1}$ is known and the inner products, $W^T s$, between the filter set W and the sample's spectrum s are determined experimentally. The filter effect on the sample can be produced either by filtering a reflecting or transmitting light of the sample, or by illuminating the sample by the synthesized light with the spectral characteristics of the filter.

3 Optical Setup

The inner products, $W^T s$ in Equation 1, between a broad band color filter set W and a sample s can be calculated optically using a liquid crystal panel [17, 18]. If the sample is illuminated by synthesized light which has the spectral characteristics of the color filter W_i, then the detected intensity of the sample corresponds to the inner product $W_i^T s$.

3.1 Spectral Synthesizer

To synthesize the light corresponding to the color filter, the optical setup shown in Figure 1 was constructed. The white light source is a halogen lamp pair with two 150W lamps. The light is introduced to a 2mm slit by a fiber light guide, which is omitted in Figure 1, then reflected by a mirror and incident on a concave grating (size 40mm × 40mm, horizontal focus 136mm). The collimated light is dispersed on the focal plane of the concave grating. On the dispersion plane there are a rectangular window with 11mm height, a cylindrical lens

(size 30mm × 50mm, focus 70mm), and a liquid crystal (LC) panel (screen size 19.8mm × 26.4mm). The transmittance of the LC-panel along the wavelength axis is controlled by a computer through a monochrome image board and a LC-driver. The light passing through the LC-panel is finally mixed by the second concave grating (size 40mm × 40mm, horizontal focus 136mm). The function of the cylindrical lens in the dispersion plane is to gather light energy effectively to the second grating, in order to prove good mixing and to make the light loss as small as possible. Mixed light from the second grating is directed to the measuring plane by a mirror. The real size of the optical setup for the spectral synthesizer is 30cm × 15cm, with the height of 7cm.

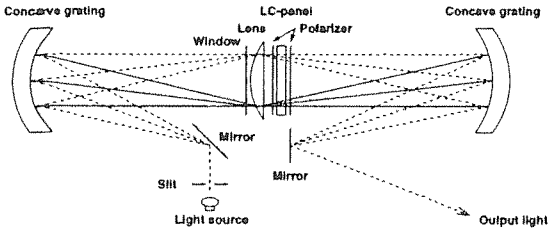

Figure 1: Optical setup for the spectral synthesizer.

3.2 Liquid Crystal Panel

The transmittance of the LC-panel, which is a component of the commercial SHARP XV-NV1 projector, is controlled by computer through a monochrome image board having 512 × 640 pixels and the LC-driver. The digital signal corresponding to the transmittance pattern containing the input levels between 0 and 255 is transferred from the computer's image board to the LC-driver, which sends the video output to the LC-panel. The screen size of the LC-panel is 19.8mm × 26.4mm containing 624 × 832 pixels. Figure 2 shows a schematic drawing of controlling the LC-panel. The LC-panel is an active matrix type with thin film transistors (TFT). This type of LC-panel is known to be free from crosstalk phenomena, which means that the transmittance of a single pixel is not affected by the transmittance of the surrounding pixels. We also confirmed this experimentally.

4 Experiments

4.1 Synthesizing the Light

In this experiment we checked the accuracy of the synthesized light. We designed a color filter set of 4 filters using the unsupervised neural network. The choice of

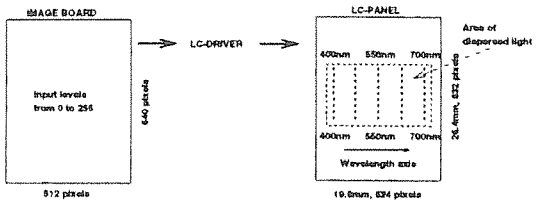

Figure 2: Schematic drawing of controlling the LC-panel.

the best dimension for the filter set is discussed later, in subsection 4.2, where we show that 4 filters is the optimal number of filters in our present system. Figure 3 shows the learned filters.

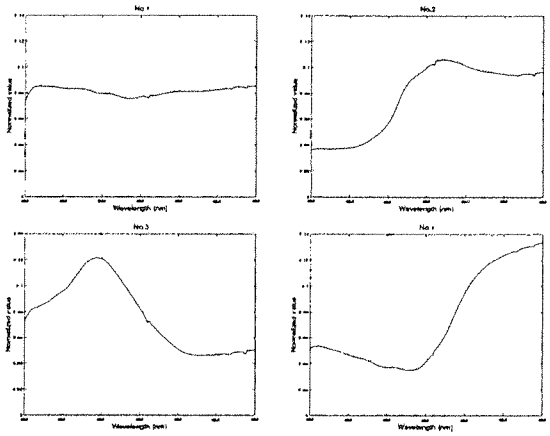

Figure 3: Filter set of 4 learned filters used in proposed spectral vision system.

We prepared the transmittance patterns for the LC-panel and measured the output spectra using a CCD-camera (SONY XC-73) with 31 narrow band interference filters. Figure 4 shows the results of the measurements, where the solid lines are the designed filter set multiplied by the light source spectrum and the dashed lines are measured output spectra when this light source is used. It can be seen that the system can synthesize the illumination corresponding to each color filter with sufficient accuracy. Filter No. 4 shows some error, which is caused by a low signal to noise ratio.

4.2 Dimension Estimation

Next we investigated experimentally the optimal dimension for our model, i.e. how many filters should be used. In this experiment we used transparent color samples,

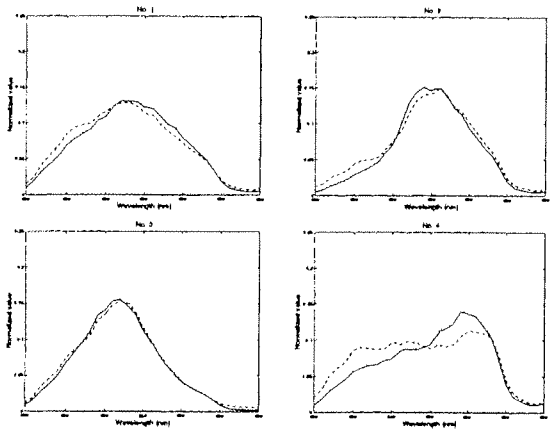

Figure 4: Optically measured results of filtered illuminator. Solid lines are the designed filters multiplied by the light source spectrum and the dashed lines are measured results.

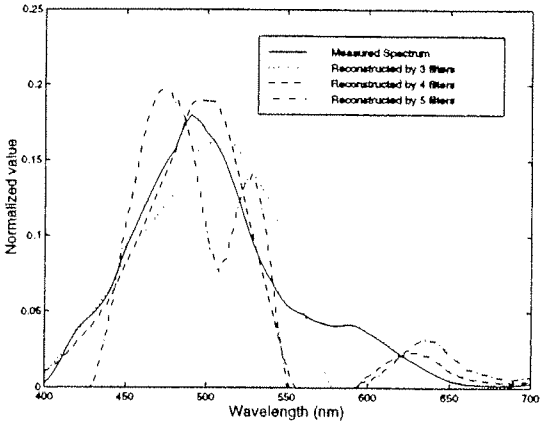

Figure 5: The spectrum of a transparent sample measured by the spectrophotometer (solid line) and the spectra measured by the spectral vision system using 3, 4 and 5 filters.

which were prepared by taking positive slides of Munsell color chips [17]. A transparent color sample was placed in front of the second mirror (see Fig. 1), it was illuminated by the synthesized lights, and the intensity data which correspond to the inner product between the color filters and sample's color spectrum were detected by the CCD-camera. The intensities were detected as average intensities inside the 10×10 pixels image window. The sample's spectrum was then reconstructed using the pseudoinverse matrix in Equation 1. The spectra of the samples were measured in advance by a Shimadzu UV-VIS 2500PC spectrophotometer to compare the results. In these experiments the spectra were sampled at 2nm intervals from 400nm to 700nm.

Figure 5 shows an example of the transparent sample's spectrum which was measured by the spectrophotometer and by our spectral vision system using different number of filters. It can be seen that the reconstruction using 5 filters approximated the peak of the spectrum from 450nm to 550nm with two peaks. In the series of experiments with transparent color samples the same phenomenon happened. When we added more filters to our system, the reconstruction errors highly increased. We investigated carefully this phenomenon and found out that the inverse matrix in Equation 1 was sometimes near singular and then a small error between the optically calculated inner product and theoretic inner product caused large reconstruction errors. In those cases we used a regularization technique based on the truncated singular value decomposition (SVD) to eliminate the effect of near singularity in the spectrum reconstruction.

We calculated the CIE xy- and CIE $L^*a^*b^*$-errors for 6 transparent color samples used in our experiments. The averaged CIE xy- and CIE $L^*a^*b^*$-errors for the filter sets of 3, 4, 5 and 6 filters are tabulated in Table 1, where the ΔE^*-value is defined as $\Delta E^* = \sqrt{\Delta L^{*2} + \Delta a^{*2} + \Delta b^{*2}}$. It can be seen that the ΔE^*-error between the filter sets of 4, 5 and 6 filters is lower than 1, and therefore we decided to use the filter set of them with the lowest dimension, *i.e.* the filter set of 4 filters. Figure 6 a) shows the sample with biggest ΔE^*-error and the sample with smallest ΔE^*-error is shown in Figure 6 b) when the filter set of 4 filters was used.

Table 1: The averaged CIE xy- and CIE $L^*a^*b^*$-errors over 6 transparent color samples between the spectra measured by the spectrophotometer and the spectra measured by the spectral vision system using 3, 4, 5 and 6 filters.

Number of filters	Averaged $(\Delta x, \Delta y)$	Averaged ΔE^*
3	0.0691	25.30
4	0.0324	10.13
5	0.0396	10.68
6	0.0350	10.90

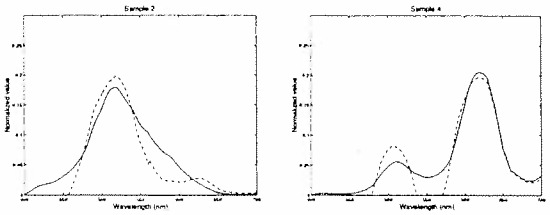

a) b)

Figure 6: The spectra of two transparent samples measured by the spectrophotometer (solid lines) and the spectra measured by the spectral vision system using 4 filters (dashed lines).

4.3 Spectral Image

Finally we acquired a spectral image from a real world object using the spectral vision system shown in Figure 7. A setup of a strawberry and a mandarin lying on a table in front of a colored panel was used as the real world scene. In this experiment we measured the sample's reflectance spectra. The distance between the second mirror in the spectral synthesizer and the sample was 40cm and the distance between the sample and the CCD-camera was 40cm. The angle between the synthesized light and the CCD-camera was 42°. The size of the synthesized light area in the measuring plane was 8cm × 5cm.

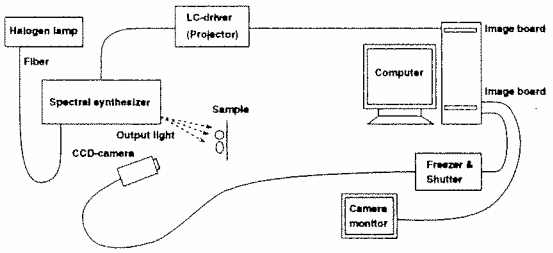

Figure 7: Spectral vision system.

The sample used is shown as a real size gray level image in Figure 8. The image was taken when the LC-panel was set to an input level of 255. The size of the sample is 397 × 290 pixels. The background of the sample are color sheets which are, from left to right: painted blue, painted green, glossy yellow and glossy red.

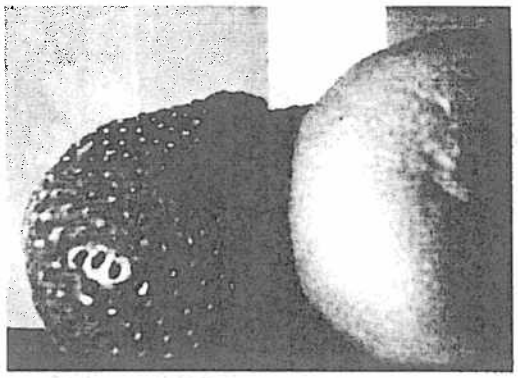

Figure 8: Sample as a real size gray level image, illuminated by the halogen lamp.

We illuminated the sample by 4 synthesized lights corresponding to the color filters shown in Figure 3 and the reflected intensity images were detected by CCD-camera. The shutter speed was 2 seconds. Figure 9 shows the detected intensity images.

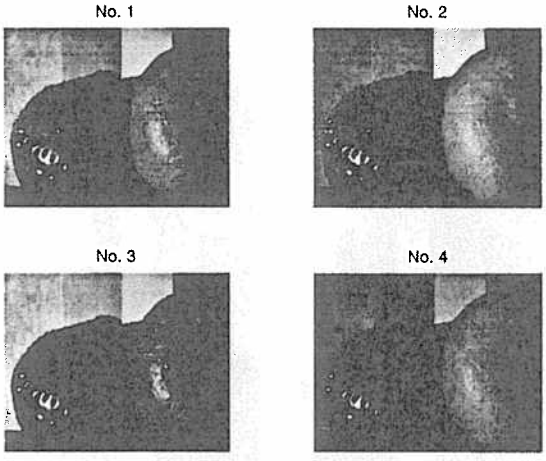

Figure 9: Detected intensity images of the sample, when the sample was illuminated by the synthesized lights which correspond to 4 color filters.

From the detected intensities, we reconstructed the spectral image on the wavelength range from 400nm to 700nm at 10nm intervals using a pseudoinverse matrix. Figure 10 a) shows the wavelength bands from 430nm to 650nm at 20nm intervals of the spectral image acquired by the spectral vision system using 4 filters.

To compare the results, we measured the same spectral image by CCD-camera with 31 narrow band interference filters covering the wavelength range from 400nm to 700nm at 10nm intervals. Light passing through a narrow band filter is highly absorbed and therefore we used a shutter speed of 8 seconds to make the measured images brighter. Figure 10 b) shows the measured results at the wavelength range from 430 to 650nm at 20nm intervals.

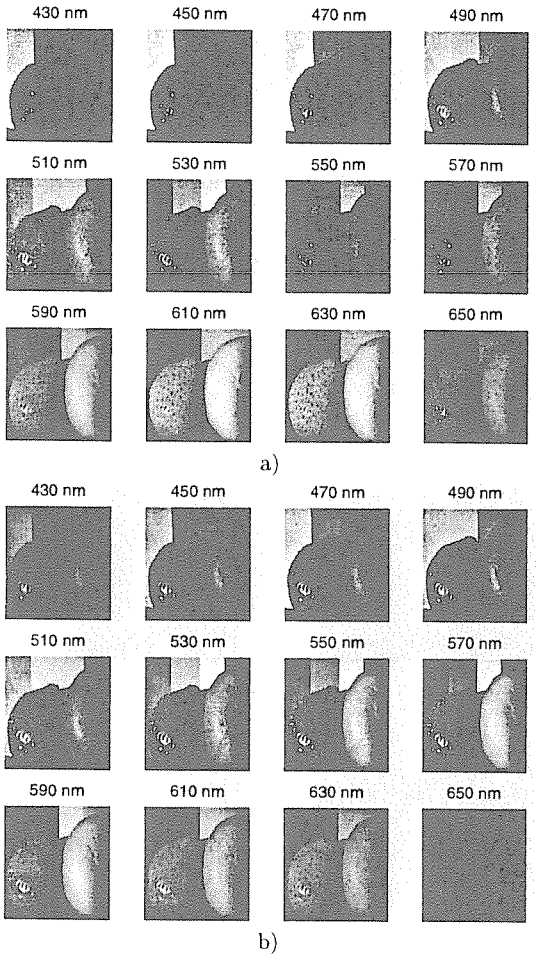

Figure 10: a) Spectral image measured by the spectral vision system using 4 filters. b) Spectral image measured by the CCD-camera with 31 narrow band interference filters.

Figure 11 shows two examples of spectra at different locations of the spectral image. The spectrum in Figure 11 a) is the spectrum of the glossy yellow color sheet and the spectrum of the strawberry is shown in Figure 11 b).

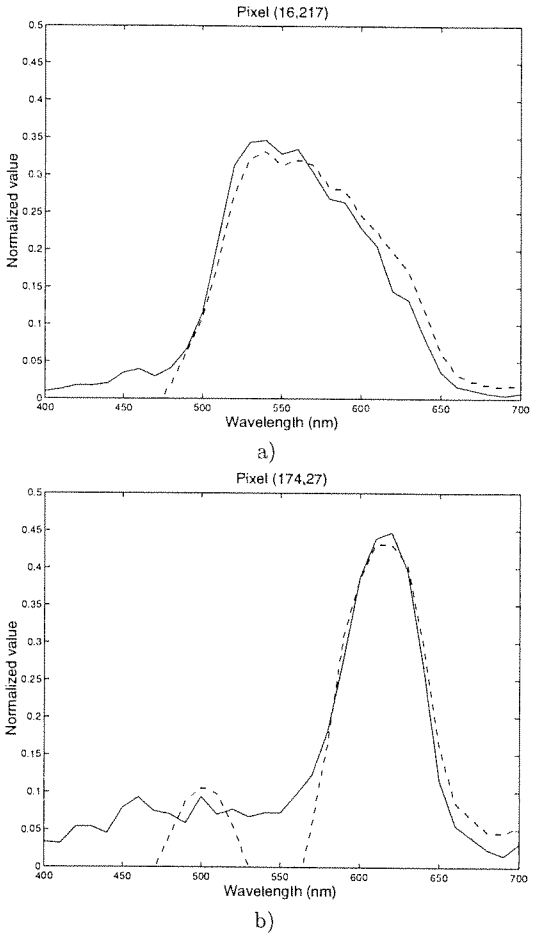

Figure 11: Spectra at two different locations of the spectral image. Solid lines correspond to the spectral image measured by CCD-camera with 31 narrow band filters and dashed lines correspond to the spectral image measured by the spectral vision system using 4 filters.

5 Discussion

We presented a spectral vision system which can be used to measure a color spectrum and two-dimensional spectral images. First we designed the low-dimensional color filter set using an unsupervised neural network. Then we constructed a compact size optical setup to synthesize the light corresponding to the color filter. This

spectral synthesizer can be also used in other applications where a certain illumination must be synthesized. We illuminated the sample with synthesized light and therefore our present system is limited to indoor-measurements. In the outdoor use a more powerful illuminator is needed. In addition, a frequent calibration procedure needs to be designed due to temporal illumination change.

We implemented the color filters optically using a LC-panel. The thin-film-transistor (TFT) type LC-panel is free from crosstalk phenomena and therefore it is easy to control. We used a halogen lamp pair as a light source. It has a low light energy in blue and red areas, but the shape of its spectrum is smooth and suitable for filtering on the dispersion plane. Another possible light source is, for example, the Xenon lamp, which has more light energy in blue and red areas, but also some sharp peaks in the visible light area, which can cause problems when filtering it on the dispersion plane. In the present system the energy of the synthesized output light was suitable for detection by CCD-camera when the sample was located at a distance of 40cm from the spectral synthesizer. The area of light in the measuring plane was 8cm $\times$ 5cm. To make the distance between the spectral synthesizer and the sample longer and the light area bigger, a light source of higher light energy or a high sensitivity camera should be used.

We decided experimentally the optimal dimension for the color filter set used in the spectral vision system. In theory, if the dimension of the filter set W in Equation 1 increases, then the estimation error between the sample's true spectrum s and the reconstructed spectrum s' decreases. In the experiments, however, we noticed that when using more than 4 filters, the estimation error started to highly grow. Tominaga [11] has also shown that the appropriate linear model dimension depends on the properties of the illuminants and on the properties of the measurement instrument. Furthermore, the dimension of the linear model may be limited, for example, by the possible noise in the optical system and by the spectral sensitivity of the CCD-camera. In the experiments, we measured the spectra of the transparent color sheets using different number of filters and we concluded that 4 filters was the optimal number of filters in our present system. We also noticed that when the inverse matrix in Equation 1 was near singular, then a very small error between optically calculated inner product and theoretic inner product caused big errors in the spectrum reconstruction. In order to avoid the problem of near singularity, we used a truncated singular value decomposition method. The filter set designed by the unsupervised neural network contains uncorrelated color filters, but inside the light source spectrum of the halogen lamp the independency becomes weaker.

In our final experiment we acquired the spectral image by our spectral vision system using 4 filters. This was compared to the spectral image measured by CCD-camera with 31 narrow band filters. The spectra measured by the both methods correlated well.

Many of the present spectral imaging systems are based on line scanning [2]. In these systems the spectra are measured with arbitrary accuracy. The acquisition time complexity for each line is $O(1)$ and for the whole image $O(N)$, where N is the number of lines in image. Extra care should be taken for acquisition of equilateral pixels when either the object or the camera is moving. In the proposed spectral vision system, the spatial resolution of the image is defined by the CCD-array and one can obtain a two-dimensional image directly. The different spectral components are, however, acquired separately. In this case the time complexity for acquiring a component image is $O(1)$ and for the whole spectral image the time complexity is $O(L)$, where L is the number of spectral components and $L << N$. Our belief is that the proposed system is easier to use and a better choice for static objects. For moving objects, the number of spectral components and the speed of image acquisition set limits of use. The most critical part is the set-up time of the LCSLM.

We showed that our spectral vision system can be used to measure spectral images. The data obtained from the filtering process is only 4 monochrome images, which can be used to reconstruct the spectral image by a pseudoinverse matrix. The acquired data is convenient for storing and transmitting the spectral image. The optical system is used to calculate the optical inner product, and therefore this system can be used in various optical pattern recognition tasks, for example in classifiers, where the classification criteria contains the inner product calculation. There are still some open questions in our system, for example, the choice of color filter set, possible system noise, near singularity of the inverse matrix and the size of the light area to be illuminated. The main result of this paper is a prototype of the spectral vision system, which can be developed further to be more accurate in its color representation.

Acknowledgments

This work was done when Markku Hauta-Kasari was visiting researcher at the Graduate School of Science and Engineering, Saitama University, Japan. Markku Hauta-Kasari was supported by scholarships from Monbusho (Japanese Ministry of Education) and from Lappeenranta University of Technology, Finland. This work was also partly supported by a Grant-in-Aid for Development Scientific Research (B) (No. 10555013) of the Japanese Ministry of Education, by Jenny and Antti Wihuri Foundation, Finland and by Emil Aaltonen Foundation, Finland. The transmittance data for

the interference filters and the spectra for the transparent samples were measured by the Shimadzu UV-VIS 2500PC spectrophotometer at the Institute of Physical and Chemical Research (RIKEN), Wako, Japan. The Munsell spectral database is available at the www-server of the Lappeenranta University of Technology, Finland, *http://www.it.lut.fi/research/color/lutcs_database.html*. We appreciate the fruitful discussions on this paper with Dr. Shigeki Nakauchi.

References

[1] S. R. Ramasamy, V. Venkatasubrmanian, and S. Anbazhagan, "Reflectance spectra of minerals and their discrimination using thematic mapper, irs and spot multispectral data," *International Journal of Remote Sensing*, vol. 14, pp. 2935–2970, 1993.

[2] T. Hyvarinen, E. Herrala, and A. Dall'Ava, "Direct sight imaging spectrograph: a unique add-on component brings spectral imaging to industrial applications," in *Proceedings, IS & T/SPIE's Symposium on Electronic Imaging: Science and Technology (EI98), San Jose, California, USA, January 25-30*, vol. 3302-21, 1998.

[3] P. K. Kaiser and R. M. Boynton, *Human Color Vision, Second Edition*. Washington DC: Optical Society of America, 1996.

[4] G. Wyszecki and W. S. Stiles, *Color science : concepts and methods, quantitative data and formulae*. New York: Wiley, 1982.

[5] M. S. Drew and B. V. Funt, "Natural metamers," *CVGIP: Image Understanding*, vol. 56, pp. 139–151, 1992.

[6] S. Kawata, K. Sasaki, and S. Minami, "Component analysis of spatial and spectral patterns in multispectral images. I. basis," *Journal of the Optical Society of America A*, vol. 4, no. 11, pp. 2101–2106, 1987.

[7] J. Hallikainen, J. P. S. Parkkinen, and T. Jaaskelainen, "Color image processing with AOTF," in *Proceedings, 6th Scandinavian Conference on Image Analysis, SCIA '89, Oulu, Finland, June 19-22*, pp. 294–300, 1989.

[8] K. Itoh, "Interferometric multispectral imaging," in *Progress in Optics XXXV* (E. Wolf, ed.), pp. 145–196, Elsevier Science, 1996.

[9] J. Parkkinen, J. Hallikainen, and T. Jaaskelainen, "Characteristic spectra of Munsell colors," *Journal of the Optical Society of America A*, vol. 6, no. 2, pp. 318–322, 1989.

[10] S. Usui, S. Nakauchi, and M. Nakano, "Reconstruction of Munsell color space by a five-layer neural network," *Journal of the Optical Society of America A*, vol. 9, no. 4, pp. 516–520, 1992.

[11] S. Tominaga, "Multichannel vision system for estimating surface and illumination functions," *Journal of the Optical Society of America A*, vol. 13, no. 11, pp. 2163–2173, 1996.

[12] S. Baronti, A. Casini, F. Lotti, and S. Porcinai, "Multispectral imaging system for the mapping of pigments in works of art by use of principal-component analysis," *Applied Optics*, vol. 37, no. 8, pp. 1299–1309, 1998.

[13] H. Haneishi, T. Hasegawa, N. Tsumura, and Y. Miyake, "Design of color filters for recording artworks," in *Proceedings, IS&T's 50th Annual Conference, Cambridge, Massachusetts, May 18-23*, pp. 369–372, 1997.

[14] R. Lenz, M. Österberg, J. Hiltunen, T. Jaaskelainen, and J. Parkkinen, "Unsupervised filtering of color spectra," *Journal of the Optical Society of America A*, vol. 13, no. 7, pp. 1315–1324, 1996.

[15] *Munsell Book of Color, Matte Finish Collection*. Baltimore, USA: Munsell Color, 1976.

[16] T. Jaaskelainen, J. Parkkinen, and S. Toyooka, "Vector-subspace model for color representation," *Journal of the Optical Society of America A*, vol. 7, no. 4, pp. 725–730, 1990.

[17] T. Jaaskelainen, T. S, S. Izawa, and H. Kadono, "Color classification by vector supscape method and its optical implementation using liquid crystal spatial light modulator," *Optics Communications*, vol. 89, no. 1, pp. 23–29, 1992.

[18] N. Hayasaka, S. Toyooka, and T. Jaaskelainen, "Iterative feedback method to make a spatial filter on a liquid crystal spatial light modulator for 2D spectroscopic pattern recognition," *Optics Communications*, vol. 119, pp. 643–651, 1995.

[19] M. Hauta-Kasari, W. Wang, S. Toyooka, J. Parkkinen, and R. Lenz, "Unsupervised filtering of Munsell spectra," in *Proceedings, The 3rd Asian Conference on Computer Vision, ACCV'98, Hong Kong, January 8-10* (R. Chin and T.-C. Pong, eds.), vol. I of *Lecture Notes in Computer Science 1351*, pp. 248–255, Springer, 1998.

[20] E. Oja, *Subspace Methods of Pattern Recognition*. Letchworth, England: Research Studies Press, 1983.

[21] S. Grossberg, *Studies of the Mind and Brain*. Drodrecht, Holland: Reidel Press, 1982.

[22] T. Kohonen, *The Self-Organizing Maps*. Berlin Heidelberg: Springer-Verlag, 1995.

[23] S. Haykin, *Neural Networks*. New York: Macmillan College Publishing Company, 1994.

LAPPEENRANNAN TEKNILLINEN KORKEAKOULU. TIETEELLISIÄ JULKAISUJA
LAPPEENRANTA UNIVERSITY OF TECHNOLOGY. RESEARCH PAPERS

35. KÄLVIÄINEN, HEIKKI. Randomized hough transform: new extensions. 1994. U.s. Diss.

36. HEIKKONEN, JUKKA. Subsymbolic representations, self-organizing maps, and object motion learning. 1994. 119 s. Diss.

37. KOSKINEN, JUKKA ANTERO. Knapsack sets for cryptography. 1994. 81 s. Diss.

38. TURUNEN, ESKO. A mathematical study of fuzzy logic: an algebraic approach. 1994. U.s. Diss.

39. JANHUNEN, ANTERO. Toimitustäsmällisyyden suunnittelumenetelmä. 1994. 161 s. Väitösk.

40. LARES-MANKKI, LAURA. Strategy implementation bottlenecks: identification, analysis and removal. 1994. 150 s. Diss.

41. French-Finnish Colloquium on Safety of French and Russian Type Nuclear Power Plants. 1994. 275 s.

42. KORPELA, JUKKA. An analytic approach to distribution logistics strategic management. 1994. U.s. Diss.

43. Third International Seminar on Horizontal Steam Generators October 18-20, 1994, Lappeenranta, Finland. 1995. 413 s.

44. AHOLA, JYRKI. Yrityksen strategiaprosessi: näkökohtia strategisen johtamisen kehittämiseksi konsernorganisaatiossa. 1995. 235 s., liitt. Väitösk.

45. RANTANEN, HANNU. The effects of productivity on profitability: a case study at firm level using an activity-based costing approach. 1995. 169 s., liitt. Diss.

46. Optics in Engineering: First Finnish-Japanese meeting Lappeenranta, 12-14th, June 1995 / ed. by P. Silfsten. 1995. 102 s.

47. HAAPALEHTO, TIMO. Validation studies of thermal-hydraulic code for safety analysis of nuclear power plants. 1995. U.s. Diss.

48. KYLÄHEIKO, KALEVI. Coping with technology: a study on economic methodology and strategic management of technology. 1995. 263 s. Diss.

49. HYVÄRINEN, LIISA. Essays on innovativeness and its evaluation in small and medium-sized enterprises. 1995. U.s. Diss.

50. TOIVANEN, PEKKA. New distance transforms for gray-level image compression. 1996. U.s. Diss.

51. EHSANI, NEDA. A study on fractionation and ultrafiltration of proteins with characterized modified and unmodified membranes. 1996. U.s. Diss.

52. SOININEN, RAIMO. Fracture behaviour and assessment of design requirements against fracture in welded steel structures made of cold formed rectangular hollow sections. 1996. 238 s. Diss.

53. OJA, MARJA. Pressure filtration of mineral slurries: modelling and particle shape characterization. 1996. 148 s. Diss.

54. MARTTILA, ESA. Ilmanvaihdon lämmönsiirtimien teknillinen ja taloudellinen mitoitus. 1996. 57 s. Väitösk.

55. TALONPOIKA, TIMO. Dynamic model of small once-through boiler. 1996. 86 s. Diss.

56. BACKMAN, JARI. On the reversed Brayton cycle with high speed machinery. 1996. 103 s. Diss.

57. ILME, JARNO. Estimating plate efficiencies in simulation of industrial scale distillation columns. 1997. U.s. Diss.

58. NUORTILA-JOKINEN, JUTTA. Choice of optimal membrane processes for economical treatment of paper machine clear filtrate. 1997. U.s. Diss.

59. KUHMONEN, MIKA. The effect of operational disturbances on reliability and operation time distribution of NC-machine tools in FMS. 1997. 133 s., liitt. Diss.

60. HALME, JARKKO. Utilization of genetic algorithm in online tuning of fluid power servos. 1997. 91 s. Diss.

61. MIKKOLA, AKI. Studies on fatigue damage in a hydraulically driven boom system using virtual prototype simulations. 1997. 80 s., liitt. Diss.

62. TUUNILA, RITVA. Ultrafine grinding of FGD and phosphogypsum with an attrition bead mill and a jet mill: optimisation and modelling of grinding and mill comparison. 1997. 122 s. Diss.

63. PIRTTILÄ, ANNELI. Competitor information and competitive knowledge management in a large, industrial organization. 1997. 175 s., liitt. Diss.

64. MEURONEN, VESA. Ash particle erosion on steam boiler convective section. 1997. 149 s. Diss.

65. MALINEN, HEIKKI. Forecasting energy demand and CO_2 -emissions from energy production in the forest industry. 1997. 86 s. Diss.

66. SALMINEN, RISTO T. Role of references in international industrial marketing - a theory-building case study about supplier's processes of utilizing references. 1997. 375 s. Diss.

67. Fourth International Seminar on Horizontal Steam Generators 11-13 March 1997, Lappeenranta, Finland. 1997. 285 s.

68. KAIKKO, JUHA. Performance prediction of gas turbines by solving a system of non-linear equations. 1998. 91 s. Diss.

69. LEHMUSVAARA, ANTTI. Improving the potentials of logistics processes: identification and solutions. 1998. U.s. Diss.

70. PIHLAJAMÄKI, ARTO. Electrochemical characterisation of filter media properties and their exploitation in enhanced filtration. 1998. U.s. Diss.

71. VIROLAINEN, VELI-MATTI. Motives, circumstances, and success factors in partnership sourcing. 1998. 232 s. Diss.

72. PORRAS, JARI. Developing a distributed simulation environment on a cluster of workstations. 1998. U.s. Diss.

73. LAURONEN, JARI. Spare part management of an electricity distribution network. 1998. 130 s. Diss.

74. PYRHÖNEN, OLLI. Analysis and control of excitation, field weakening and stability in direct torque controlled electrically excited synchronous motor drives. 1998. 109 s. Diss.

Sarjan uusi nimi: ACTA UNIVERSITATIS LAPPEENRANTAENSIS

75. SAARNIO, ANTTI. Choice of strategic technology investment - case of pulp production technology. 1999. 225 s. Diss.

76. MATTILA, HEIKKI. Merchandising strategies and retail performance for seasonal fashion products. 1999. 219 s. Diss.

77. KAUKONEN, JUKKA. Salient pole synchronous machine modelling in an industrial direct torque controlled drive application. 1999. 138 s. Diss.

78. MÄNTTÄRI, MIKA. Fouling management and retention in nanofiltration of integrated paper mill effluents. 1999. U.s. Diss.

79. NIEMELÄ, MARKKU. Position sensorless electrically excited synchronous motor drive for industrial use based on direct flux linkage and torque control. 1999. 142 s. Diss.

80. LEPPÄJÄRVI, SEPPO. Image segmentation and analysis for automatic color correction. 1999. U.s. Diss.